Prehydrated Electron and Its Role in Ionizing Radiation Induced DNA Damage and Molecular Mechanisms of Action of Halogenated Sensitizers for Radiotherapy of Cancer

by

Chunrong Wang

A thesis
presented to the University of Waterloo
in fulfillment of the
thesis requirement for the degree of
Doctor of Philosophy
in
Physics

Waterloo, Ontario, Canada, 2012

©Chunrong Wang 2012

AUTHOR’S DECLARATION:

I hereby declare that I am the sole author of this thesis. This is a true copy of the thesis, including any required final revisions, as accepted by my examiners.

I understand that my thesis may be made electronically available to the public.

This thesis is based on following publications:

[1] **Chun-Rong Wang,** Anmin Hu and Qing-Bin Lu, 'Direct Observation of the Transition State of Ultrafast Electron Transfer Reaction of a Radiosensitizing Drug Bromodeoxyuridine', J. Chem. Phys. 124, 241102 (2006). [selected for republications in the Virtual Journal of Biological Physics Research (July 1, 2006) http://www.vjbio.org and in the Virtual Journal of Ultrafast Science (July 2006), http://www.vjultrafast.org].

[2] **Chun-Rong Wang** and Qing-Bin Lu, 'Real-Time Observation of Molecular Reaction Mechanism of Aqueous 5-halo-2'-deoxyurimidines under UV/Ionizing Radiation', Angew. Chem. Int. Ed. 46, 6316 (2007).

[3] **Chun-Rong Wang**, Kristine Drew, Ting Luo, Mei-Jun Lu and Qing-Bin Lu, 'Resonant Dissociative Electron Transfer of the Presolvated Electron to CCl_4 in Liquid: Direct Observation and Lifetime of the $CCl_4{}^{*-}$ Transition State', J. Chem. Phys.128, 041102 (2008).

[4] **Chun-Rong Wang**, Ting Luo and Qing-Bin Lu, 'On the Lifetimes and Physical Nature of Prehydrated Electrons in Liquid Water', Phys. Chem. Chem. Phys. 10, 4463 (2008) [Selected as a **Hot Article** for PCCP].

[5] **Chun-Rong Wang**, Jenny Nguyen and Qing-Bin Lu, 'Bond breakage of nucleotides by dissociative electron transfer of nonequilibrium prehydrated electrons: a new molecular mechanism for reductive DNA damage', J. Am. Chem. Soc. 131, 11320 (2009)

[This paper was highlighted in a News & Views article in NATURE 461, 358 (2009)].

[6] **Chun-Rong Wang** and Qing-Bin Lu, 'Molecular Mechanism of the DNA Sequence Selectivity of 5-Halo-2'-Deoxyuridines as Potential Radiosensitizers', J. Am. Chem. Soc. 132, 14710 (2010).

Abstract

Despite advances in technology and understanding of biological systems in the past two decades, modern drug discovery is still a lengthy, expensive, difficult and inefficient process with low rate of new therapeutic discovery. The search for new effective drugs remains a somewhat empirical process. There is compelling need for a more fundamental, mechanistic understanding of human cancers and anticancer drugs to design more appropriate drugs.

Radiotherapy is still the major therapy of cancer. It uses high-energy ionizing radiation such as x-rays and charged particle beams to destroy cancer cells. DNA is well known to be the principal biological target of radiotherapy, but the molecular mechanism of ionizing radiation induced DNA damage was elusive. The conventional thought of the ·OH radical as the major origin for ionizing radiation induced DNA damage is questionable. Although various strategies and types of compounds have been designed and developed as potential radiosensitizers to enhance the radiosensitizing efficiency of radiotherapy, none of them have been approved for clinical use. The general outcomes of clinical trials have been disappointing.

This thesis presents an innovative molecular-mechanism-based drug discovery project to develop novel drugs for effective radiotherapy of cancer through the emerging

femtomedicine approach. Its ultimate goal is to develop more effective radiosensitizers, based on our unique molecular understandings of ionizing radiation induced DNA damage and halopyrimidines as a family of potential radiosensitizers.

Direct, real-time observation of molecular reactions is of significant importance in diverse fields from chemistry and biology, environmental sciences to medicine. *Femtosecond time-resolved laser spectroscopy* (fs-TRLS) is a very powerful, direct technique for real-time observation of molecular reactions. Its key strength lies in short duration laser flashes of a time scale at which reactions actually happen - femtoseconds (fs) (1fs = 10^{-15} second). Since the late 1980s, its application to study chemical and biological systems led to the births of new subfields of science, called femtochemistry and femtobiology. Recently, *femtomedicine* has been proposed as a new transdisciplinary frontier to integrate ultrafast laser techniques with biomedical methods for advances in fundamental understandings and treatments of major human diseases. This the remarkable opportunity afforded through real-time observation of biochemical reactions at the molecular level. Femtomedicine holds the promise of advances in the radiotherapy of cancer.

Several important findings were made in this thesis. First, our results of careful and high-quality fs-TRLS measurements have resolved the long existing controversies about the physical nature and lifetimes of a novel ultrashort-lived electron species (e_{pre}^-) generated in radiolysis of water. These results have not only resolved the large

discrepancies existing in the literature but provided new insights into electron hydration dynamics in bulk water. Such information is important for quantitative understanding and modeling of the role of non-equilibrium e_{pre}^- in electron-driven reactions in diverse environmental and biological systems, from radiation chemistry and radiation biology to atmospheric ozone depletion.

Second, our fs-TRLS results have unraveled how e_{pre}^- plays a crucial role in ionizing radiation induced DNA damage. We found that among DNA bases, only T and especially G are vulnerable to a dissociative electron transfer (DET) reaction with e_{pre}^- leading to bond breaks, while the electron can be stably trapped at C and especially A to form stable anions. The results not only challenge the conventional notion that damage to the genome by ionizing radiation is mainly induced by the oxidizing OH radical, but provide a deeper fundamental understanding of the molecular mechanism of the DNA damage caused by a reductive agent (e_{pre}^-). Our findings have led to a new molecular mechanism of *reductive* DNA damage.

Third, halopyrimidines, especially BrdU and IdU, have passed Phase I to II clinical trials as potential hypoxic radiosensitizers, but the outcome of Phase III clinical trials was disappointing. Our results of fs-TRLS studies have provided a new molecular mechanism of action of halopyrimidines (XdUs, X=F, Cl, Br and I) in liquid water under ionizing radiation. We found that it is the ultrashort-lived e_{pre}^-, rather than the long-lived e_{hyd}^-, that is responsible for DET reactions of XdUs. This reaction leads to the formation

of the reactive dU ·radical, which then causes DNA strand breaks and cancer cell death. Our results have challenged a long accepted mechanism that long-lived e_{hyd}^- would be responsible for the radical formation from halogenated molecules. Furthermore, we found that the DET reaction efficacy leading to the formation of the reactive dU ·radical is in the order of FdU << CldU < BrdU < IdU. Thus, only BrdU and IdU could be explored as potential radiosensitizers, in agreement with the results of bioactivity tests and clinical trials.

Fourth, our fs-TRLS studies have provided a molecular mechanism for the DNA sequence selectivity of BrdU and IdU in radiosensitization. We found the DET reactions of BrdU/ IdU with $dAMP^{*-}$ and $dGMP^{*-}$ formed by attachment of e_{pre}^- generated by radiolysis of water in aqueous BrdU-dAMP/dGMP and IdU-dAMP/dGMP complexes under ionizing radiation. This new mechanistic insight into the interaction of BrdU and IdU with DNA provides clues to improve the halogen familty as potential radiosensitizers and to develop more effective radiosensitizers for clinical applications.

Fifth, based on our molecular mechanistic understandings of DNA damage induced by ionizing radiation and halopyrimidines as potential radiosensitizers, we develop more effective new radisensitizing drug candidates through the femtomedicine approach. We have performed a fs-TRLS study of the DET reaction of a candidate compound (RS-1) with e_{pre}^-, and found that the DET reaction of e_{pre}^- with RS-1 is much stronger than that of IdU (and certainly BrdU and CldU). Moreover, we have tested the

radiosensitizing effect of RS-1 against human cervical cancer (HeLa) cells exposed to various doses of x-ray irradiation through DNA damage measurements by gel electrophoresis and cell viability/death assays by MTT. Our results have confirmed that RS-1 can largely enhance the radiosensitivity of treated human cervical cancer (HeLa) cells to x-ray (ionizing) radiation. It is clearly demonstrated that RS-1 has a much better radiosensitizing effect than IdU. Although these are just preliminary results, our results have shown promise of developing more effective radiosensitizers.

In summary, our studies have demonstrated the potential of *femtomedicine* as an exciting new frontier to bring breakthroughs in understanding fundamental biological processes and to provide an efficient and economical strategy for development of new anticancer drugs.

Acknowledgments

Many people deserve to be acknowledged for their help during my graduate studies. To all of those not mentioned here specifically, you have my deepest gratitude for your efforts. Several individuals deserve a special mentioning and I wish to take this opportunity to express my appreciation.

I am extremely grateful to my research advisor, Prof. Qing-Bin Lu, for giving me the opportunity to be involved in this exciting project and for numerous fruitful scientific discussions. His invaluable supervision, profound guidance, and foresighted sense to numerous scientific issues were indispensable to my successful completion of this Ph.D study and research. His incredible enthusiasm for femtomedicine research has been inspiring and contagious.

My gratitude also goes to my committee members, Prof. Bae-Yeun Ha, Prof. Bruce Greenberg, Prof. Jeff Chen, and Prof. Hartwig Peemoeller, for their input along the way and valuable discussions. Also I like to thank all my previous and current group members for their discussion, kind help and friendship.

Thanks are also due to my good friends, Hai-Tang Wang, Xi Chen, Mei Huang, Hao Liang, Ying Jiang, Zhao Ren, Xiao-Jian Chang and Yi-Jie Hu, for their precious friendship, encouragement and kind help.

Special gratitude goes to two special friends, Yi-Zhen Guo and Yuan-Shui Zheng,

even though they are not in Canada with me. Every time when I share my happiness and bitterness with them, they are always there and have been incredibly considerate, patient, and supportive.

I also like to thank my amazing family, for giving me their love, support, and encouragement all the time.

I am also indebted to Judy McDonnell for providing valuable help. I would also like to thank all the staff members and postgraduate students of the department for their hospitality, help and friendship.

Finally, financial supports to this project from the Canadian Institutes of Health Research (CIHR) are acknowledged.

To my family

Contents

List of Figures

List of Tables

Chapter 1

Introduction to Cancer Therapies

This thesis is part of our project aiming to obtain new-molecular-level understanding of ionizing radiation induced DNA damage and of mechanisms of the action of existing anticancer drugs such as potential radiosensitizers bromodeoxyuridine (BrdU) and iododeoxyuridine (IdU) and so as to develop new anticancer drugs. In this chapter, I shall introduce some background information about this thesis.

1.1. Cancer

1.1.1. What is cancer?

Among the most challenging diseases, cancer is very difficult to cure. Cancer might be thought to be a single disease, but as a matter of fact, it is a kind of diseases in which abnormal cells divide too quickly and out of control [1]. They result from the uncontrolled cell growth of abnormal cells in the body [1-4]. If the DNA in a cell is mutated and the mutations affect normal cell growth and division, cells may not die when they are supposed to. It is possible for

the extra cells to form a tumour, as shown in Fig. 1.1 [1]. But not all the cancers are tumours, such as leukemia.

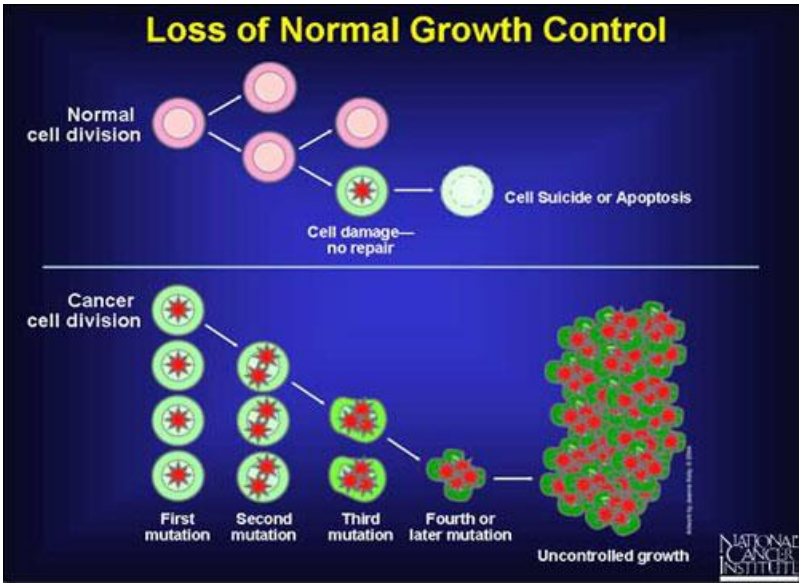

Figure 1.1. Cancer arises from a loss of normal growth control [1].

There are many different kinds of cancers. They can be divided into mainly six categories, including carcinoma, sarcoma, leukemia, lymphoma, myeloma, and central nervous system cancers [5-7]:

- carcinoma: they are malignancies of epithelial tissues, such as skin or tissues covering internal organs. Approximately 80~90 percent of all cancers fall into this category [5].
- sarcoma: cancers that initiate in connective or supportive tissues, such as bones, fat, and blood vessels.

- leukemia: they arise from blood-forming tissues such as the bone marrow. They are usually linked to overproduction of white-blood cells, which do not perform as well as they should. Moreover, the function of red blood cells is also affected by leukemia.
- lymphoma: they originate in the lymphatic system.
- myeloma: they start in the plasma cells of bone marrow.
- central nervous system cancers: they initiate in the tissues of the brain or spinal cord. They are among the most devastating cancers [8].

Also, cancer can develop in many different organs or tissues, such as the breast, ovary, lung, brain, kidney, cervix, liver, colon, skin, bones, nerve tissue, etc (almost every organ or tissue). Cancers can be caused by different origins, including genetic problems, toxic chemicals (e.g., benzene), over drinking of alcohol, over exposure of sunlight, exposure to ionizing radiation, environmental toxins (e.g., posionous mushrooms), viruses, obesity, etc [9]. Moreover, the causes of many cancers are still unknown [9].

1.1.2. Microenvironment of cancer

The surrounding normal cells, molecules, and blood vessels feed a tumor cell. A tumor can alter its microenvironment, and the microenvironment can affect how a tumor grows, spreads and responds to the treatment. There are some characteristic features distinguishing a solid tumour from its corresponding normal tissue. These include *high interstitial fluid pressure (IFP), low oxygen tension (hypoxia), and low extracellular PH (acidosis)* [10-12]. All of them can contribute to the resistance of cancer therapy and affect the treatment outcomes [12]. Therefore,

some research efforts in cancer treatments have been focused on the tumor microenvironment as a therapeutic target. Below, a brief discussion on the microenvironment of tumor is given.

A tumour has unique vasculature, which leads to the tumour specific conditions [10]. Tumor vasculature is drastically different from normal vascular networks. The latter are well-organized architecture with dichotomous branching and hierarchic order [13]. They consist of arterioles, capillaries, and venules [13-14]. Under normal conditions, blood flows from arterioles to capillaries, and then to venules in a regular manner. Also, there is a network of lymphatics to drain fluid and cellular by-products from interstitium [15-16]. In contrast, tumor vascular networks are highly disorder with a complete lack of lymphatics [15-16]; tumour vessels are dilated, saccular, and tortuous, and are more permeable than those in normal tissues [13-14].

Interstitium refers to the space between the cells and the vascular compartment. It is important to transport molecules between the cells and blood vessels. Permeable tumor vessels with leak ends and a complete lack of lymphatics in a tumor cause an abnormal accumulation of fluid contents in the tumor tissue [12-16]. Because lymphatic fluid and waste products are not efficiently transported away from the tumor microenvironment, the interstitial fluid pressure (IFP) in the tumor tissue is higher than for normal tissues. The IFP in normal tissues is about equal to the atmospheric pressure (76 mmHg), while the IFP in a tumor tissue could be increased to up to 100 mmHg [12]. The increased IFP can hinder transcapillary fluid flow and convective transport of therapeutic molecules into the tumor [17].

Due to the poor tumor vasculature, the blood flow through tumor is impaired. The oxygen delivery in tumor is thus reduced. Oxygen cannot be diffused into the tumor areas distant from the blood vessels [18]. They develop temporary or chronically hypoxic regions. The pO_2 of

normal tissues lies in the range between 10 and 80 mmHg, while it could be < 5 mmHg for certain areas of tumor [12, 19-20]. Moreover, the blood flow is temporally heterogeneous (unstable), which can lead to acute hypoxia in tumors [12-14].

The metabolic environment of the tumor is also affected by the unique tumor vasculature and the resultant oxygen depletion. Acidic metabolites in the tumor cannot be adequately carried away. Hypoxia in the tumor microenvironment results in acidosis, because lactic acid builds up due to anaerobic glycolysis [21-22]. Therefore the PH value in tumor is lower than those in normal tissues.

1.1.3. Typical cancer treatments

There are a few typical cancer treatments, including surgery, radiotherapy, and chemotherapy [3]. The choice of treatment depends on the type of cancer and its stage. The latter refers to how much a cancer has grown and whether the cancer cells have spread from the original tumor location. If a tumor is still localized and the cancer cells have not spread to other organs or tissues, the most common treatment to cure the cancer is surgery. If the cancer cells have only spread to local lymph nodes, it is still possible to remove all of the cancer cells by surgery. In contrast, if the cancer cells have spread to other organs or tissues, it is difficult or impossible to remove all of the cancer cells by surgery and the patients may be treated by radiotherapy or chemotherapy, or the combination of both. In some cases, cancer patients may need a combination treatment of the three approaches (surgery, radiation, and chemotherapy).

Surgery removes a solid tumour with some surrounding healthy tissue while keeping the surrounding normal tissues to a minimal injury [23]. Radiotherapy uses high-energy ionizing radiation, such as x-rays, γ-rays, or charged particles to cause irreparable DNA damage and kill the cancer cells [23]. It is used to target small areas and usually not used to treat cancers that have spread. Chemotherapy uses anti-tumour compounds to kill malignant tumour cells. It is used as the primary therapy for cancers in an advanced stage and often used in combination with other localized treatments such as surgery and radiotherapy [23]. In the case of solid tumours, the first treatment is usually the surgery to remove a tumour with a margin of normal tissues. Then radiotherapy is used to destroy any possible residuals of the tumour. In many cases, an anti-cancer drug is also used to kill residual cancer cells and any possible cancer cells spread to other areas in the body.

Moreover, there are emerging, unconventional cancer treatments such as photodynamic therapy, photothermal therapy, gene therapy, hormone therapy, bone marrow transplantation and virus therapy [3, 23]. For example, photodynamic therapy (PDT) is a novel clinical method [24]. It uses the combination of photosensitizers and specific lasers to treat a number of tumours, such as skin cancer and non-small cell lung cancer. It is comparatively non-invasive, can be targeted accurately and has fewer side effects [24].

1.1.4. Effects of tumour microenvironment on conventional cancer therapies

The microenvironment of tumor can have significant impacts on the outcomes of cancer treatments [12]. First, the poor vasculature in tumor places a physical constraint on the

microenvironment and can cause an ineffective drug delivery [25-26]. In the tumor, the acidosis (low pH values) of the microenvironment and the high interstitial pressure also make drug delivery difficult [25-26]. It has been shown that patients with lymphoma and melanoma had better response to chemotherapy if their IFP dropped during treatment [27]. An additional contributor to this hostile environment is the heterogeneous nature of the tumor and its local environment. Different areas of the tumor are unevenly hypoxic or acidic, since blood flow within the tumor is not constantly stable because of the abnormal vasculature. Also, the extracellular matrix is different from normal environmental conditions. Low extracellular PH also decreases the uptake of many chemotherapeutic drugs [28]. Many drugs, such as doxorubicin, are most efficiently passing through both plasma membranes and intracellular membranes in a neutral state [28]. However, they tend to become charged states when they exist in the acidic environment of the tumor [28]. This can cause a significant reduction of drug uptake.

Hypoxic conditions also appear to promote tumor survival and growth in cancer therapies [29-30]. Hypoxia affects several types of chemotherapy drugs. Oxygen is required for some drugs, such as mephalan, bleomycin, and etoposide, to achieve a maximal efficiency [29]. Moreover, the low oxygen level could cause cell cycle arrest and thus reduce the therapeutic efficacy of the drugs that are more effective against proliferating cells [30]. For radiotherapy, hypoxia has been well known to inhibit effective radiation killing of cancer cells [31-34]. Indeed, oxygen itself is an effective radiosensitizer. It is a well-known fact that well-oxygenated cells required a radiation dose only about one third of that required for anoxic cells to achieve a given level of cell killing [35]. For photodynamic therapy (PDT), its therapeutic efficiency depends on the distribution of photosensitizers, the propagation of the photoactivating light and the amount of oxygen in the tumour [36]. In particular, the activation of PDT is to generate reactive

oxygen species that then causes biological effects such as cell apoptosis and necrosis [24]. Therefore, PDT efficiency is certainly dependent on the oxygen level in the tumor. Unfortunately, the poor tumour vasculature results in reduced photosensitizer and oxygen delivery in tumor tissues.

However, the tumor microenvironment may be exploited as an advantage to develop anti-cancer drugs that targets at the tumor preferentially. For example, "reductive" hypoxic radiosensitizers may kill hypoxic cancer cells effectively while have a less toxicity against oxic cells in healthy tissues, as will be discussed in Section 2.7 of Chapter 2.

1.2. Drug discovery and development

1.2.1. Drug discovery history

Drug discovery history is a long, slow process. In the ancient times, people used an almost completely empirical method to treat diseases and recover from their illness. For instance, healing herbs were discovered by a process of trial and error. To the beginning of the 19th century, pharmacologically active compounds were extracted from plants by a method called solvent extraction [37-38].An example was theisolation of morphine from opium by Serturner in 1805 [38]. This allowed people to study morphine without the interference of other constituents of the opium mixture. It was the infancy of *pharmacology*. Soon after, additional alkaloids were

isolated from opium. Their comparative biological evaluations marked the beginning of *modern medicinal chemistry* [38].

Then, urea was synthesized by Wohler in 1828 [38]. The progress established the science of *synthetic organic chemistry*. William Perkin discovered mauveine in 1856 [37]. It represented that for the first time in history, the development of new drugs did not necessarily come from natural products. The subsequent successful synthesis of chloral hydrate in 1868 and sodium salicylate in 1875 represented the start of the industrial production of *synthetic drugs* [37-38].

At about the turn of the 20th century, Nobel laureate Paul Ehrlich used the term *chemotherapy* to describe the application of chemicals with known composition to the treatment of parasites [38]. Till the 1960s, the discovery of new drugs depended mostly on the discovery of natural product analogs. By then, the activity of a compound was tested in the whole animal system [38]. Since the late 1960s, molecular biology started to develop rapidly. DNA helix structure was discovered and genes were found to express as proteins. It was also found that some proteins, when they were overexpressed or incorrectly expressed, cause many human diseases. Therefore, some drugs were designed to target these proteins for the treatment of related diseases [38].

In the second half of the 20th century, medicinal chemists manipulated the chemical structures to control the transportations of drugs to their targets and to obtain optimal uptakes [37-38]. With the advances in biochemistry in the 1970s and breakthroughs in molecular biology in the 1980s, it became possible to identify leads by screening a large number of compounds for many new targets in human genome. A new age of drug discovery emerged in the early 1990s: *high throughput screening* (HTS) and *combinatorial chemistry* were born [37-38]. Since then,

people have learned how to control the production of proteins that were responsible for some diseases and have tested the efficacy of potential drugs. Screening a huge number of compounds through HTS has been one of the major methods in modern drug discovery [38].

1.2.2. Limitations of modern drug discovery and development

There has been a great progress in the drug discovery and development in the past two decades. The technology and understanding of biological systems have been increasingly advanced. However, modern drug discovery is still a lengthy, expensive, difficult and inefficient process with low rate of new therapeutic discovery [39]. On the average, it takes about 20 years to develop a single new medicine [40], and the research and development cost of a new drug is about US $1.8 billion [41].

Here is an example given to show that modern drug discovery is an inefficient process. Cisplatin is an effective cancer chemotherapy drug. It is now the cornerstone agent in treating a variety of cancer, including ovarian cancer, testicular cancer, cervical cancer, bladder cancer, lung cancer, head and neck cancer, lymphomas cancer, brain tumors, malignant pleural mesothlioma and neuroblastoma [42-44]. However, its application is often limited by severe toxic side effects and resistance possessed by various cancers. Over three thousands of platinum analogues have been synthesized and screened for anticancer activity in an attempt to overcome the drawbacks of cisplatin and to broaden the range of treatable tumors in the past 40 years [42-44]. Among the compounds, only two have been approved by the FDA: oxilaplatin and carboplatin for the treatment of some cancers. This might imply the lack of a precise

understanding of the molecular mechanism of the cytotoxicity of cisplatin [45-46]. This example indicates that there is a pressing need for mechanistic understanding of action of existing anticancer drugs at the molecular level, which can, in turn, lead to mechanism-based design of new anticancer drugs.

In this thesis, we present an innovative molecular-mechanism-based drug discovery project to develop novel drugs for effective radiotherapy of cancer through the emerging femtomedicine approach. This approach aims to integrate ultrafast laser techniques with biomedical methods aims for advances in fundamental understanding and treatment of major human diseases, notably cancer [47].

Chapter 2

Ionizing-Radiation-Induced DNA damage and Radiotherapy

Radiotherapy is currently the major modality of cancer therapy. It uses high energy x-rays, or charged particles to destroy cancer cells. DNA is the major target of radiotherapy. In some applications, compounds (the so-called radiosensitizers) are used as drugs to make cancer cells more sensitive to radiotherapy. In this chapter, the physical and chemical basis of radiotherapy will be briefly introduced. The current status of the study of DNA damage induced ionzing radiation will then be reviewed, and finally the main types of potential radiosensitizers will be reviewed and discussed.

The ultimate goal of this project is to develop more effective radiosensitizers, based on our unique molecular understanding of ionizing radiation induced DNA damage and halopyrimidines as a family of potential radiosensitizers. To achieve this ultimate goal, we need to understand how ionizing radiation causes DNA damage and how radiosensitizers enhance the therapeutic efficacy of radiotherapy.

2.1. Radiation energy deposition

Ionizing radiation used in radiotherapy includes high energy photons and charged particles such as x-rays, γ-rays, electrons and ions. The energy deposition into the matter by ionizing radiation is a random process [48]. Generally, an ionizing particle will have a high energy that is far sufficient to remove an orbital electron from any atom with which it interacts. Therefore any atom may randomly lose an electron and is ionized.

If a complex system (one consisting of more than one kind of molecules) is irradiated with ionizing radiation, the ionization probability is proportional to the number (concentration/density) of molecules present in the system. When cells or tissues are irradiated, most of the radiation energy is absorbed by water, because cells are made up of more than 70% in mass of water [12]. Ionizing radiation results in not only ionization, but also excitation of water molecules.

2.2. Target of radiotherapy

DNA is the principal target of radiotherapy. It is critical for cell survival [49]. Other bioactive molecules, such as RNA, amino acids, peptides, proteins, lipids, and inorganic ions can also be damaged by ionizing radiation, because the way ionizing radiation deposits its energy is non-selective. But cells can still be alive even when these bioactive molecules lose most of their biological activity. For example, if most of the RNA is damaged, good RNA can still be transcribed from good DNA. In contrast, if DNA is damaged and not repaired, the transcribed

RNA and translated proteins will have problems. The cells will be mutated or killed finally. DNA as the principal target of ionizing radiation has been confirmed by some experimental results [50-53]. It was shown that if radiation was absorbed by the outer membrane and the cytoplasm of eukaryotic cells, little lethal damage to cells was observed [53]. But when the radiation reached the nucleus, lethal damage dramatically increased [50-53].

In the living systems, ionizing radiation causes DNA damage through direct and indirect interactions [12, 49]. In the direct effect, ionizing radiation energy is directly deposited into DNA. DNA molecules will be directly ionized or excited, initiating a chain reaction that leads to biological effects. The direct effect is thought to be dominant under high LET (linear energy transfer) radiation, such as neutrons, α-particles, and high energy argon ion beam [12]. In the indirect action, ionizing radiation firstly reacts with cellular environment, mostly water, generating different types of reactive radicals. These radicals then react with the DNA, causing damage to the DNA. The indirect effect plays a major role in DNA damage caused by low LET radiation - such as β particles, x-rays, and γ-rays.

2.3. Direct effect of DNA damage

2.3.1. Caused by high energy ionizing radiation

The primary effect of direct ionizing radiation damage to duplex DNA is the formation of cationic and anionic radicals [54-61]. In DNA irradiated at low temperature, researchers have suggested that the hole (positive charge) migrates to and stabilizes on guanine [59, 61]. In 1991, Sevilla et al. [61] reported an ESR (electron spin resonance) study of the relative distribution of ion radicals formed in DNA equilibrated with D_2O and irradiated by γ–rays at 77 K. Their result gave DNA ion radicals' relative abundances as about 77% $C^{\cdot -}$, 23% $T^{\cdot -}$ for anions and >90% $G^{\cdot +}$ for the cations; about equal amounts of anions and cations were present. In the next year, the same group reported the free-radical distribution in γ–irradiated frozen samples of single stranded DNA (ssDNA) and double stranded DNA (dsDNA) [62]. They suggested a more uniform distribution of the radical ions on the DNA bases for the ssDNA than that for the dsDNA: thymine anion $T^{\cdot -}$ (30-35%), cytosine anion $C^{\cdot -}$ (20-28%), guanine cation $G^{\cdot +}$ (26-28%), and adenine cation $A^{\cdot +}$ (8-17%), with small amounts of purine anions or pyrimidine cations. ESR studies of irradiated DNA at low temperatures indicated that the major radical species stabilized at 77K are localized predominantly on the DNA bases [54-62].

There have been several studies of DNA constituents irradiated with ion beams [63-67]. A significant decrease in radical yields and new radical species were observed with increasing LET [63-66]. In 1994, Wang et al. [68] suggested the possible existence of sugar radicals in γ-irradiated hydrated DNA at elevated radiation doses. Free radicals located on the deoxyribose

moiety were the likely precursors to strand breaks. The C1' ·might result in an abasic site [69], and the C1' ; C3' ; C4' ·and C5' ·radicals might result in strand breaks [70]. Razskazovskii et al. [71] reported the first clear ESR spectrum of the C1' ·radical in a DNA double helix in 1998. In 2004, Sevilla and coworkers [72] reported that photoexcitation of previously stabilized guanine cation radicals, G^+ ·resulted in the formation of C1' ·radicals in double–stranded DNA at 77K. In 1996, Becker et al. [67] firstly identified the C3' ·(or C4' ·) radicals at 77K $^{16}O^{8+}$ ion-irradiated hydrated DNA. Subsequently, the C3' ·radicals were also reported by Weiland et al. [73], Debije et al. [74], and Becker et al. [75].

ESR studies also identified sugar-phosphate radicals [67, 75, 76]. Beck et. al identified a phosphate radical of the type $ROPO_2^-$ ·in hydrated DNA irradiated by $^{16}O^{8+}$ ion [67], argon–ion [75], and γ-ray [75]. They suggested that this result from P-O bond cleavage [75, 76]. The same group also identified a sugar moiety radical resulting from rupture of the C3'-O bond in hydrated DNA irradiated by argon–ion [75], and γ-ray [75]. These radicals are the direct products of strand breaks.

2.3.2. Caused by low energy free (kinetic) electrons (LEFEs)

An isolated molecule may dissociate and/or form a negative ion by interaction with a low energy free (kinetic) electron (LEFE). There are basically two mechanisms [77]: dipolar dissociation and dissociative attachment. For a diatomic molecule AB, these processes could be represented by following equations, respectively:

$$e + AB \rightarrow AB^* + e \rightarrow A^+ + B^- + e \quad \text{..... 2.1}$$

$$e + AB \rightarrow AB^{*-} \rightarrow A + B^- \quad \text{..... 2.2}$$

The first reaction (Eq. 2.1) proceeds via an excited state AB* and is called dipolar dissociation (DD); the second reaction (Eq. 2.2) proceeds via a transient vibrationally-excited anion AB^{*-} and is a resonance process called dissociative electron attachment (DEA). Depending on electron energy, electron can cause DNA damage through ionization, dipolar dissociation (DD), and dissociative electron attachment (DEA) processes. DEA occurs for free electrons at low kinetic energies of 0-20 eV [78-79].

Low energy secondary free (kinetic) electrons are produced in abundance in nearly all types of radiation tracks [12]. In the 1980s and 1990s, theoretical calculations suggested that energy deposition of > ~100 eV correlated with double strand break (DSB) yields [80-81] and such energy depositions in low LET irradiation arises mostly from low energy secondary electrons [81-83]. In 1997, by computational modelling and calculations, Nikjoo et. al [84] concluded that 90% of total energy depositions were due to events less than 60 eV, but the largest DSB yield was due to energy depositions in the range 60-150 eV for all three electron energies (300 eV, 1.5 keV, and 4.5 keV). They suggested that the DNA damage is due to the low energy secondary electrons. The same year, Botchway et. al. [85] used characteristic aluminum K (Al_K) (energy of 1.5 keV) and copper (Cu_L) (energy of ~0.96 keV) x-ray to study the effect of the numerous low energy secondary electrons produced by low LET ionizing radiation on DNA. They suggested that clustered damage such as DSBs was produced predominantly by low energy electron "track ends". It should be noted that in these theoretical and experimental studies, the electron solvation dynamics were not taken into account.

In 2000, Boudaiffa et al. [78] showed DNA strand breaks by low energy (3-20 eV) free (kinetic) electrons. They irradiated plasmid DNA under dry, ultrahigh vacuum (UHV) conditions with a low energy free (kinetic) electron (LEFE) gun, and found that dissociative electron attachment (DEA) of low energy (3-20 eV) free (kinetic) electrons can cause SSBs and DSBs of the dry DNA. It was found that under 15 eV, kinetic electrons with energies around 10 eV had the resonance in causing SSBs and DSBs. LEFEs with energies 3-5 eV, caused some SSBs, but no DSBs. In 2004, the same group studied DNA strand breaks induced by 0-4 eV free electrons [86]. They showed a higher yield of DNA SSBs at ~1 eV but no yields of DSBs induced by (0-4 eV) free electrons. In 2005-2006, Illenberger et al [87-88] reported experimental results for DEAs of near 0 eV electrons to gaseous DNA bases and the phosphate group. It was found that the compound undergoes DEA reaction within a low energy resonance feature at 1 eV and a further resonance peaking at 8 eV. They suggested that the direct effect of SSBs caused by LEFEs is due to DEA directly to the phosphate group.

On the theoretical point of view, Simons and co-workers [89] in 2002 reported the first theoretical studies of the effect of the DNA solvation in an aqueous environment on DEA-induced SSBs, proposing that SSBs can effectively occur via forming a (π^*) shape anion resonance at the DNA base after attachment of an access electron of ~1 eV if the DNA is solvated in water. In 2004-2006, the same group [90-91] suggested that it is highly unlikely that electrons having kinetic energies near 0 eV can attach directly to DNA's phosphate group's P=O π^* orbital, while electron kinetic energies in the 2-3 eV range attach directly to phosphate group's P=O π^* orbital. In 2006-2008, a number of groups [92-96] reported theoretical studies of DEAs of near 0 eV electrons to nucleotides in both the gas phase and aqueous solution. Generally, these theoretical studies were focused on the energetic stability of nucleotide anions

and gave rather controversial results [91-96]. For example, Simons and co-workers [91] suggested that DNA bases can attach electrons having kinetic energies even below 1 eV range and subsequently undergo phosphate-sugar O-C bond cleavage. They also suggested that electrons with kinetic energies in the 2-3 eV attach directly to the phosphate group, while electrons with energies near 0 eV are highly unlikely to attach to the phosphate group's P=O π^* orbital. Bao et. al [92] investigated LEFE attachment induced $C_{5'}$-$O_{5'}$ σ bond breaking of pyrimidine nucleotides (5'-dCMPH and 5'-dTMPH). Their calculated results indicated that the pyrimidine nucleotides are able to capture electrons around ~0 eV to form electronically stable anions in both the gas phase and aqueous solution. Sevilla and co-workers [95] calculated that the barrier height for adiabatic $C_{5'}$-$O_{5'}$ bond dissociation of 5'-dTMP anion radical in aqueous environment is substantially higher than in the gas phase such that it would not contribute to DNA strand cleavage in the aqueous system.

However, none of the above-mentioned experimental studies with (0-20 eV) free (kinetic) electrons were performed in aqueous solutions. These gas phase experimental results could not be applied to real biological systems, in which water constitutes a major component. The water environment is unlikely to enhance DEAs of molecules at free electron energies >1.0 eV. Indeed , Lu and Sanche [97-99] have observed that DEAs of molecules to free electrons with energies $\geqslant$ 1.0 eV, effective in the gas phase, are completely quenched when they are adsorbed on H_2O ice, while the DEA cross section at ~0 eV electrons are significantly enhanced by H_2O ice. The latter is due to a dissociative electron transfer (DET) mechanism, which will be discussed in later Chapters.

2.4. Indirect effect of DNA damage

As mentioned in Section .2.1, most of the ionizing radiation energy is absorbed by water. In the indirect effect, DNA is damaged by the radicals generated from the radiolysis of water.

2.4.1. Radiolysis of water

In radiation chemistry, G-values are defined as the number of molecules formed or lost per 100 electron volts of energy absorbed [49, 100].

G= (number of altered molecules) /100 eV.

G may also be expressed as 'molar concentration of altered entities per unit dose':

$$G = 9.64 \times 10^6 \frac{C}{D\rho}$$

where C is the molar concentration in M, D is the dose in Gy (J / kg), and ρ is the density of the medium in g/cm^3.

H_2O molecules can either be ionized or excited by ionizing radiation (Eqs. 2.3 and 2.4). In the ionization process, a water radical cation (H_2O^+) and an electron are generated (Eq. 2.3).

$H_2O \rightarrow H_2O^+ + e^-$ ……………………………… 2.3

$H_2O \rightarrow H_2O^*$ …………………………………… 2.4

The water radical cation (H_2O^+) is a strong acid. It reacts with another water molecule, forming an H_3O^+ and a OH· radical (Eq. 2.5). The electron reacts with surrounding water molecules, and becomes the solvated electron (Eq. 2.6)

$$H_2O^+ + H_2O \rightarrow H_3O^+ + OH\cdot \quad \text{..... 2.5}$$

$$e^- + n\,H_2O \rightarrow e_{solv}^- \quad \text{..... 2.6}$$

The excited water molecule can dissociate into either an H-atom and a ·OH radical or a water radical cation (H_2O^+) and an electron (Eq. 2.7):

$$H_2O^* \rightarrow H\cdot + OH\cdot \text{ or } H_2O^+ + e^- \quad \text{..... 2.7}$$

The free radicals(OH ; e_{solv}^- and H ·) either react with one another or diffuse into the bulk of the solution, reacting with anything that they encounter, producing H_2O, H_2O_2, molecular hydrogen and some other free radicals such as HO_2 (hydrogen peroxide) [12, 49, 100-101].

Since ionizing radiation deposits its energy non-selectively, essentially all the radiation energy is absorbed by water in $\leqslant$ 0.1 M aqueous solution [101]. In the conventional context of radiobiology, the free radicals of radiolysis of water are long known to be e_{solv}^-, ·OH, H·, H_2O_2 and H_2 [100-102]. Their quantum yields (G values) per 100 eV energy deposited were measured to be 2.8, 2.4, 0.6, 0.8, and 0.4 at 10^{-6} s after irradiation, respectively [100-102].

2.4.2. Reactions of free radicals with DNA

Free radicals (·OH, e_{solv}^-, H ·) can react with biological molecules and change them. The ·OH radical is a strongly oxidizing species [102-106], while e_{solv}^- and H ·radicals are reducing agents [61].

The highly reactive ·OH radical often abstracts carbon-bound hydrogen atoms more or less non-selectively [102, 106]. ·OH radicals can directly abstract H atoms from biomolecules, especially DNA. Moreover, ·OH radicals add to the unsaturated bonds of biomolecules [108-110], or further react with other radicals to form new reactive active radicals such as: O^-, O_2^-, HO_2 ·etc [106]. These reactions then result in molecular degradation or initiate damaging chain reaction processes.

e_{solv}^- reacts with DNA bases to form electron adducts [110-113]. The formed electron adducts undergo protonation reactions [110-113]. H ·radicals react with DNA to form H ·adduct radicals [110 and references therein].

2.5. Types of DNA damage induced by ionizing radiation

Ionizing radiation induces several types of DNA damage, including base damage, abasic sites, single-strand breaks (SSBs), double-strand breaks (DSBs), DNA-protein cross-links, DNA intra-/ inter- cross links, and multiply damage sites (MDS).

For base damage, at least thirteen modified bases were detected in calf thymus DNA irradiated by γ-rays [110]. Thymine glycol, cytosine glycol, 5-hydroxy-5-methyl-hydantoin, and 5,6-dihydrothymine are the major products for pyrimidines [114-116]. 8-oxo-guanine (8-oxo-Gua) and 8-oxo-adenine, and ring-ruptured species such as 2,6-diamino-4-hydroxyl-5-formamidopyrimidne (FAPyGua) and 4,6-diamino -5-formamidopyrimidine (FAPyAde) are the major products for purines [116-120]. Thymine glycol blocks DNA replication [110 and references therein]. 8-oxo-Gua directs misincorporation of adenine by DNA polymerase [121], and ring-ruptured DNA base blocks DNA synthesis [122].

When deoxyribose is damaged, abasic sites (as shown in Fig. 2.1) and deoxyribose fragments are formed [110]. The oxidized AP (apurinic / apyrimidinic site) lesions 2-deoxyribolactone (deoxyribonic acid) and 2-deoxypentose-4-ulose are produced in DNA by x-rays [102].

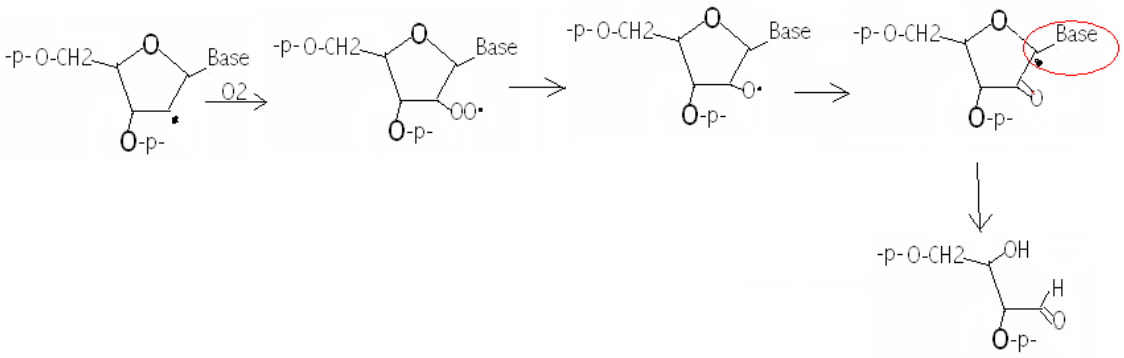

Figure 2.1 Reaction mechanism of base loss [110].

Damage to the deoxyribose-phosphate backbones may cause scission of the backbone and result in the breakage of DNA strands. Breakage of the bond between C3'-C4' or between C4'-C5' can produce a single strand break [110]. Single strand breaks can be easily and quickly repaired by intracellular enzymes [12, 49]. If the strand breaks occurred in two opposite DNA strands and are separated by only a few base pairs, this may lead to a DSB [123]. DSBs are believed to be the most important lesions produced in chromosomes by radiation [12, 49, 123]. The interaction of two DSBs may result in cell death, carcinogenesis, or mutation [12, 49, 123].

The DNA, protein free radicals generated by ionizing radiation can also react with each other to form DNA-protein cross links, DNA intra- / inter- cross links, as shown in Fig 2.2 [110]. DNA-protein cross-link can also be formed by adding a DNA radical to an aromatic amino acid of a protein, or by adding a protein radical to a DNA base [110].

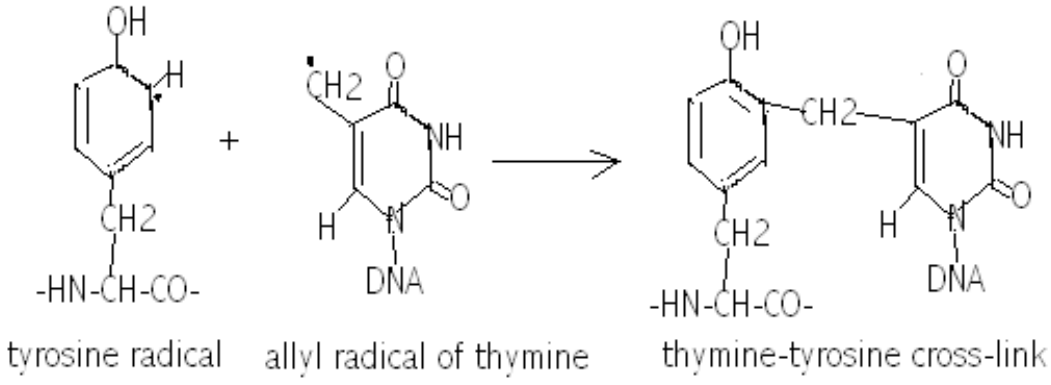

Figure 2.2. Formation of DNA-protein crosslink [65]

Numbers of early physical and biochemical changes for mammalian cells irradiated with 1Gy of low LET radiation are shown in Table 2.1 [12].

Table 2.1. DNA damage produced in one cell by 1Gy x-ray [12].

Damage	No. per cell
Damaged bases	1000-2000
Damaged sugars	1200
SSBs	1000
DSBs	40
Abasic sites	250
Cross-links	200-400

2.6. ·OH radical – mainly responsible for ionizing radiation induced DNA damage?

Cellular endpoints and strand breakage in cellular DNA can be manipulated by compounds that are known to be OH scavengers, such as isopropanol [124], t-butanol [125-126], and DMSO [127-128].Thus it was believed that OH radicals are predominantly responsible for the indirect effect of ionizing radiation induced DNA damage.

In 1967, Block et al. [129] firstly attributed inactivation of single-strand DNA of the bacteriophage ϕX174 to OH radicals. They observed the large increase of the 37% survival dose,

when ·OH radical scavenger --- iodide ions were added. From then on, different experiments were conducted and the results suggested that ·OH radicals were the major culprit for indirect effect of DNA damage. N_2O converts e_{solv}^- into ·OH radicals. It was found that DNA sample bubbled with N_2O increased the yield of DNA damage by a factor of 2 [129].The addition of alcohols (methanol, ethanol, t-butanol) protected DNA molecules of mammalian cells from radiation-induced single-strand breaks [125].

Since the above mentioned experiments showed that ·OH radical scavengers significantly decreased the amount of DNA damage [124-129], ·OH radicals were long thought to be mainly responsible for the indirect effect of DNA damage induced by ionizing radiation. However, it has also been observed that even very high concentrations of ·OH scavengers cannot completely quench the DNA damage, especially DSBs [124-131]. That 'nonscavengable' DNA damage (~30% SSB, and ~30-65% DSB) was therefore attributed to direct action of radiation in the DNA [124-131]. This assignment, however, conflicts with another important observation made by Ito et al. [132]. The experiments conducted by Ito et al. [132] were to gain knowledge of the dependence of the yield of DNA strand breaks induced by γ-rays on water content. Ito et al. [132] compared DNA damage induced by ^{60}Co γ-rays under three irradiation conditions, the DNA in a dry, humid and aqueous states. They found that water content plays a very critical role in the yields of DNA strand breaks induced by γ rays. The presence of water molecules enhances the yields of SSBs and DSBs by more than 10 fold in the humid state, and by over 1000 fold in the aqueous state. That is: DNA stand breaks in aqueous state = 100 fold DNA damage in humid state = 1000 fold DNA damage in dry state. In this experiment, only ~1% of DNA strand breaks were caused by the direct effect (DNA with hydrated water as an integral). Indirect effect contributes to ~99% of DNA strand breaks. If ·OH radicals play a dominant role in the indirect

effect, then, high concentration of ·OH scavenger should be able to scavenge ~99% of DNA strand breaks in aqueous solution, which is obviously contradictory to the fact that there is still 30-65% 'nonscavengable' DSBs, even when very high concentrations of ·OH scavengers up to 2M were used [12].

Moreover, it is worthwhile to note that the damage produced by ·OH radicals is similar to that produced during oxidative metabolism [133-135]. At the mean lethal dose of ionizing radiation for mammalian cells, the number of ·OH-induced DNA-damaged sites is low compared to the spontaneous background of about 10,000-150,000 oxidative DNA damaged sites per human cell per day [136-137]. In repair proficient cells, all DNA damage produced by ·OH radicals is removed [12, 49]. H_2O_2 is known to produce ·OH radicals by a Fenton-type reaction and it induces lesions in cells similar to those from ionizing radiation [12, 138]. It was found that SSBs introduced into the DNA of mammalian cells by the treatment of H_2O_2 at 0℃ cause no cell killing [138].

The above observed facts imply that there may be some important processes missing in the conventional understanding of radiation-induced DNA damage.

With the birth of femtosecond (fs) time-resolved laser spectroscopy, the solvation dynamics of free electrons in water has been studied at an unprecedented level. It has become clear that the electron is solvated through two major steps: before it becomes fully solvated electron (e_{solv}^-), the electron is located in a weakly bound pre-existing trap, and is called presolvated electron (e_{pre}^-) with a finite lifetime < 1 ps [139-142]. The processes can be expressed as:

$$e + nH_2O \rightarrow e_{pre}^- \rightarrow e_{solv}^-$$

Here, e_{pre}^- is a novel species, which was first experimentally observed in 1987 [139]. The G value of e_{pre}^- is nearly double that of its ending product e_{solv}^- [142]. The DNA damage caused by e_{pre}^- was not taken into account in current radiobiology. It is very likely that e_{pre}^- plays an important role in DNA damage induced by ionizing radiation, as will be addressed in later Chapters of this thesis.

2.7. Radiosensitizers

Radiotherapy is currently utilised in ~50% of patients with solid tumours at some stage of their treatment [143]. The most common ionizing radiation sources used in radiotherapy are low LET ionizing radiation (IR) sources such as x-rays and γ-rays, whose cytotoxicity results from their ability to induce DNA damage, particularly DNA double-strand-breaks (DSBs)due to the formation of free radicals within the cells [12, 49, 143]. Although refinements in IR fractionation have optimised dose delivery and new technology developments such as intensity-modulated and image-guided radiotherapy (IMRT and IGRT) have increased the precision of irradiation to the target tumour, there are still limitations in doses and effectiveness that cause failure in treatments [143]. This is linked to the fact that many tumours exhibit intrinsic or acquired resistance to ionizing radiation as part of the carcinogenic process or during the course of radiotherapy [144]. Therefore the use of radiosensitizers may overcome radioresistance and enhance the radiosensitivity of tumour cells. This has long been explored to enhance tumour control and

minimise the radiation toxicity toward healthy tissues through using lower radiation doses [144]. However, current radiosensitizers are still largely unsatisfactory, since existing radiosensitizing agents often cause a high rate of unacceptable treatment-related morbidity [144-145]. Therefore, continuing efforts in experimental and translational oncology research have been to identify more effective radiosensitizing agents [146-147].

A number of radiosensitizing agents with various modes of action have been developed. Table 2.2 [144] listed the traditional anticancer agents that are currently used in clinical trials. However, owing to their inherent cytotoxocity, these agents can cause normal tissue damage and ionizing radiation-related side effects when combined with radiotherapy. The derivatives of those compounds listed in Table 2.2 have been designed and developed [145-146], with the hope to improve their therapeutic effects and to avoid the side effects. However, few of those compounds have been used in clinical treatments [145-146].

Table 2.2. Mechanisms of cytotoxicity and radiosensitization of anticancer drugs as radiosensitizers [144].

Compound	Cytotoxicity	Radiosensitization
5-Fluorouracil	Inhibition of thymidylate synthase, incorporation into DNA and inhibition of RNA maturation [147]	Inhibition of the repair of IR-induced DSBs and impairment of cell cycle checkpoints.
IdU BrdU	Inhibition of ribonucleotide reductase and incorporation into DNA [147]	Augmentation of IR-induced DSBs and inhibition of their reapir
TAS-106	Inhibition of thymidylate synthase and RNA synthesis [148]	Abrogation of G2/M checkpoint, enhancement of IR-induced tumor cell apoptosis associated with an inhibition of the expression of HIF-1α and of the antiapoptotic protein, surviving.
Gemcitabine	Depletion of deoxynucleoside triphosphates resulting in DNA polymerase and ribonucleotide reductase inhibition [147].	Induction of nucleotide misincorporation during DNA replication that augments cell death following IR. Enhanced by mismatch repair deficiency.
Clofarabine	Inhibition of DNA polymerases and ribonucleotide reductase and incorporation into DNA [149]	Inhibition of the repair of IR-induced DSBs at low doses and induction of DSBs at high doses.
3-AP (Triapine)	Inhibition of ribonucleotide reductase in blockade of DNA synthesis and repair [147, 150]	Inhibition of the repair of IR-induced DSBs
Temozolomide	Methylation of guanine at O6 position resulting in DNA mismatch pairing, DNA strand breakage and cell death [151]	Inhibition of the repair of IR-induced DSBs leading to increased mitotic catastrophe
Platinum analogues	Covalent binding to purine DNA bases causing interstrand and intrastrand crosslink [152]	Inhibition of the repair of IR-induced DNA damage, induction of apoptosis and formation of IR-induced toxic platinum intermediates
Camptothecin analoguues	Inhibition of topoisomarase I, resulting in irreversible DNA DSBs [153]	Worsening of IR-induced DNA lesions and inhibition of their repair.
Taxanes, epothilones	Stabilisation of microtubules through tubulin binding resulting in cell cycle arrest in G2-M and cell death [144, 154]	Synchronisation of tumour cells in G2-M at a point of maximum radiosensitivity

As mentioned in Chapter 1 (Section 1.1.4), the hypoxia of tumor microenvironment can seriously affect the outcome of radiotherapy. Hypoxic cells are 2~3 times more resistant to killing by ionizing radiation than normal oxic cells, largely due to the lower yield of DNA-damaging oxygen radicals [155-161]. Overall, similar to case in photodynamic therapy, the hypoxia of solid tumours represents a major cause of treatment failure in radiotherapy [155-156]. Over the past decades, several strategies have been explored to overcome the problem of radioresistance associated with tumour hypoxia [146, 155-156, 162]. These include strategies to improve tumour oxygenation during radiotherapy [145-146, 162], to target hypoxia-inducible factor (HIF)-1, a transcription factor that promotes the survival of hypoxic tumour cells [163-166], and to target hypoxic tumor cells. The latter strategy involves the development of hypoxic radiosensitizers [146, 155, 162, 167], which consist mainly of two types: oxygen-mimicking hypoxic sensitizers and hypoxic cytotoxins (bioreductive radiosensitizers) [12, 123].

For hypoxic sensitizers, the strategy is to develop drugs that have similar properties to oxygen as a radiosensitizer [12]. This strategy is based on the idea that oxygen shows the radiosensitization because of its electron affinity and that other molecules with large electron affinities might show similar radiosensitizing properties. Some molecules from the classes of halopyrimidines [168-177] and nitromidazoles [178-180] have been observed to show some radiosensitization to hypoxic cancer cells in both cell line and animal experiments. Halopyrimidines, expecially bromodeoxyuridine (BrdU) and iododeoxyuridine (IdU), have passed phase I to Phase II clinical trials, but a very limited radiosensitivity enhancement was observed in phase III clinical trials [181-183] and no clinical uses of halopyrimidines as

radiosensitizers have been approved. For nitromidazole compounds, misonidazole has been tested in many studies, which showed a preferential killing of hypoxic cells *in vitro* in a dose-dependent manner [12, 184]. The *in vivo* results of misonidazole showed a good correlation with the *in vitro* results at high acute radiation doses [184], whereas the radiosensitivity enhancement was decreased when misonidazole was used in combination with fractionated radiation doses [185]. Many nitromidazoles have also been studied, and 9 such compounds have been tested in clinical trials [146, 186]. However, the overall results from the clinical trials have not been as good as expected [123], and the trials with less toxic drugs such as etanidazole [187-188] and nimorazole [189-190] showed some inconsistent results. So far, only 5-nitroimidazole has been used with some success for radiotherapy of head and neck cancers in Denmark [162].

For hypoxic cytotoxins, the strategy is to develop bioreductive drugs that utilize tumor hypoxia as a therapeutic advantage and target hypoxic cancer cells specifically [12, 123]. Among bioreductive drugs of current clinical interest, the leading agent is tirapazamine (TPZ) [123, 191]. Under hypoxia, TPZ is preferentially cytotoxic to hypoxic cells in the tumor because its one-electron reduction leads to the formation of a radical which can cause DNA strand breaks and kill the hypoxic cells. For oxygenated cells, in contrast, the reactive radical can be oxidized back. TPZ has also been tested in combination with cisplatin (an effective but toxic chemotherapeutic drug) to enhance its treatment efficiency [123, 192]. TPZ was evaluated in clinical trials and showed some effectiveness, for example, in treating non-small-cell lung carcinoma and advanced head and neck cancers by combination with radiotherapy and cisplatin [12, 193-194]. However, the *in vivo* test of TPZ in mouse tumor models also showed a significant increase in toxicity to normal tissues [165, 195]. Efforts have been made to improve

therapeutic properties of TPZ by making its analogues [196]. Another type of bioreductive drugs is represented by nitrobenzindoles [197]. But the radiosensitizing activity of these compounds in tumors was not reported. Currently, for bioreductive drugs targeting at tumor hypoxia, PR-104 [198-199], AQ4N [167], and EO9 [145] are still under clinical trials.

Although various strategies and types of compounds have been designed and developed as potential radiosensitizers, none of them have been approved for clinical use, except for 5-nitroimidazole, which is used for radiotherapy of head and neck cancers in Denmark [162]. In spite of great efforts and resources invested in developing effective radiosensitizers in the world wide, clinical results have been unsatisfactory. The radiosensitizing effects of these compounds either were found accidentally, such as cisplatin and BrdU, or were designed based on some biological results. What chemicals reaction do those compounds undergo and what triggers the chemical reactions under ionizing radiation remains essentially unknown. For example, many radiosensitizers, whether hypoxic sensitizers or hypoxic cytotoxins, were designed on the basis of the intrinsic effect of oxygen in radiotherapy, while the widely accepted mechanism for the function of oxygen is the oxygen-fixation hypothesis (OFH) that was proposed in the early 1950s. At that time little was known about the basis of molecular biology. The OFH explains that the function of oxygen is to stabilize DNA damage induced by free radicals generated during ionizing radiation. However, the OFH is not a totally successful explanation of O_2 as a radiosensitizer [12, 123]. As a matter of fact, the molecular mechanisms of action of most radiosensitizers including cisplatin in clinical trials or use are unknown or not well understood. This is probably a typical problem in modern drug discovery and development. The identification of successful anticancer agents remains a somewhat empirical process [200]. Without a specific mechanistic understanding, it is difficult to learn from the success and failure

of the therapies and existing anticancer drugs [200]. The compelling need is for a more fundamental, mechanistic understanding of human cancers and anticancer drugs to design more appropriate drugs.

2.8. Major objectives of this thesis

(1) In this chapter, DNA damage caused by ionizing radiation has been reviewed. The role of ·OH as the major culprit for ionizing radiation induced DNA damage is questionable. We speculate that the prehydrated electron (e_{pre}^-) may play an important role in causing DNA damage. *The first goal of this thesis is to investigate the possible effect of* e_{pre}^- *on ionizing-radiation induced DNA damage.*

(2) Halopyrimidines, especially bromodeoxyuridine (BrdU) and iododeoxyuridine (IdU), have been explored as important hypoxic radiosensitizers in Phase I to III clinical trials, but their precise molecular mechanism of action is unknown. In particular, an important characteristic of BrdU and IdU as photo- or radio-sensitizers is that their radio-/photo-sensitivity depend on the DNA sequence [125-126]. They will cause the most significant DNA damage when they are adjacent to the adenine base (i.e. 5'-dABrdU). Currently proposed mechanisms in the literature could not explain this phenomenon well. I have studied the reaction mechanism of BrdU/IdU with e_{pre}^- produced by 2 UV photon excitation of water in my M.Sc study [201], which will be outlined in Chapter 4. *The second goal of this thesis is to continue my study in revealing the precise molecular mechanisms of BrdU and IdU as potential hypoxic*

radiosensitizers and particularly of the DNA sequence selectivity in their radiosensitivity, using our state-of-the-art femtosecond time-resolved (pump-probe) laser spectroscopy.

(3) Modern drug discovery and development prove to be an inefficient and expensive process. We present an innovative molecular-mechanism based drug discovery project to develop novel drugs for effective radiotherapy of cancer. Based on our unique understanding of the molecular mechanisms of the role of e_{pre}^- in ionizing-radiation induced DNA damage and of halopyrimidines as hypoxic radiosensitizers, *the third goal of this thesis is to develop new radiosensitizers that could have better radiosensitivity enhancement than BrdU and IdU.*

Chapter 3
Experimental Methodology

3.1. Femtochemistry, Femtobiology and Femtomedicine

3.1.1. Elementary chemical reaction and transition state

A chemical reaction is a process that results in the transformation of one set of chemical substances to another. Classically, a chemical reaction involves changes associated with the motion of electrons in forming and breaking of chemical bonds between atoms, and can often be described by a chemical equation. A chemical reaction is often composed of a sequence of multiple sub-steps, the so-called elementary reactions. An elementary reaction is the smallest step in a chemical reaction and has no intermediate products. In theories describing elementary reactions, it is usually assumed that there is *a transition state* through which an assembly of atoms in the reactants must pass on going from reactants to products [202]. As shown in Fig. 3.1, the transition state of a chemical reaction is a particular configuration along the reaction coordinate, and is defined as the state corresponding to the highest energy along this reaction coordinate. A molecular reaction mechanism is the step by step sequence of elementary reactions [202-204].

By definition, the species in the transition state is neither a reactant nor a product. It has more free energy than the reactants or products, and therefore is the least stable state. The transition states determine how the chemical reaction happens, that is, how the chemical bonds are broken or formed during the reaction.

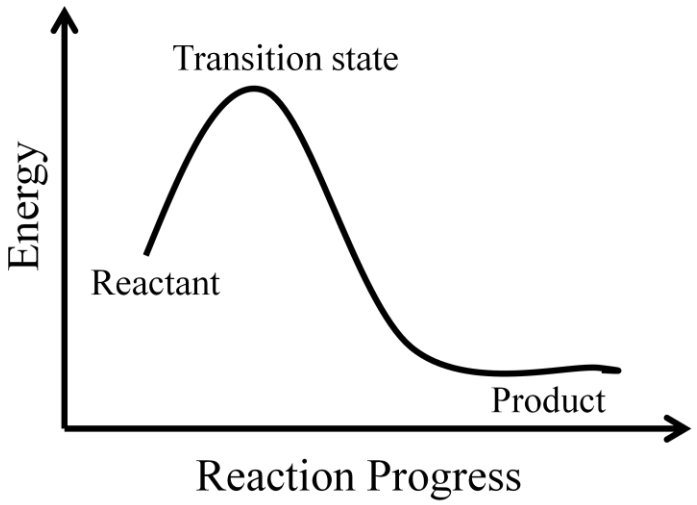

Figure 3.1. Reaction coordinate of an elementary chemical reaction

The transition state theory (TST) was developed slowly through various approaches. The earliest one is the thermodynamic treatment. In 1884, Jacobus van't Hoff (the first Nobel laureate in Chemistry, 1901) proposed the Van't Hoff equation describing the temperature dependence of the equilibrium constant for a reversible reaction (A⇌B) [205]:

$$\frac{d \ln K}{dT} = \frac{\Delta U}{RT^2},$$

where ΔU is the change in internal energy, K is the equilibrium constant of the reaction, R is the universal gas constant, and T is the thermodynamic temperature. Then in 1889, based on experimental work, Svante Arrhenius (Nobel laureate in Chemistry 1903) proposed a similar expression for the reaction rate constant, integration of which leads to the well-known Arrhenius equation [206]:

$$\text{reaction rate constant} \quad k = Ae^{\frac{-E_a}{RT}},$$

where A is the pre-exponential coefficient and E_a is the activation energy.

By the early 20th century, many researchers had accepted the Arrhenius equation, which was widely used to determine energies for the reaction barriers. But the Arrhenius equation was derived from empirical observations and ignored any mechanistic considerations, such as whether one or more reactive intermediates are involved in the reaction converting a reactant into a product [205]. Therefore, further development was obviously required to understand the two parameters associated with this law, the pre-exponential factor (*A*) and the activation energy (E_a). This led to different theories of how chemical reactions occur, including kinetic theory treating reacting molecules as hard spheres colliding with one another and neglecting entropy changes and statistical-mechanical treatment [205]. The latter played a significant role in the development of TST, concluding that the activation energy of a reaction is equal to the average energy of all molecules undergoing reaction minus the average energy of all reactant molecules [205].

However, the concept of potential energy surface played a very important role in the development of TST. The foundation of this concept was laid by Marcelin, who proposed that the progress of a chemical reaction could be described as a point in a potential energy surface

with coordinates in atomic momenta and distances [207]. Then, the most important contributions were made by Henry Eyring and by Meredith Gwynne Evans and Michael Polanyi simultaneously in 1935 [208]. These led to the Eyring equation, successfully addressing the two parameters (A and E_a) [208]. The now called TST was therefore developed, which is also referred to as 'activated-complex theory', or 'theory of absolute reaction rates'. The theory essentially assumed that the transition state was crossed very rapidly, on the time scale that applies to molecular vibrations (on the time scales of 10^{-15} seconds) [208]. No one ever dreamed of possible experimental observations of the transition state in such short time scales [209].

3.1.2. First direct observation of the transition state —the Birth of Femtochemistry

But that was what exactly made by Dr. Ahmed Zewail at Caltechin in his pioneering experiments using femtosecond ($1fs=10^{-15}$ s) laser spectroscopy [210-211]. At the end of the 1980s, Dr. Zewail performed a series of experiments using flashes of laser light that last for femtoseconds, which led to the birth of the research field now called *femtochemistry.* Femtochemistry is the branch of physical chemistry that involves the study of chemical reactions on extremely short timescales, approximately 10^{-15} seconds. The steps in chemical reactions typically occur in the timescales of femtoseconds to picoseconds and sometimes form intermediate products. These intermediate products cannot always be deduced from observing the reactants and the products. With time-resolved (pump-probe) femtosecond spectroscopic techniques, it was the first time to observe in real time (by analogy to 'slow motion' in TV shows) what happens as the reaction barrier is crossed over by reactants during a chemical reaction and

therefore to obtain a mechanistic understanding of Arrhenius' formula for the temperature dependence of the reaction rate constant. Overall, femtochemistry allows real-time studies of the molecular mechanisms of chemical reactions in an unprecedented level. Dr. Zewail was therefore awarded the Nobel Prize in Chemistry in 1999 '*for his studies of the transition states of chemical reactions using femtosecond spectroscopy*' [211].

3.1.3. From femtochemistry and femtobiology to femtomedicine

Parallel with the development of femtochemistry, *femtobiology* was initially developed to study ultrafast elementary processes often occurring on the picosecond (ps) timescale (from a few to tens or hundreds of ps) in biological systems [212]. Both fields of femtochemistry and femtobiology have been well developed in the past 25 years. Recently, Dr. Lu further proposed a new approach which aims to integrate ultrafast spectroscopy and imaging techniques with biomedical methods for the study of initial biological processes occurring on the timescale of femtoseconds that are closely linked to diseases and their treatments. This new strategy may lead to the opening of a new frontier called *femtomedicine* [213]. It is generally believed that many biological processes such as DNA damage and cell death are rather slow processes that could occur in the time scales of microseconds or longer. As mentioned in the above, however, chemical reactions (e.g., for production of reactive radicals) that initiate these biological effects often occur in the time scales from femtoseconds to picoseconds [210]. Thus, biological events occurring at slow processes may be regulated by initial processes occurring in ultra-short time scales. It is therefore of significance to use ultrafast physical techniques to study initial

biochemical reactions so that one may obtain a complete picture of relevant biological processes. For instance, femtomedicine may be able to provide a new-level understanding of slower biological effects such as DNA damage, cancer initiation and cancer cell death, and may therefore lead to major advances in the therapy of cancer [213].

Through a series of successful studies [214-221], Dr. Lu's team has demonstrated the high potential of femtomedicine to bring breakthroughs in understanding the fundamental processes regulating biological function and in improving the therapeutic efficacy of diseases such as cancer. For example, the femtomedicine studies has led to the findings of the molecular mechanisms of action of cisplatin as the most widely-used anticancer drug for combination with radiotherapy [214] and for (mono) chemotherapy [215] and halopyrimidines as potential sensitizers for radiotherapy of cancer [216-218, see also Chapters 4 and 7], a new molecular mechanism of reductive DNA damage [219, 220, see also Chapter 6] and the development of more effective therapies of various types of human cancers including ovarian, cervical and lung cancers [221]. This is the exciting opportunity afforded through real-time femtosecond spectroscopic observation of biochemical reactions at the molecular level.

3.2. Pump-probe femtosecond laser spectroscopy

3.2.1. Basic principle

Femtosecond (fs) time-resolved (pump-probe) laser absorption spectroscopy (fs-TRLS) is a very powerful technique to study molecular reactions. The basic principle of the femtosecond laser spectroscopy appears to be simple and straightforward. A schematic diagram to illustrate the principle of a time-resolved fs laser spectroscopy is shown in Fig. 3.2. First, a pump pulse is used to initiate the reaction; at a certain time delay after the pump pulse, a probe pulse is used to detect the reaction transition state, intermediate, or reaction generated radicals. It is like an ultrafast camera taking a picture of the system at a time. By successively delaying the probe pulse with respect to the pump pulse, a 'film' is obtained of the course of the reaction. The reacting molecules or new species are observed by measuring certain characteristic properties, e.g., an optical transmission. The transition species detected at chosen wavelengths have specific spectra that serve as fingerprints, and they can therefore be identified and characterized. Under this condition, the molecular reaction pathway leading to the formation of the radical R· is directly observed in real time. For example, if we probe at the absorption wavelength of the excited state ICG*, the formation and decay of ICG* is real-time observed, as shown in Fig. 3.3. Therefore, the reaction of the transition species ICG* with another molecule (e.g., oxygen) can be observed and the reaction efficiency can be determined.

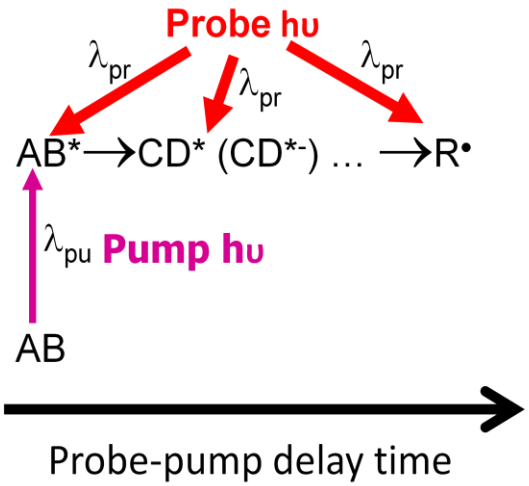

Figure 3.2. Basic principle of pump-probe fs laser spectroscopy

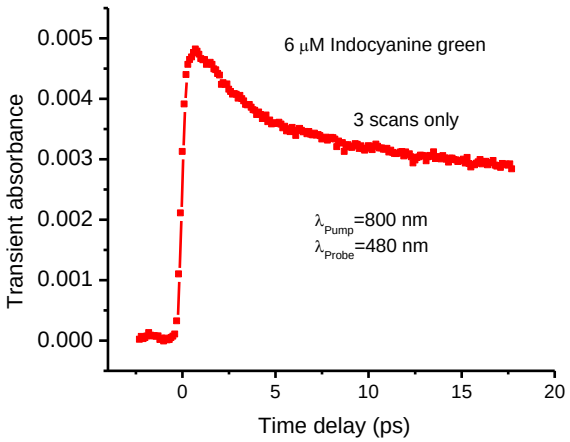

Figure 3.3. High-sensitivity femtosecond time-resolved laser transient absorption kinetic trace of an excited state of a photosensitizer, where the pump and probe pulse energies are only 12 and 0.2 nanojoule (nJ), respectively.

3.2.2. Experimental Setup

Dr. Lu has successfully home built a high-sensitivity time-resolved fs laser spectroscopy laboratory in the Department of Physics of the University of Waterloo. As shown in Fig. 3.4, in this technique, an ultrafast laser is used to generate a femtosecond width 800 nm laser pulse. This laser pulse is split out into two pulses, one as a pump pulse and the other as a probe pulse. Both laser pulses are sent to nonlinear optical devices, such as optical parametric amplifiers (OPA) to obtain the desired wavelengths. In our lab, the time-resolved fs laser spectroscopy used a Ti: sapphire laser system producing 100~120 fs, 1 mJ laser pulses centered at λ=800 nm at a repetition rate of 1 kHz. The two optical parametric amplifiers (OPAs) offer a wide wavelength extension from ultraviolet (UV) (≥266 nm) to near infrared (NIR) for pump and probe pulses. The polarization of pump and probe pulses was set at the magic angle (54.7 °) to avoid contribution from polarization anisotropy due to orientation motions of molecules.

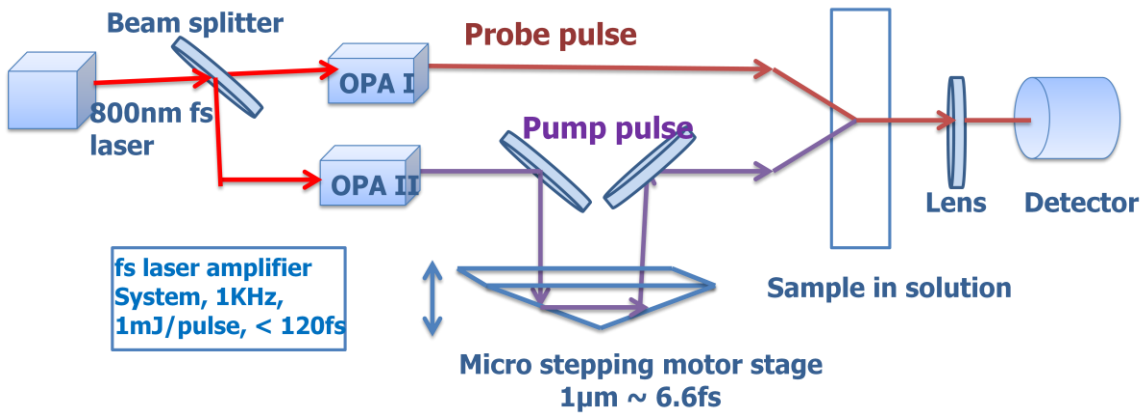

Figure 3.4. Schematic diagram of pump-probe absorption spectroscopy

The time delay between the pump and the probe pulses is controlled by a precise microstepping motor stage, and time resolution in fs can therefore be achieved with the use of fs laser pulses. Changing the microstepping motor stage by 1 μm, the time delay between the probe and pump pulses will be changed by 6.67 fs.

$$\nabla t = \frac{\nabla S}{c} = \frac{2 \times 10^{-6}\ \mathrm{m}}{3 \times 10^{8}\ \mathrm{m/s}} = 6.67 \times 10^{-15}\ \mathrm{s} = 6.67\ \mathrm{fs}$$

The detectors recording the spectrum and the motion controller are integrated into a computer program that directly gives rise to a transient absorption or fluorescence spectrum (as a function of delay time or wavelength) to show the real-time evolution of a particular transition state. Once intermediate species are identified, the reaction pathway can be determined.

In femtosecond pump-probe laser spectroscopy experiments, to obtain an extremely high signal to noise ratio is not only required but a challenging task for biological studies. This is because that even a moderate-energy 100 fs laser pulse at 5 μJ/pulse, its peak power is very high (~5×10^{7} W). This will inevitably cause instant damage to the sample and generate non-linear artificial effects, disabling the capability of the spectroscopy to observe the true reaction of the intact biological molecule. Typically, pump pulse energies smaller than 0.1 μJ/pulse (≤100 nJ/pulse) are required for reliable biological experiments. Under this condition, to observe a sufficient intensity of the detected *transient* signal will require extremely high detection efficiency with a very high signal to noise ratio. For instance, it should be able to detect a transient absorbance signal as low as 1×10^{-4} (a.u.), in comparison with the typical absorbance

of 1.0-2.0 measured with a commercial spectrophotometer. As shown in Fig. 3.3, fortunately, this capability has been typically achievable in Dr. Lu's home-built fs-TRLS.

To determine the precise formation and decay lifetimes of a transition-state species, the instrument response function must be taken into account to fit the obtained transient absorption kinetic trace. The time-dependent transient absorption signal is given by a number of exponential functions [222]. These exponential terms are convoluted with the instrument response function repressed by a Gaussian function $G(t) = (1/\sqrt{2\pi}\sigma)\exp(-t^2/2\sigma^2)$, where σ is the standard deviation for the Gaussian and is related to the FWHM (Full Width at Half Maximum) of the pump-probe cross-correlation function by $\sigma = FWHM/2\sqrt{2\ln 2}$ [222]. The resulting time-dependent signal S(t) is given by

$$S(t) = \sum_{i=1}^{n} c_2 \int_{-\infty}^{t} G(t')\exp(-\frac{t-t'}{\tau_i})dt' \qquad \text{..... 3.1 [222]}$$

where negative (positive) c_i is the amplitude of the component i with rising (decay) time τ_i. Eq. (3.1) can be solved analytically to give the following equation:

$$S(t) = \sum_{i=1}^{n} c_i \frac{1}{2}\exp(\frac{\sigma^2}{2\tau_i^2} - \frac{t}{\tau_i}) \times [1 - erf(\frac{1}{\sqrt{2}}(\frac{\sigma}{\tau_i} - \frac{t}{\sigma}))] \qquad \text{..... 3.2 [222]}$$

where erf is the error function. The best fits to the experimental data were obtained by using a least-square fitting program.

3.3. DNA gel electrophoresis

DNA gel electrophoresis is an important analytical tool in biology. It can easily separate DNA fragments by their sizes and visualize them. It is a commonly used diagnostic tool in molecular biology labs. The typical setup of DNA gel electrophoresis is shown in Fig. 3.5 [223].

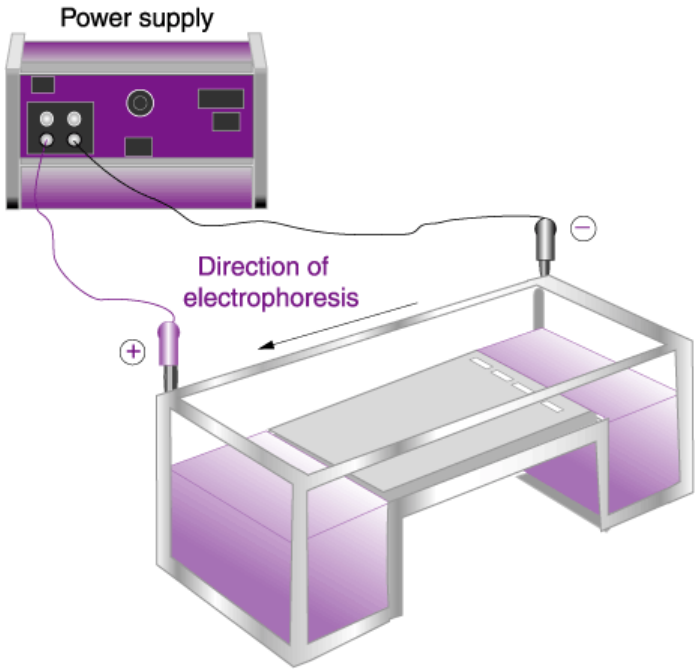

Figure 3.5. Typical setup of DNA gel electrophoresis [223].

At neutral PH, DNA is negatively charged due to its phosphate backbone. When an electrical potential is applied onto DNA molecules, they will move toward the positive electrodes, as shown in Fig. 3.6.

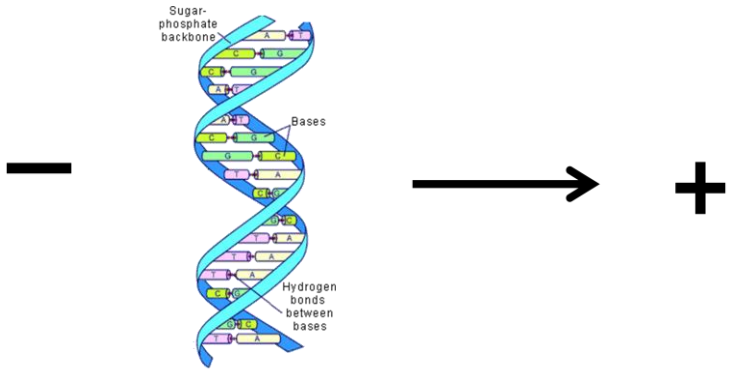

Figure 3.6. A diagram showing the movement of DNA under electrical potential

In this thesis, the agarose gel is made by adding 1% agarose into 1×TAE (Tris-acetate-EDTA) buffer. The agarose forms a porous lattice in the buffer solution. DNA molecules must pass through the holes to move toward the positive electrode. In a same agarose gel, the moving rate of DNA is determined by its electric charge, conformation, and size. The migration rate of DNA fragments V could be quantified by the following equations [224]:

$$V = Ez/f \quad \ldots\ldots\ldots\ldots\ldots\ldots\ldots\ldots\ldots\ldots\ldots\ldots\ldots\ldots\ldots\ldots \quad 3.3$$

$$f = 6\pi\eta r \quad \ldots\ldots\ldots\ldots\ldots\ldots\ldots\ldots\ldots\ldots\ldots\ldots\ldots\ldots\ldots\ldots\ldots\ldots \quad 3.4$$

where V is the migration rate, E is the electric field strength, f is the friction force, η is the viscosity of the gel, and r is the radius of DNA molecule.

For the same conformation, smaller DNA molecules move faster than larger ones. Therefore, a mixture of different sizes of DNA molecules of same conformation can be separated by their sizes.

If supercoiled circular DNA is SSB damaged, its conformation changes to nicked circular. The mass is still the same, but the volume becomes larger, thus the moving rate of SSB DNA is slower than that of its undamaged supercoiled form. If supercoiled circular DNA is DSB damaged, its conformation changes to linear. Typically, the rate of linear DNA migration is slower than that of its supercoiled form, but faster than its circular form. The moving rate of different conformations of the same DNA is in the order of: supersoiled (undamaged) > Linear (DSB) > circular (SSB).

DNA fragments are visualized by staining with ethidium bromide when they migrate enough. Ethidium bromide intercalates between DNA bases and emits fluorescence under the exposure of UV light.

In this PhD project, we use the plasmid DNA (Pgem 3Zf(-), 3197kbp) extracted from Escherichia coli JM109 to test the radiosensitizing effects of some compounds. The undamaged DNA is supercoiled circular DNA. Our treatments to the DNA cause single strand breaks (SSBs) and double strand breaks (DSBs), which are nicked circle and linearized form respectively. The images we will get will be similar to the one shown in Fig. 3.7. The undamaged supercoiled circular DNA moves the fastest and moves farthest from the loading well, followed by DSBs and SSBs.

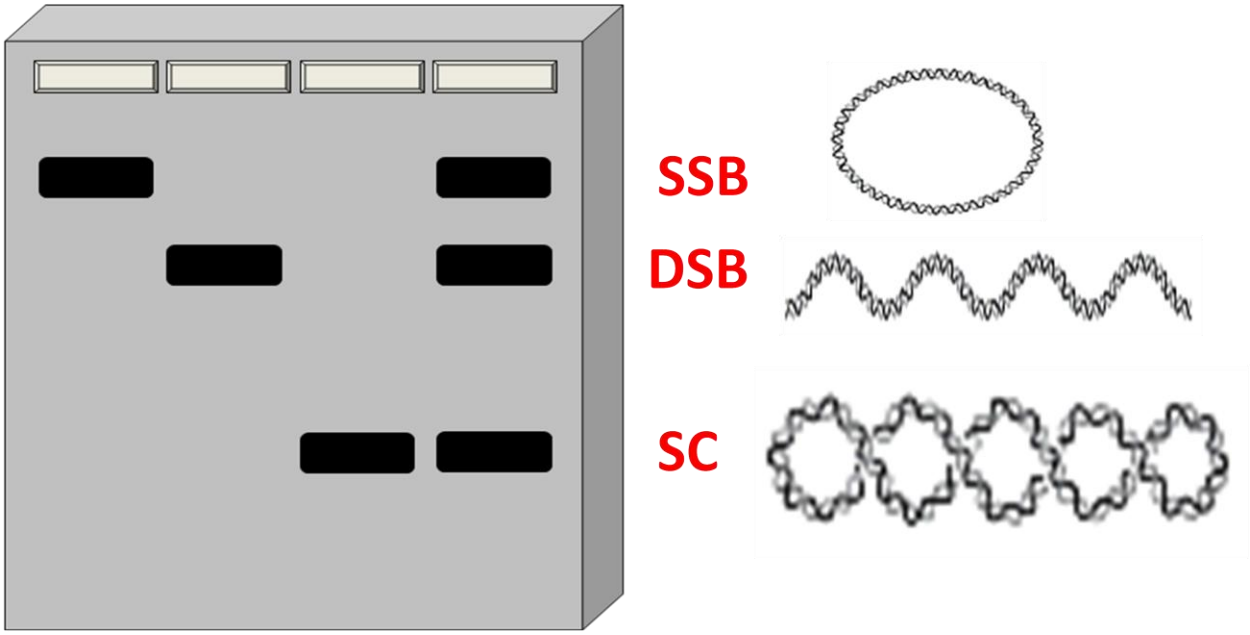

Figure 3.7. DNA gel images of SSB, DSB and SC from the same DNA.

3.4. MTT assay

MTT (3-(4,5-Dimethylthiazol-2-yl)-2,5-diphenyltetrazolium bromide) assay is usually used to assess the viability and the proliferation of cells. This method can be used to test the cytotxicity of potential medicinal agents since these agents influence cell viability and proliferation.

The full name of MTT is 3-(4,5-dimethylthiazol-2-yl)-2,5-diphenyltetrazolium bromide. It is a yellow tetrazole. It is reduced to purple formazon in living cells by mitochondrial reductase, as shown in Fig. 3.8 [225]. The insoluble purple formazon is dissolved by a solubilization solution, such as DMSO or a solution of the detergent sodium dodecyl sulfate (SDS) in diluted hydrochloric acid, to form a colored solution. The absorbance of this colored solution is measured at a certain wavelength (usually in the range of 500 to 600 nm) by a spectrophotometer, as shown in Fig. 3.9 (picture taken in our lab). If DMSO is used as a solvent, absorbance wavelength 540 nm will be used, while 570 nm will be used if SDS is the solvent.

For the same cell type, the absorbance shows a linear relationship on the survived cell numbers. As shown in Fig. 3.10, the absorbance is linear dependent on the number of HeLa cells grown in our lab. In the MTT experimental results, higher absorbance means that there are more survived cells.

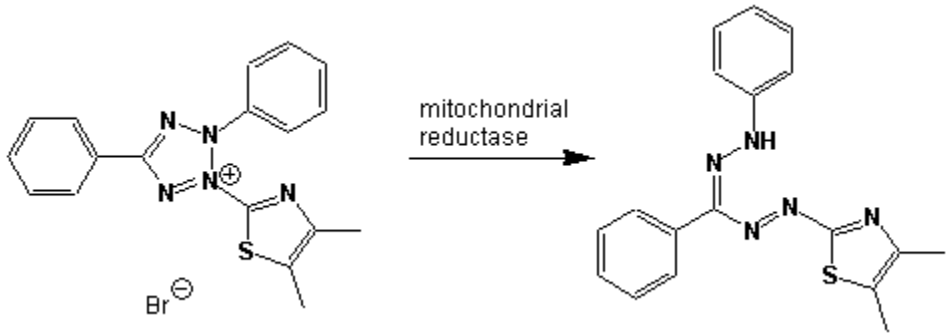

Figure 3.8. MTT is reduced by mitochondrial reductase [225].

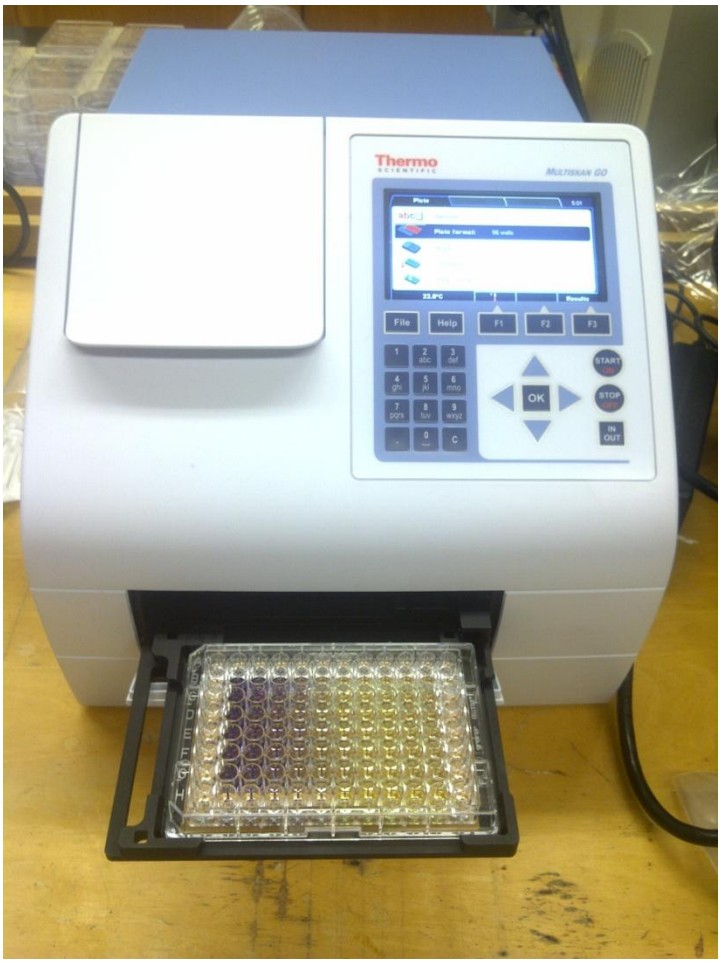

Figure 3.9. Use of microplate reader (@PHYS337, University of Waterloo) to measure the absorbance of cells treated with MTT.

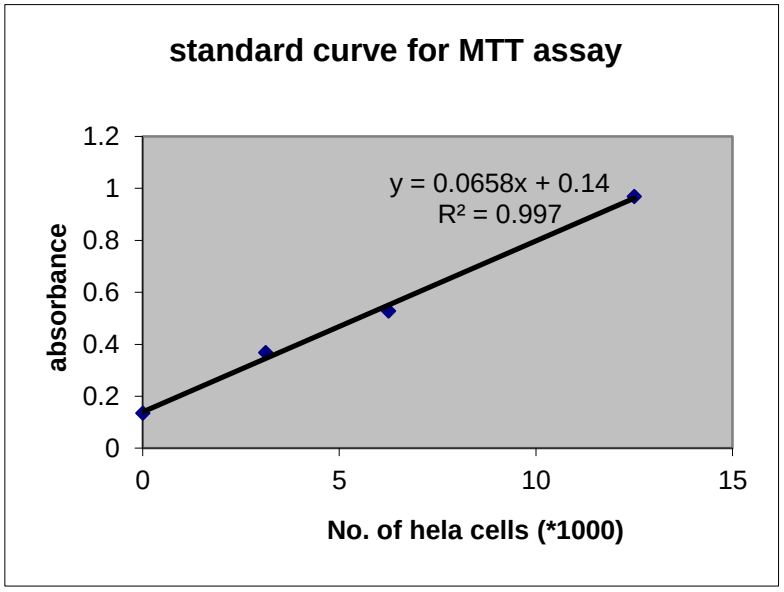

Figure 3.10. Absorbance measured in MTT assay shows a linear dependence on HeLa cell numbers.

Chapter 4

Prehydrated Electrons and Molecular Reaction Mechanism of Halopyrimidines as Potential Radiosensitizers

Replacement of thymidine in DNA by halopyrimidines such as bromodeoxyuridine (BrdU) and iododeoxyuridine (IdU) has been known to enhance DNA damage and cell death induced by ionizing radiolysis [168-169, 171, 174, 226-228] and UV photolysis [229-235] since the 1960s. Identified as potential sensitizers for radiotherapy of cancer, BrdU and IdU have been tested in several Phase I - Phase III clinical trials [181-183]. Generally, however, the clinical results have been unsatisfactory and therefore neither BrdU nor IdU have been approved for clinical use. This is probably related to the fact that the precise molecular mechanism of BrdU and IdU as potential hypoxic radiosensitizers is not well understood. In this Chapter, our state-of-the-art fs time-resolved laser spectroscopic studies will unravel the molecular mechanism of action of BrdU and IdU in liquid water under ionizing radiation. A dissociative electron-transfer (DET) reaction mechanism of BrdU/IdU with *the prehydrated electron (*e_{pre}^-) is discovered. Furthermore, we show that the e_{pre}^- states are electronically excited states and have lifetimes of ~180 and 540 fs. Our results demonstrate that *e_{pre}^-, a novel species of electrons produced in radiolysis of water, is a fascinating species due to its fundamental importance in chemistry, biology and environment*.

4.1. Electron solvation (hydration) dynamics

There has been long and continued interest in studying the solvation dynamics and reactivity of excess electrons in liquid water [107, 139-142, 236-245]. First discovered in the 1960s [236], the hydrated electron (e_{hyd}^-) is a well-known species produced by radiolysis of water under ionizing radiation and its reactivity with various molecules has been well determined [107]. Since the advent of femtosecond (fs) (1fs=10^{-15} s) time-resolved laser spectroscopy (fs-TRLS), the precursor to e_{hyd}^- (denoted e_{pre}^-) has been directly observed [139-142, 240]. Below is a brief introduction to electron hydration dynamics.

4.1.1. The solvated (hydrated) electron

4.1.1.1. What is solvation?

Interactions of molecular entities with surroundings in the liquid or solid state are generally regarded as ***solvation phenomena***. 'Solvation' represents the phenomenon of interaction of a solute particle with the host solvent. Solvation results in stabilization of the solute species in the solution [237].

Polar solvents like water are those with molecular structures that contain dipoles. They can solvate ions because they orient the appropriate partially –charged portion of the molecule towards the ion due to electrostatic attraction. This stabilizes the system and creates a solvation

shell. Water is the most common and well-studied polar solvent, but others exist, such as ammonia and ethanol [237].

4.1.1.2. Differences between free electron e^- and solvated electron e_{sol}^-

A free electron diffusing through matter undergoes elastic and inelastic scattering processes. Finally it will be trapped by one of the following two processes. It may be incorporated into the orbital of an atom or molecule which has a positive electron affinity, and forming a negative ion. Or, as it migrates through condensed matter, and be trapped in a potential energy 'trap' induced by its own polarization field. The 'trapped' electron cannot migrate. freely any more. But it can be released from the trap by absorbing energy [107].

The electron trapped in a solvent distinguishes from a free electron by being less mobile and more localized. Trapped electrons have negative free energy of formation and they are thermodynamically more stable [238]. The solvated electron in water is called a hydrated electron, denoted as e_{hyd}^-. e_{hyd}^- is trapped in a deep potential well at –3.2—3.5 eV in water [238].

4.1.1.3. Properties of e_{solv}^-

In bulk water, the absorption spectrum of e_{hyd}^- is in the range from 220 to 1000 nm, peaking at 720 nm [107]. It has a molar extinction coefficient of 1.85×10^4 $M^{-1}cm^{-1}$ at 720 nm [107]. In bulk water, e_{solv}^- is believed to be confined in a small cavity and to occupy an s-like ground state at −3.2—3.5 eV from the vacuum level [238]. The hydrated electron e_{solv}^- is a stronger reducing agent than the ·H radical by a different reducing potential of 0.67 eV [107].

e_{hyd}^- was discovered in the 1960s [236]. Many of its properties and reactivities have been well studied. It is a well-bound electron donor. It reacts with both inorganic and organic compounds, such as N_2O, MnO_4^-, NO_3^-, carbonyl group and iodoaliphatic compounds, with typical reaction rate constants in the range of 10^9-10^{10} $M^{-1}s^{-1}$ [238]. However, e_{solv}^- is believed to be ineffective at inducing biological damage due to its large binding energy of 3.2–3.5 eV [12, 102].

4.1.2. The Pre-solvated electron e_{pre}^-

With the advent of pump-probe femtosecond (fs) ($1fs=10^{-15}$ s) laser spectroscopy in late 1980s, electron solvation dynamics in bulk water has been studied on an unprecedented level. Following the first direct observation of the prehydrated electron (e_{pre}^-) by Migus et al. [139], researchers have intensely studied this ultrashort-lived species [139, 239-245, 247-255]. It is now well known that the solvation of an excess electron (e.g., produced via two-UV-photon excitation) in

water proceeds essentially through two major stages: the electron is first localized in a weakly-bound preexisting trap and is called a precursor to the hydrated electron, denoted as e_{pre}^-, with a lifetime <1 ps [139, 239-245]. However, these studies reported quite diverse lifetimes and physical properties of e_{pre}^- over the past two decades; the reported lifetimes ranged from 10fs, 50 fs, 110 fs, ~200 fs, ~300 fs, 540 fs to ~1 ps [139, 239-245]. The quantum yield of e_{pre}^- is nearly double that of its end product (e_{hyd}^-) [31] or the ·OH radical. Thus, there has been significant interest in studying the reactivities of e_{pre}^- with various molecules [97-99, 245, 256-258]. In particular, there is evidence that *e_{pre}^- can be effectively attached to amino acids and nucleotides* [256-258]. More significantly, Lu and co-workers [97-99] have proposed that e_{pre}^- causes the large enhancements in electron-induced *bond breaking* of halogenated molecules such as chlorofluorocarbons (major ozone-depleting substances) adsorbed on water ice via a dissociative electron transfer (DET) mechanism, which can be relevant to the formation of the ozone hole in earth's atmosphere. However, the role of e_{pre}^- in electron-driven processes in aqueous environments is generally poorly understood and is relevant to several critical issues facing environmental scientists and radiation biologists [246]. Direct observation of electron transfer (ET) reactions between e_{pre}^- and molecules is thus of great interest. Such reactions have been difficult to study because of the ultrashort lifetimes of e_{pre}^-, on the fs time scale.

4.2. BrdU / IdU as potential radiosensitizers

As mentioned in Chapter 2, halopyrimidines, especially BrdU and IdU, are an important family of potential hypoxic radiosensitizers [168-169, 171, 174, 226-228]. They are halogenated thymidine analogues. Their molecular structures are shown in Fig. 4.1. Cells undergoing DNA synthesis cannot distinguish efficiently between thymidine and BrdU / IdU. If cells are treated with BrdU or IdU for a sufficiently long period before irradiation, significant incorporation into DNA occurs. Under ionizing radiation, replacement of thymidine in DNA by BrdU/IdU causes large enhancement of DNA damage and cell death. The DNA damage caused by BrdU/IdU includes, single-strand breaks (SSBs), double strand breaks (DSBs), interstrand cross-links [232], and chromatid aberrations, especially sister chromatid exchange (SCE) [259-260].

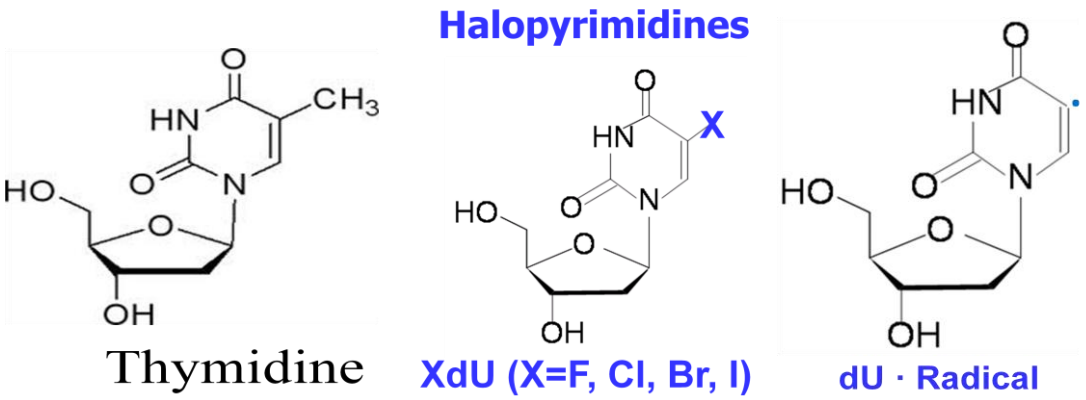

Figure 4.1. Molecular structures of thymidine, XdU, and dU• radical.

As potential radiosensitizers, BrdU/IdU have passed phase I to phase II clinical trials, but showed small efficiency in phase III trials [181-183]. This is probably related to the poor understanding of the molecular reaction mechanism of BrdU/IdU.

Since the phenomenon was first noted by Zamenhof, De Giovanni and Greer [261], a large number of experiments have confirmed that cells containing DNA in which thymidine has been partially replaced by BrdU are more sensitive to killing by UV light and ionizing radiation than their un-substituted counterparts. However, the sensitization mechanism remained unknown. In 1967 [262], Adams suggested that the presence in substituted DNA of the highly electro-negative bromine moiety on BrdU would greatly increase the cross section for radiation-produced electron trapping over un-substituted DNA and result in hydrated electron (e_{hyd}^-) migration to the 5 position of the BrdU nucleotides. The $BrdU^-$ anions thus formed were hypothesized as undergoing dissociation to bromide ion and uracil-type radicals, which cause permanent damage to the DNA. The reaction is represented as:

$$BrdU + e_{hyd}^- \rightarrow BrdU^- \rightarrow Br^- + dU^\bullet \quad \text{.....4.1}$$

The uracil-type radicals have been detected by different methods [263-264]. In the presence of a source of abstractable hydrogen, the uracil-5-yl ($U^\bullet$) radical is expected to react to produce uracil (HU). Indeed, the production of uracil had been detected by spectrophotometric techniques and conductometric pulse radiolysis [265-266].

For a very long time, e_{hyd}^- was believed to play a critical role in the generation of the uracil radical in the molecular mechanism of action of halopyrimidines. At that time when this

mechanism was proposed, nothing was known about e_{pre}^-. Previous nanosecond (ns)-resolved pulse radiolysis experiments on BrU showed a transient absorption peak at ~330 nm, which was attributed to the transition state BrU^{*-} [267]. *But without a fs resolution it was impossible to observe the formation of the real transition state and therefore to determine which species,* e_{pre}^- *or* e_{hyd}^-*, leads to the reaction and the formation of the reactive radical*.

Real-time observation of the transition state in a chemical reaction is of great interest. It is important to know the properties of the transition state if one is to predict, understand and modify the course of a reaction [209-210]. The application of time-resolved femtosecond (fs) laser spectroscopy to the studies of transition states has led to the birth of new fields called femtochemistry and femtobiology [210]. In this chapter, we report the first real-time observation of the transition state of the ultrafast ET reaction of e_{pre}^- with halopyrimidines.

4.3. Experiments

The methodology for pump-probe femtosecond transient absorption measurements has been described in Chapter 3. We used a Ti:sapphire laser system producing 100-120 fs, 1mJ laser pulses centered at λ=800 nm at a repetition rate of 1 kHz, two optical parametric amplifiers producing pump and probe pulses with wavelengths from UV to infrared. A pump wavelength of 318-322 nm was used to generate excess electrons in water and a probe wavelength at 330-340 nm was used to probe the intermediate state XdU^{*-} of the reaction of e_{pre}^- with a XdU (X=F, Cl,

Br, and I). The polarization of pump and probe pulses was set at the magic angle (54.7°) to avoid contribution from polarization anisotropy due to orientational motions of molecules. A small pump pulse energy (≤0.3 μJ) was used to make the solvated electron signal negligible when detected at (probe) wavelengths around 330 nm and to avoid any nonlinear effects. The sample was held in a 5 mm cell with a stirring bar to avoid any photoproduct accumulation. Ultrapure water with a resistivity of > 18 MΩ/cm was used and halopyrimidines (FdU, BrdU, CldU, and IdU) from Sigma-Aldrich were used as supplied.

4.4. Results and Discussion

The production of the precursor electron and the solvated electron via two-UV-photon excitation in water is shown in Fig. 4.2. The absorption spectrum of BrdU is shown in Fig. 4.3. It has absorption peaks at 210 nm and 279 nm and a tail extending up to 315 nm. To avoid the possible absorption of the pump pulse by BrdU, we used 318 nm as the pump wavelength to generate e_{pre}^-. A probe pulse 330 nm was used to observe the transition state of the ultrafast electron reaction of BrdU with the e_{pre}^-. The fs-TRLS transient absorption kinetic traces for the formation and decay of the dissociative transient anion of $BrdU^{*-}$ with different concentrations are shown in Fig. 4.4.

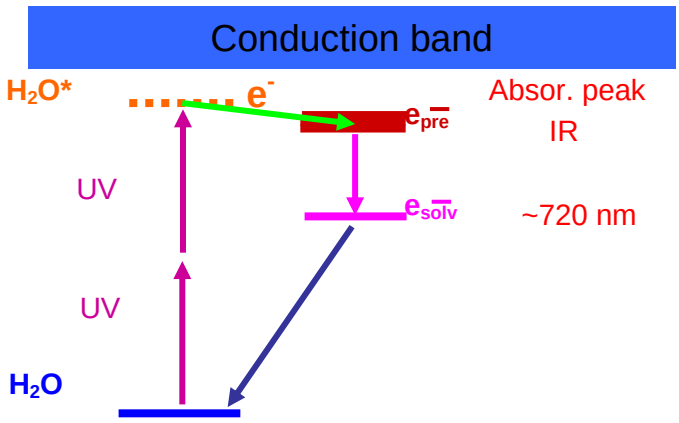

Figure 4.2. Schematic diagram for the production of the precursor electron and the solvated electron via two-UV-photon excitation in water.

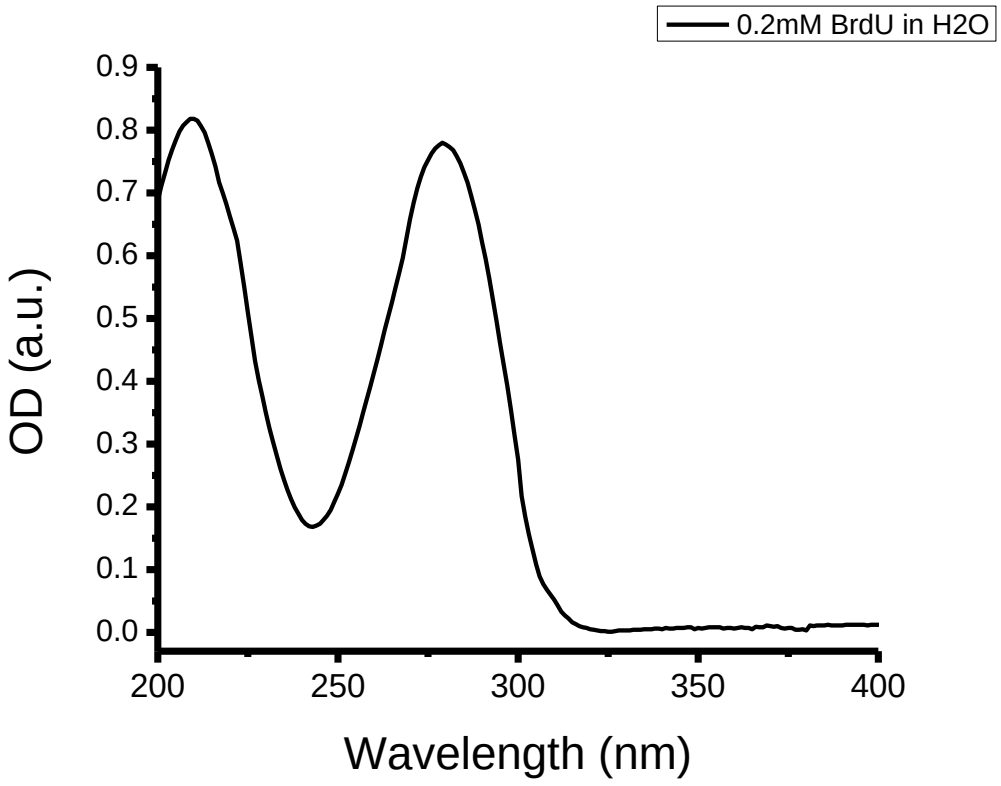

Figure 4.3. Static absorption spectrum of BrdU

Our fs-resolved results reveal novel features of the formation and decay kinetics of $BrdU^{*-}$. The result in Fig. 4.4a shows that there is a clear rise in the signal that peaks at ~0.55 ps. The transient absorption kinetic traces simply exhibit a linear dependence on BrdU concentration in the measured range of 10 to 31 mM. This indicates that the transient species must result from a single BrdU molecule. By subtracting the transient absorption kinetic trace for the pure water from that of BrdU, the 'spike' can be removed nearly completely (Fig. 4.4b). This makes it possible to make a theoretical fit to the experimental kinetic trace, and hence the formation and decay times of the transient species can be quantitatively obtained. From the fitting, we obtain a formation (rising) time of ~150±40 fs and two decay times: one is of ~1.5±0.3 ps and the other on the scale of ns. The ns decay component seems consistent with the result observed in previous ns radiolysis experiments [267]. Moreover, the yield of the transient absorption at 330 nm now shows a quadratic dependence on the pump pulse energy, as shown Fig. 4.5. The possibility to attribute this transient absorption to the BrdU** state produced via 2-photon excitation of BrdU can be ruled out by the observation that no transient absorption signal was detected as the pump wavelength was ≥400 nm, while the 2-photon excitation cross section of BrdU has maxima at 534 nm and 558 nm. Also, electron production from 2-photon excitation or ionization of BrdU molecules is negligible since the molecular density of BrdU (10-31 mM) is at least 3 orders of magnitude less than that of H_2O (~50 M). Even a small yield of $BrdU^+$ ions is created by 2-photon ionization of BrdU, they cannot contribute to the transient signal observed in Fig. 4.4. because, like the BrdU* signal, $BrdU^+$ signal would not show a clear rising time. These results indicate that the detected transient species must originate from the transfer of electrons generated via 2-photon excitation of H_2O molecules.

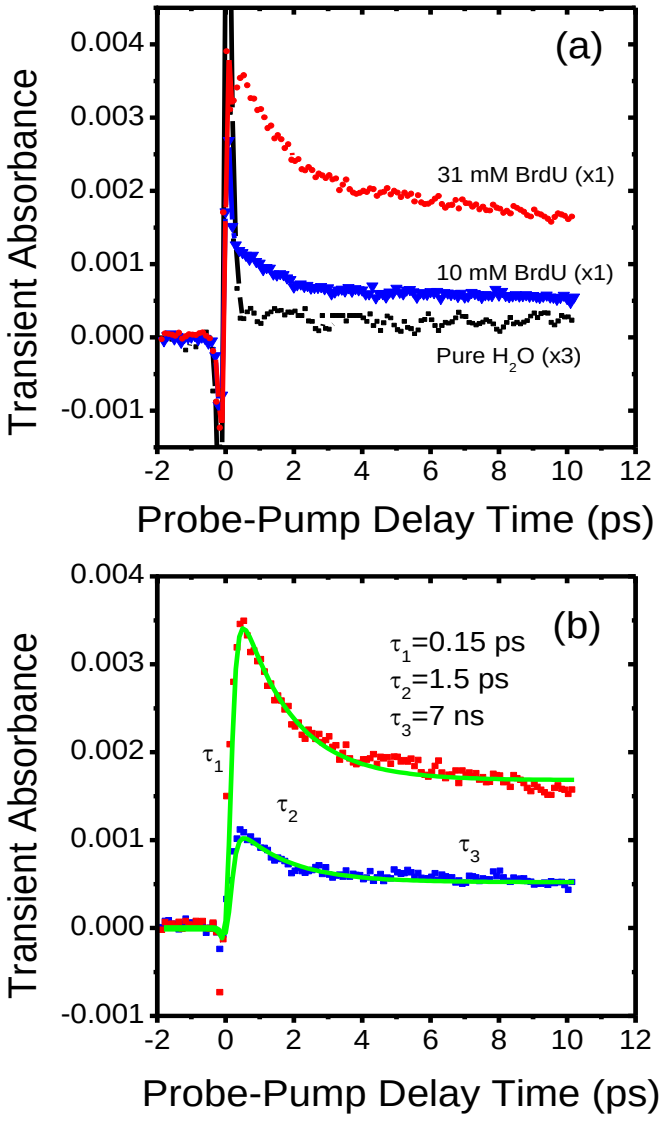

Figure 4.4. Femtosecond transient absorption kinetic traces of BrdU in water, pumped at 318 nm and probed at 330 nm: (a) original data, where the sharp peak at time zero is the coherence "spike" observed when λ_{pump} and λ_{probe} are close to each other; (b) after the subtraction of the kinetic for the pure water. The solid lines in (b) are the best fit to the experimental data, giving a rise time τ_1=0.15 ps and two decay times τ_2=1.5 ps and τ_3=7 ns.

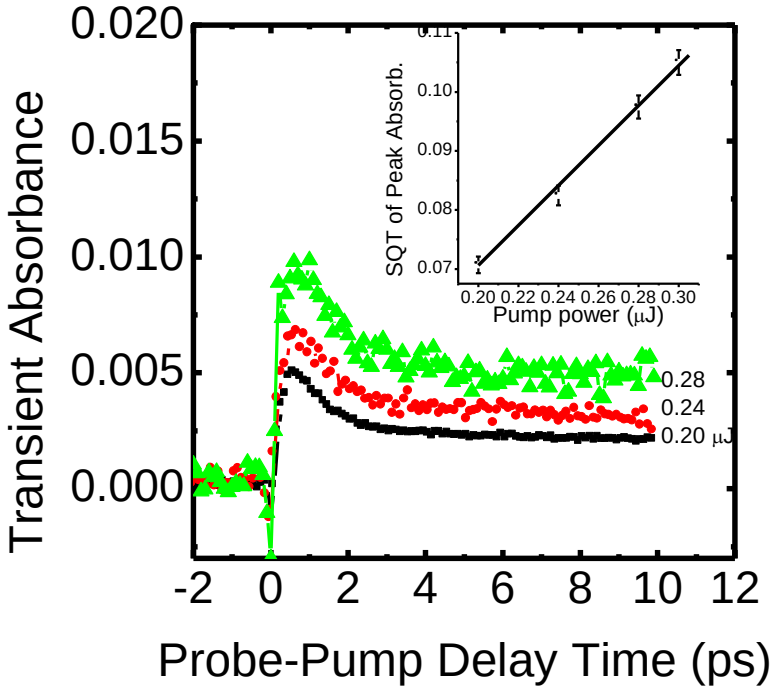

Figure 4.5. Femtosecond transient absorption kinetic trace of 10 mM BrdU in water, pumped at 318 nm with various pulse energies and probed at 330 nm, after the subtraction of the kinetic trace for the pure water. The inset is the square root (SQR) of the absorbance peak intensity at 0.55 ps versus pump pulse energy.

The above results show that the electron transfer reaction is complete within 0.2 ps after the electronic excitation by 318 nm, leading to the formation of a transition state $BrdU^{*-}$ that has a lifetime of ~1.5 ps. The lifetime of a transition state usually lies in the range of 10^{-15} s (fs) up to a few 10^{-12} s (ps) [209-210]. Beyond this, the transition state of the molecule either has dissociated into fragments or has relaxed into a nondissociative, vibrationally-relaxed anionic state that has a lifetime in the ns range. Indeed, the lifetimes of transient (AB^{*-}) states of many halogenated molecules (ABs) are measured to be in the range of 0.1 to a few ps [268]. Thus, it is reasonable to assign the faster decay of 1.5±0.3 ps to the dissociation of $BrdU^{*-}$ into Br^- and $dU^\bullet$. The reaction can be presented as:

$$BrdU + e_{pre}^- \rightarrow BrdU^{*-} \rightarrow Br^- + dU^\bullet \quad \text{..... 4.2}$$

Our observation of the rapid formation of $BrdU^{*-}$ on a time scale of ≤0.2 ps is of particular significance, which clearly demonstrates that this transition species does not result from the fully solvated, well-bound electron (e_{solv}^-), which would be generated in later stages ≥1.0 ps. Only the precursor electron, e_{pre}^-, can be responsible for the formation of the transient species in such a short period of time following the electronic excitation. If e_{solv}^- led to the formation of the transition state $BrdU^{*-}$, the formation of $BrdU^{*-}$ would correspond to its lifetime, which is in the μs timescale and we would not be able to observe its decay in the ps time scale. In contrast, our results show that the formation of $BrdU^{*-}$starts almost immediately after the electrons were generated by two UV (318nm) photon excitation, and is complete within 0.2 ps. Thus it is concluded that it is e_{pre}^-, rather than e_{hyd}^- that leads to the formation of the

dissociative BrdU*$^-$transition anion. This is the first real-time observation of the transition state of the ultrafast electron transfer reaction of e_{pre}^- with a biologically important halogenated molecule, BrdU [216].

After studying the molecular reaction mechanism of BrdU as a radiosensitizer, we extended the study to all four halopyrimidines (FdU, CldU, BrdU, and IdU). Femtosecond transient absorption kinetic traces of XdUs probed with λ_{probe}=330 nm are shown in Fig. 4.6, together with the absorption for the pure water. The transient absorption signal intensities detected at the peaks in Fig. 4.6 as a function of probe wavelength with the same pump wavelength are shown in Fig. 4.7. Moreover, the linear dependence of the transient absorption signal for XdU*$^-$ on XdU concentration is confirmed for other XdUs, as shown in Fig. 4.8 for IdU. Thus, higher XdU (X=Br, Cl and F) concentrations were used to obtain the signal intensities comparable with that for IdU in Fig. 4. 6.

The results in Fig. 4.7 show that the absorption spectra of XdU*$^-$ transition states indeed exhibit a peak around 330 nm for all XdUs, consistent with the observation by nanosecond radiolysis experiments [267]. This indicates that the transient species observed in ns resolved experiments actually evolves from the short-lived species revealed in current fs experiments. The ps-lived dissociative vibrationally-excited XdU*$^-$ states have electronic UV absorption nearly identical to their relaxed, nondissociative XdU$^-$ states. It turns out that the ns-resolved radiolysis experiments [267] correctly showed the relevance of the reactive radical formation to the reactions of XUs with electrons generated in radiolysis and the absorption of anionic states peaking around 330 nm. But they actually showed the transient absorption spectra of ns-lived, vibrationally-relaxed XU$^-$, rather than the ultrashort (ps)-lived *dissociative* vibrationally-excited

XU^{*-} that is the *true* transition state of the ultrafast electron transfer reaction. Without a fs-resolved technique, it was impossible to observe the real ultrafast molecular reaction involving an electron species that has a lifetime less than 1 ps.

In Fig. 4.6, we observe that the transient absorption trace for FdU exhibits no considerable peak in the first ps after the pump excitation, indicating that essentially no DET of any weakly bound e_{pre}^- to FdU could occur. Instead only an extremely weak, flat (long-lived) signal was observed for FdU, which can be attributed to the nondissociative anion FdU^- [216, 269]. In contrast, CldU shows transient absorption kinetics similar to that for BrdU: it exhibits a single signal peak at the delay time of ~0.55 ps with one fast decay time of 1-2 ps superposed on a long-lived (ns), slow decay tail; the transient absorption intensity for CldU is significantly weaker than that for BrdU. The fitted transient absorption kinetic traces, also give a rise time of τ_1~150 fs, a fast decay time of 1.5 ps and a slow decay time in ns range for both BrdU and CldU, respectively. Since the absorptions of XdU^{*-} states are identical to their relaxed XdU^- states, the decay kinetics of the transient absorption can be solely attributed to the dissociation of XdU^{*-}. This is also confirmed by the above-described results with FdU (no DET leads to no decay in the signal). Thus, the rise time, the ps decay and the ns decay times of the transient absorption are due to the formation and the dissociation of $BrdU^{*-}$ ($CldU^{*-}$) and the lifetime of the nondissociative $BrdU^-$($CldU^-$), respectively [216]. These results indicate that the same excited-state precursor contributes to the formation of both $BrdU^{*-}$and $CldU^{*-}$. Most strikingly, the transient absorption signal for IdU is much stronger than for BrdU and CldU even when the concentration of IdU is about one order of magnitude lower. *For IdU, the transient absorption spectrum exhibits a second bump just visible at ~1.0 ps, beside the first peak at ~0.55 ps.* This

indicates that there are two precursor (e_{pre}^-) states contributing to the formation of IdU*$^-$. Assuming two consecutive e_{pre}^- states in water [139, 142, 239, 241, 243], the best fit to the transient absorption kinetic trace of IdU, shown in Fig. 4.6, gives two rise times, a fast decay time in ps and a long-lived tail in ns. They are τ_1=170 ±40 fs, τ_2=540±40 fs, τ_3=1.80 ±0.20 ps and τ_4 fixed at 10 ns, respectively. Similar to the case for BrdU [216] and CldU, the τ_1 rise time, the τ_3 and τ_4 decay times correspond to the lifetime of a precursor e_{pre}^-, the dissociative lifetime of IdU*$^-$ and the lifetime of the long-lived molecular anion IdU$^-$, respectively. *Interestingly, the fact that* IdU*$^-$ *has two rise times provides clear evidence of two* e_{pre}^- *states contributing to its formation*. Thus, IdU*$^-$ results from not only the first precursor e_{pre}^- of a ~170 fs lifetime but a second precursor e_{pre}^- that has a lifetime of ~540 fs. Indeed, fs laser spectroscopic studies have previously reported several consecutive e_{pre}^- states, having lifetimes of ~200 fs and 540-1000 fs, following two-photon excitation of H_2O by a UV (266-320 nm) pump pulse [139, 239-245, 247-255].

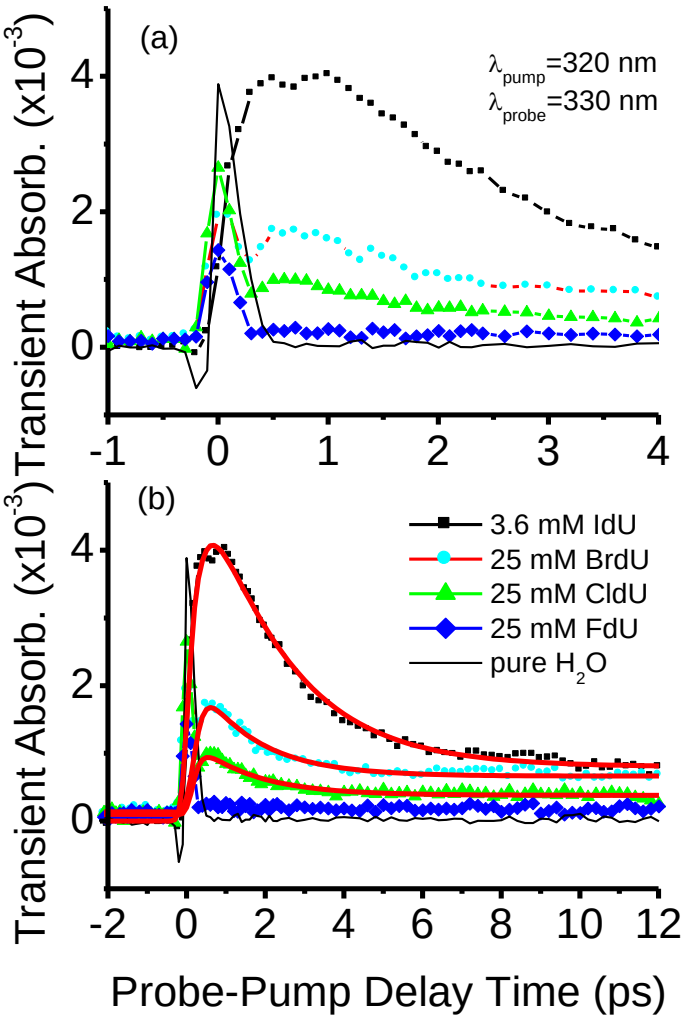

Figure 4.6. Femtosecond time-resolved transient absorption kinetic traces in the delay time ranges of (a): −1 to 4 ps and (b): −2 to 12 ps, of the pure water (solid line), 3.6 mM IdU, 25 mM BrdU, 25 mM CldU and 25 mM FdU with the pump and probe wavelengths indicated. The sharp peak at time zero is the coherence "spike". The solid lines in red are the best fits to the experimental data.

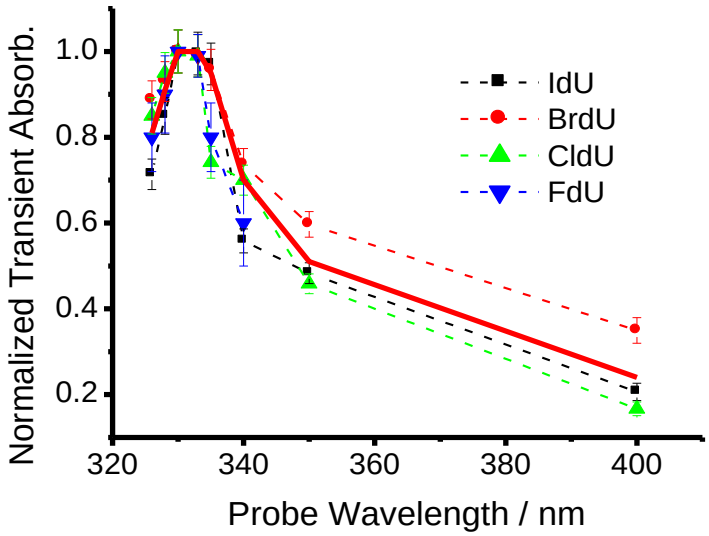

Figure 4.7. Transient absorption spectra of IdU, BrdU, CldU and FdU detected at the peaks in Fig. 4.6 versus probe wavelength in the 325–400 nm range with the pump wavelength fixed at 318 nm. The absorption intensities are normalized to those at the probe wavelength of 330 nm. The solid line in red is an aid to eye.

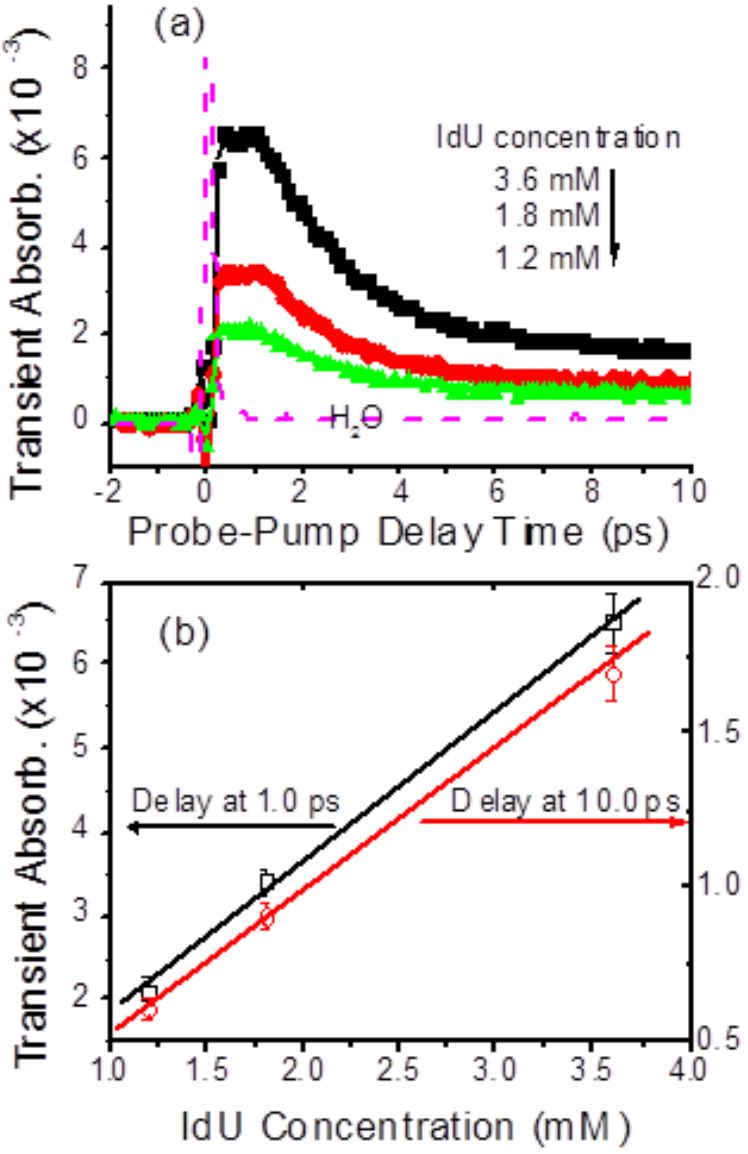

Figure 4.8. (a) Femtosecond time-resolved transient absorption kinetic trace of IdU with various concentrations, probed at 330 nm; the dashed line is the kinetic trace for the pure water; (b) Transient absorption intensities at 1.0 ps and 10.0 ps versus IdU concentration.

The excess energy ΔE for zero eV–electron-induced C-X (X=I, Br, Cl and F) bond breaks in XUs in the gas phase is given by $\Delta E \approx E_A(X) - E_{BD} \equiv \Delta E^0$, where $E_A(X)$ is the electron affinity of the halogen atom X and E_{BD} the C-X bond dissociation energy. In the condensed phase, the excess energy of reaction is increased by the polarization energy (E_P) of the medium: $\Delta E = \Delta E^0 + E_P$. With the gaseous ΔE^0 values (–0.9 to –1, 0.01, 0.24 and 0.42 eV for FU, ClU, BrU and IU, respectively) [270] and $E_p \approx 1.0$ eV for water [271], zero eV-electron-induced C-X bond breaks for CldU, BrdU and IdU in water are exothermic by 1.01, 1.24 and 1.42 eV, respectively, while the C-F bond break for FdU in water is nearly thermoneutral ($\Delta E \approx 0$ eV). This means that the lowest-energy limits of the anion resonance states CldU*$^-$, BrdU*$^-$ and IdU*$^-$ lie at –1.01, –1.24 and –1.42 eV, respectively, while the lowest FdU*$^-$ state lies around the vacuum level (0 eV). DET resonances are therefore expected to occur for CldU and BrdU with the first weakly-bound e_{pre}^- state that has the energy slightly higher than the p-like excited state of the hydrated electron. In bulk water, the absorption of e_{hyd}^- peaks at 1.7 eV (~720 nm) is believed to be a transition from the s-like ground state at ~–3.2 eV to a p-like excited state at ~—1.5 eV below the vacuum level [238, 272]. Thus, a second DET channel can additionally occur for IdU with the p-like excited state which is very close to the lowest-energy IdU*$^-$ state at ~–1.42 eV when energy-level broadening is taken into account. In contrast, no precursor states are available for DET to FdU. Thus, ultrafast electron transfer from excited-state e_{pre}^- to XdUs is expected to occur efficiently, leading to DET to IdU, BrdU and CldU with the expected efficiency: IdU>BrdU>CldU, but no DET to FdU. This is schematically shown in Fig. 4.9. This prediction is in good agreement with the observed results.

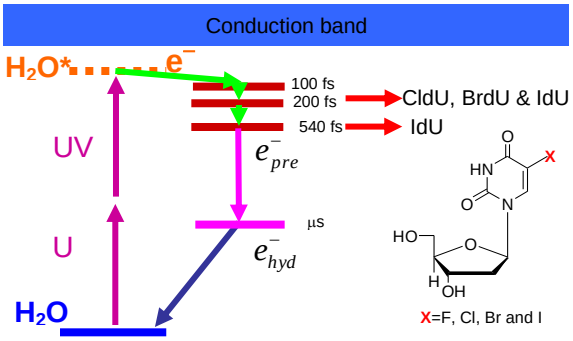

Figure 4.9. Schematic diagram for the production of the precursor electron (e_{pre}^-) and the hydrated electron (e_{hyd}^-) through two-UV photon excitation in water and the dissociative electron transfer (DET) reaction of e_{pre}^- with halopyrimidines (XdUs), whose structures are also shown.

4.5. Conclusion

Our results described in this Chapter have multiple-fold significance. First, our results prove that it is the e_{pre}^- states, rather than e_{hyd}^-, that are responsible for DET reactions to XdUs. This reaction leads to the formation of the reactive radical, which is a key step in the mechanism of action of these pro-drugs in radiotherapy of cancer. Our results have challenged a long accepted mechanism that long-lived e_{hyd}^- would be responsible for the radical formation from halogenated molecules [246, 267, 273], which would predict a formation time of XdU^{*-} in the time scale beyond ns corresponding to the e_{hyd}^- lifetime. Second, we have clearly revealed that the DET reaction efficiency is IdU>BrdU>CldU, whereas no DET of e_{pre}^- to FdU occurs. This is due to

the availability of two e_{pre}^- states for DET to IdU, of one e_{pre}^- state for DETs to BrdU and CldU, and no e_{pre}^- for DET to FdU. Thus, IdU should be explored as the most effective radiosensitizer. As a more general conclusion, our results demonstrate that despite their ultrashort lifetimes in subpicoseconds, nonequilibrium e_{pre}^- can play a crucial role in many ET reactions occurring in aqueous environments, especially for chlorine-, bromine- and iodine-containing molecules.

***Special statement**: As stated in Section 2.8 (the major objectives of this thesis) of Chapter 2, the results in this chapter have been presented in my MSc thesis [71]. The purpose to outline / represent these results here is for a better understanding of the whole PhD project that continued from my MSc work and for a better, smooth reading of this thesis.*

Chapter 5

Resolution of the Controversies about the Lifetimes and Physical Nature of Prehydrated Electron (e_{pre}^-)

5.1. Introduction

As mentioned in Chapter 4, despite intense studies over decades, the lifetimes and physical properties of the prehydrated electron (e_{pre}^-) remains very controversial. From the experimental point of view, studies by femtosecond (fs) time-resolved laser spectroscopy (fs-TRLS) have reported quite diverse lifetimes and properties of the prehydrated electron (denoted as e_{pre}^-) in bulk water. The reported lifetimes have covered 50 fs, 110 fs, ~200 fs, ~300 fs, 540 fs and ~1 ps [139-142, 239-245]. The first fs laser spectroscopic measurement by Migus et. al [139] gave a lifetime of 240 fs for the precursor of the fully solvated state in water. Subsequently, Eisenthal et al. [239-240] proposed that the e_{pre}^- has a 180 fs or 300 fs rise time and a 540±50 fs decay time, inferred from their measurements of the appearance dynamics of e_{hyd}^- probed at 620 nm, is the wet electron that is the lowest electronically excited p-like state, consistent with the nonadiabatic process theoretically predicted by Rossky and Schnitker [247]. Eisenthal et al. [239] also observed an ultrafast component (<50 fs), which was attributed to the formation and decay of the photoionization product H_2O^+. A non-adiabatic decay lifetime of ~300 fs for the p

state, followed by a ~1 ps relaxation in the s ground state, was subsequently proposed by Barbara et al. [241-242]. Later, both observed e_{pre}^- states with 200 fs and 540 fs lifetimes which were attributed to the s ground-state electron embedded in hot solvation shells [140-142], while a 45-fs ultrafast rise in the kinetic trace of e_{pre}^-, after ~800 nm excitation of the equilibrium e_{hyd}^-, was attributed to the decay lifetime of the p-state [243]. The latter was also reported to be ~50 fs in a similar 3-pulse experiment by Wiersma et al [244]. Lu, Baskin and Zewail [245] also reported a rise time of ~210 fs and a decay time of ~720 fs for e_{pre}^- with water held in a 5-mm sample cell, while *at a photon flux density 2 to 3 times higher*, a rise time of 90±10 fs and a decay lifetime of 370 ±30 fs was observed for a ~300 μm jet of water. This difference was attributed to a pulse-transient-time mismatch Δt_g induced by a group-velocity dispersion of pulses transmitted in the cell [245]. As described in Chapter 4, we have obtained more direct evidence of electronically excited e_{pre}^- states that have lifetimes of ~150 fs and ~540 fs, respectively, by real-time fs-TRLS measurements of the DET reactions of halopyrimidines XdUs (X=Cl, Br and I) with e_{pre}^- [216-217].

Equally, from the theoretical point of view, the simulated results on electron hydration dynamics have also covered a very wide range from 10 to ~1000 fs. The lifetime of the p excited state was first reported to be ~1.0 ps or ~730 fs by Rossky et al. [247-248], ~220 fs by Neria et al. [249] and ~300 fs by Staib and Borgis [250]. Jay-Gerin and co-workers [251-252] proposed that e_{pre}^- is an electron localized at a preexisting trap related to the Urbach tail extending below the water conduction band. Using different mixed quantum/classical simulation algorithms, Larsen, Bedard-Hearn and Schwartz [253] predicted a range of 400-700 fs for the average lifetime of the excited hydrated electron. In 2006, Zharikov and Fischer [254]

reported a lifetime of 50 fs for the p state, consistent with some of the experimentally reported values [243-244], while Borgis, Rossky and Turi [255] predicted an extremely short lifetime of ~10 fs for a hypothetical equilibrium excited state based on the golden rule model. The latter authors, however, pointed out that the calculated lifetime is very sensitive to the equilibrium energy gap used in the simulations. Most recently, these authors have re-examined the issue and obtained an effective excited-state lifetime of ~330 fs, by using the same golden rule approach but setting up a realistic, gap dependent kinetic rate equation [274]. The latter value is generally consistent with some earlier experimental reports of 300 fs by Barbara et al. [243] or 370 fs by Lu et al. [245] and is also close to the value of 540 fs observed by Eisenthal et al. [239-240] and us [216-217]. These new experimental and theoretical values are, however, clearly inconsistent with the excited-state lifetime of ~50 fs.

The experimental and theoretical results reviewed above indicate that there exist large discrepancies about the lifetimes and physical nature of non-equilibrium e_{pre}^- states, despite the fact that e_{pre}^- has been intensely studied over the past two decades. Therefore, it is important to closely examine why there exist large discrepancies in experimental data for electron hydration dynamics in bulk water and to remove the discrepancies. This will be essential to obtaining true and reliable conclusions about the physical properties, reactivity and role of e_{pre}^- in biological, chemical and environmental systems. Our work described in this Chapter will resolve the long-standing discrepancies about the electron hydration dynamics (the lifetimes and physical nature of non-equilibrium e_{pre}^- states).

5.2. Experiments

The standard methodology for pump-probe femtosecond transient absorption measurements has been described in chapter 3. We used a Ti:sapphire laser system producing 100－120 fs, 1 mJ laser pulses centered at λ=800 nm at a repetition rate of 0.5 kHz, two optical parametric amplifiers producing pump and probe pulses with wavelengths from visible to IR. The polarizations of pump and probe pulses were set at the magic angle (54.7°) to avoid contribution from polarization anisotropy due to orientational motions of molecules. For studies of electron hydration dynamics in pure water, pump wavelengths from 266 to 320 nm were used to generate excess electrons in water. Probe wavelengths at visible (600-720 nm) and at IR (1200-1300 nm) were used to probe the signals of e_{hyd}^- and e_{pre}^-, respectively. For the experiments with iododeoxyuridine (IdU), a pump wavelength at 320 nm was used in order to avoid the direct absorption of the pump pulse by IdU. Probe wavelengths around 330 nm were selected to search the transition state IdU^{*-} of the reaction of e_{pre}^- with IdU. In latter experiments, a relatively low pump power was chosen so that the e_{hyd}^- signal was barely detectable at probe wavelengths around 330 nm and any nonlinear effects were avoided. The best fits to the experimental data were obtained by using a least-squares fitting program. The time-dependent transient absorption signal is described by a number of exponential functions. These exponential terms are convoluted with the instrument response function represented by a Gaussian function. In our fits, the time zero and the FWHM (=300 fs) of the pump-probe cross-correlation function were *not* adjustable fitting parameters, but were fixed at the values determined in-situ by the coherence spike appearing in the kinetic trace for pure water. This procedure should give rise

to more reliable fitted results. All measurements were conducted at room temperature. The sample was held in a 5 mm cell with a stirring bar to avoid any photoproduct accumulation. Ultrapure water with a resistivity of > 18 MΩ/cm was obtained from an ultrapure water system (Barnstead's Nanopure). IdU from Sigma-Aldrich was used as supplied and its concentrations were calibrated by taking static absorption spectra from a UV/visible spectrophotometer (Beckman, Life Science).

5.3. Results and Discussion

As illustrated in Fig. 4.2, the absorption of two UV photons at wavelengths ≥266 nm by water leads to the generation of electrons lying in energy below the conduction band and the initiation of the electron hydration sequence [274-275]. We used a pump wavelength of 318 (320) nm with a pulse width of 100~120 fs to produce the excess electron in water. Under these conditions, no electrons are excited into the conduction band and thus any relatively slow electron solvation process is avoided. Fig. 5.1 shows typical fs transient absorption kinetic traces of the precursor electron and the fully hydrated electron in pure water pumped at 318 nm with a power of 0.55 μJ/pulse, probed at 1200 nm and 600 nm respectively. The kinetic trace for e_{pre}^- (Fig. 5.1a) is very similar to those reported by Laubereau et al [142] with λ_{pump}=273 nm and λ_{probe}=990 or 1600 nm and by Barbara et al. [243] with λ_{pump}=266 nm and λ_{probe}=1000 nm. The fit to our data with an instrument response function of 300 fs gives a rise time of 182 fs and a decay time of 570 fs, which are close to the reported values of 200 fs [142, 243] and 540 fs [241] for e_{pre}^-, respectively. These values are longer than those (110 fs rise and 240 fs decay) obtained by

Migus et al. [139] and those (90 fs rise and 370 fs decay) obtained at a high photon flux density by Lu et al. [245], though the probe wavelength used in those experiments is exactly or nearly identical to that used in the present experiments. The kinetic trace for e_{hyd}^- (Fig 5.1b) is nearly identical to those obtained by Eisenthal et al. [239] with λ_{probe}=625 nm and by Barbara et al. [243] with λ_{probe}=720 nm. However, caution should be exercised in the fitting of the e_{hyd}^- kinetic trace. The fit by the latter [243] gave a single rise time of 276 fs for the e_{hyd}^- signal, while the former [239] assumed two rise components in their fit and obtained a 180 fs and a 540 fs rise time. Here, we find that equal quality fits to the present data can be obtained with either a single rise time or two rise times, giving a single rise time of ~300 fs or two rise times of 180-200 fs and 540 fs. If one takes a single rise time, however, it would be difficult to understand why the time scale for the electron solvation to form the fully hydrated e_{hyd}^-, which is supposed to be the appearance kinetics of e_{hyd}^-, is much shorter than the sum of the formation and decay times of the precursor electron e_{pre}^-. In view of the fact that the kinetic trace of e_{pre}^- clearly shows a rise and a decay time of the e_{pre}^- signal (Fig. 5.1a), it has clearer physical meaning to fit the e_{hyd}^- signal with two rise times. Our fitted results are nearly identical to those obtained by Eisenthal et al. [239] and Laubereau et al. [142], though those two groups gave different pictures about the physical nature of these two e_{pre}^- states, as mentioned above. Before resolving this discrepancy, we first present our results to show how a hidden effect in pump-probe experiments could give rise to an extremely short lifetime for the p-like excited-state e_{pre}^-.

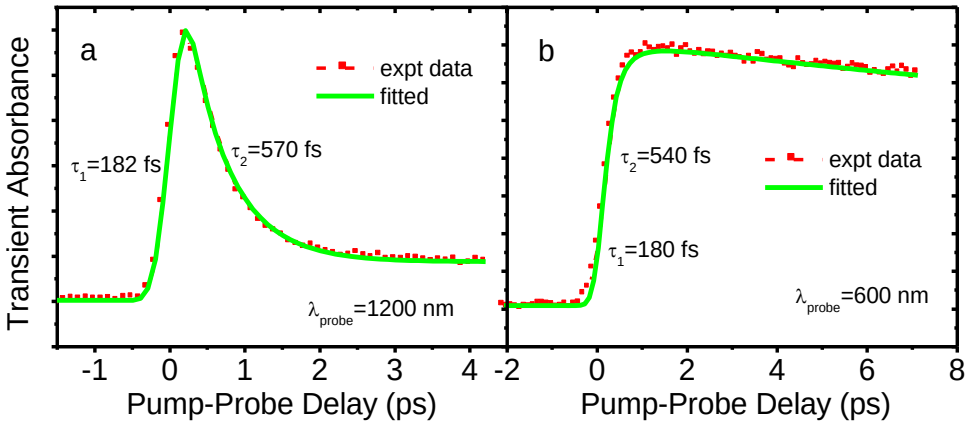

Figure 5.1 Femtosecond transient absorption kinetic traces for (a) e_{pre}^- and (b) e_{hyd}^-, at the probe wavelengths indicated, for two-photon excitation of pure water at 318 nm; the pump-probe pulse spatial overlap point in water is at ~500 μm from the front surface of a 5-mm cell. The theoretical fits are also shown with the fitted rise and decay times indicated

Interesting results are shown in Fig. 5.2 and Fig. 5.3, which were obtained with nearly the same experimental conditions as in Fig. 5.1 but with a photon flux density of 3~4 times higher. An interesting effect now shows up: the kinetic trace shapes of e_{pre}^- and e_{hyd}^- show strong dependence on the pump power. For the kinetic trace of e_{pre}^- at both low and high pump power (Figs. 5.2a-5.2f), there is clearly no rise time with the instrument response function taken into account. At higher pump power, there are two decay times for e_{pre}^-: the fits to the data give a dominant ultrashort decay of 20~30 fs and a slower decay of 520~550 fs, measured at various pump-probe spatial overlap positions (300 or 500 μm in water measured from the front surface of the sample cell). At low pump power, most strikingly, the slower decay completely disappears and only a *symmetric* narrow peak now exhibits at delay (time) zero (Fig. 5.2c and

5.2f). One could thus deduce a nearly zero fs rise and zero fs decay time if this sharp peak is taken as the kinetic trace for e_{pre}^-. It is most interesting to note that the intensity of the symmetric sharp peak shows excellent *linear* pump-power dependence (see inset in Fig. 5.2f). For the kinetic trace of e_{hyd}^- shown in Fig. 5.3, similar results are observed. At high pump power, there is an ultrafast "rise" or a sharp peak at delay zero and a slower rise that is similar to the one shown in Fig. 5.1b. In contrast, at low pump power, the slower rise completely disappears, leaving only a narrow peak at delay zero (Fig. 5.3c) or just an extremely sharp onset (Fig. 5.3f and Fig. 5.3i), at various pump-probe spatial overlap positions (150, 500 and 800 μm from the front cell surface). It is also most interesting to observe that the addition into water of 1 M KNO_3, which (NO_3^-) is a well-known strong scavenger for precursor electrons [276], does not affect the narrow peak at delay zero for the trace of e_{pre}^- or e_{hyd}^-, as shown in Fig. 5.2i, Fig. 5.3h and Fig.5.3i.

One might argue that the above-observed pump-power dependence of the decay dynamics of e_{pre}^- or the rise dynamics of e_{hyd}^- could be attributed to the effect of conduction-band electrons, which would be trapped and would relax at a site remote from the initial excitation site. This possibility must be ruled out by the following two facts. (1) At high pump power, the fitted slower decay time (520~540 fs) in Fig. 5.2 is no larger than the 570 fs decay observed in Fig. 5.1a and the 540 fs rise in Fig. 5.1b obtained with a low photon flux density. (2) At low pump power, the slower decay component becomes zero and the intensity of the symmetric sharp peak at delay time zero shows excellent *linear* pump-power dependence (see inset in Fig. 5.2f). This latter observation rules out not only the possibility of the sharp peak at delay zero being the electron signal (as no electrons could be generated by single-photon

excitation of water at 318 nm) but also the assignment of this peak to the absorption of H_2O^+ produced by two-photon excitation of H_2O (proposed in ref. 239, as the H_2O^+ intensity would have a *quadratic* pump-power dependence). In fact, as the pump power was so low that no efficient two-photon excitation of water occurs, no significant number of e_{pre}^- (e_{hyd}^-) electrons were produced and thus no H_2O^+ ions are detectable.

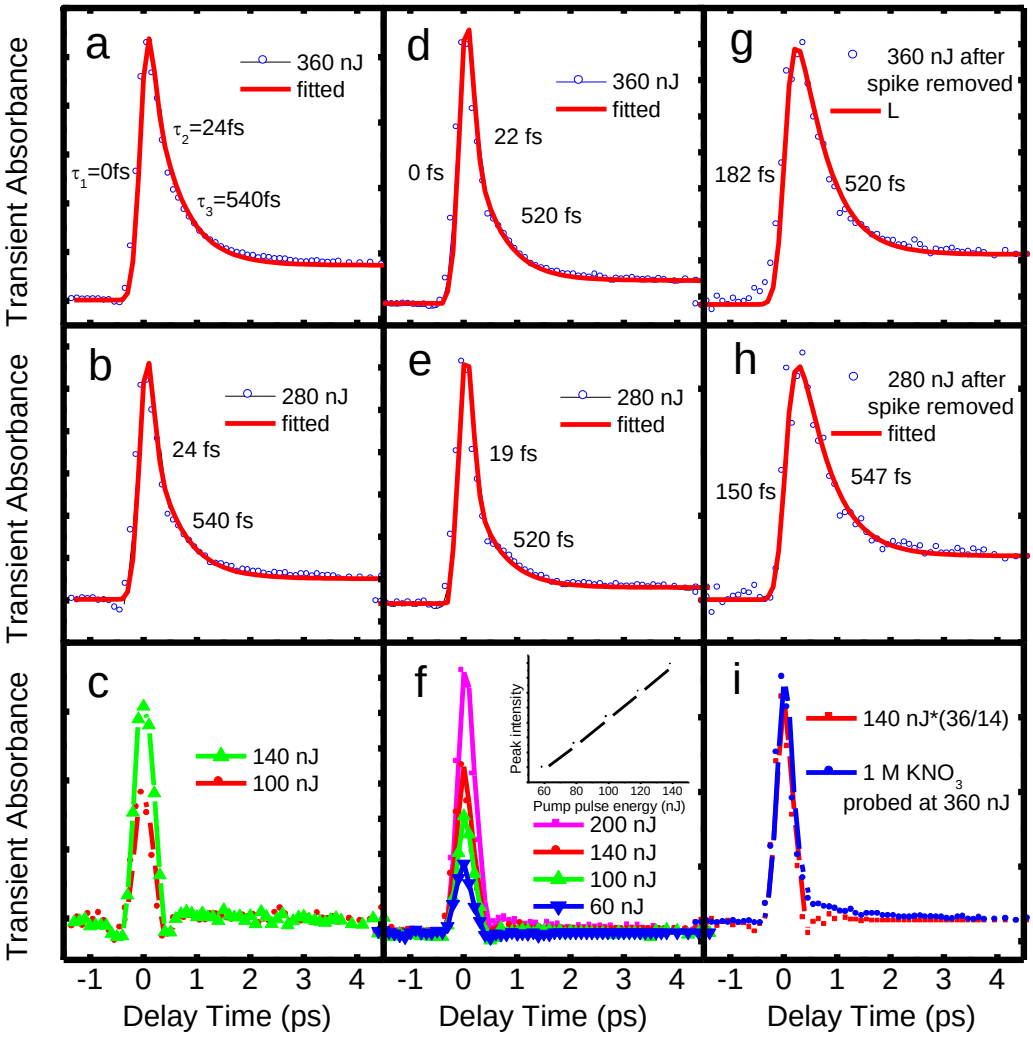
a
360 nJ
fitted
τ2=24fs
τ1=0fs
τ3=540fs
d
360 nJ
fitted
22 fs
0 fs
520 fs
g
360 nJ after
spike removed
L
182 fs
520 fs
b
280 nJ
fitted
24 fs
540 fs
e
280 nJ
fitted
19 fs
520 fs
h
280 nJ after
spike removed
fitted
150 fs
547 fs
c
140 nJ
100 nJ
f
Peak intensity
60 80 100 120 140
Pump pulse energy (nJ)
200 nJ
140 nJ
100 nJ
60 nJ
i
140 nJ*(36/14)
1 M KNO3
probed at 360 nJ
Transient Absorbance
Transient Absorbance
Transient Absorbance
-1 0 1 2 3 4
Delay Time (ps)
-1 0 1 2 3 4
Delay Time (ps)
-1 0 1 2 3 4
Delay Time (ps)

Figure 5.2.

Figure 5.2. Femtosecond transient absorption kinetic traces of the precursor electron e_{pre}^-, generated by 318 nm two-photon excitation of pure water with a pump photon flux density 3~4 times higher than that used to obtain Fig. 5.1, probed at 1224 nm. Left column (*a*—*c*): the data were collected with various pump power (360—100 nJ/pulse), at the pump-probe pulse spatial overlap position in water of ~500 μm from the front surface of a 5-mm cell; at this position, the electron signal was optimized. Center column (*d*—*f*): the data were collected with various pump power (360—60 nJ/pulse), at the pump-probe overlap position moved from ~500 μm to 300 μm without re-optimization of the electron signal; an excellent linear dependence of the sharp peak intensity at delay zero on pump power under 140 nJ/pulse is shown in the inset of *f*. Right column (*g*—*i*): *g* and *h* show the corrected kinetic traces from the traces *d* and *e* (center column), after the artificial spike was linearly extrapolated from the lowest pump power to the corresponding pump power and was subtracted from the traces *d* and *e*, respectively. In *g* and *h*, the fitted curves and results are also given. *i* shows the measured kinetic traces for the presence of an effective precursor-electron scavenger: 1M KNO_3, in water with pump power at 360 nJ/pulse, and the extrapolated spike by multiplication of the pure spike obtained at 140 nJ/pulse (see *f*) with a factor 360/140. The results in *i* indicate that the strong electron scavenger does not affect the sharp peak at delay time zero, which is identified as the artificial coherence spike.

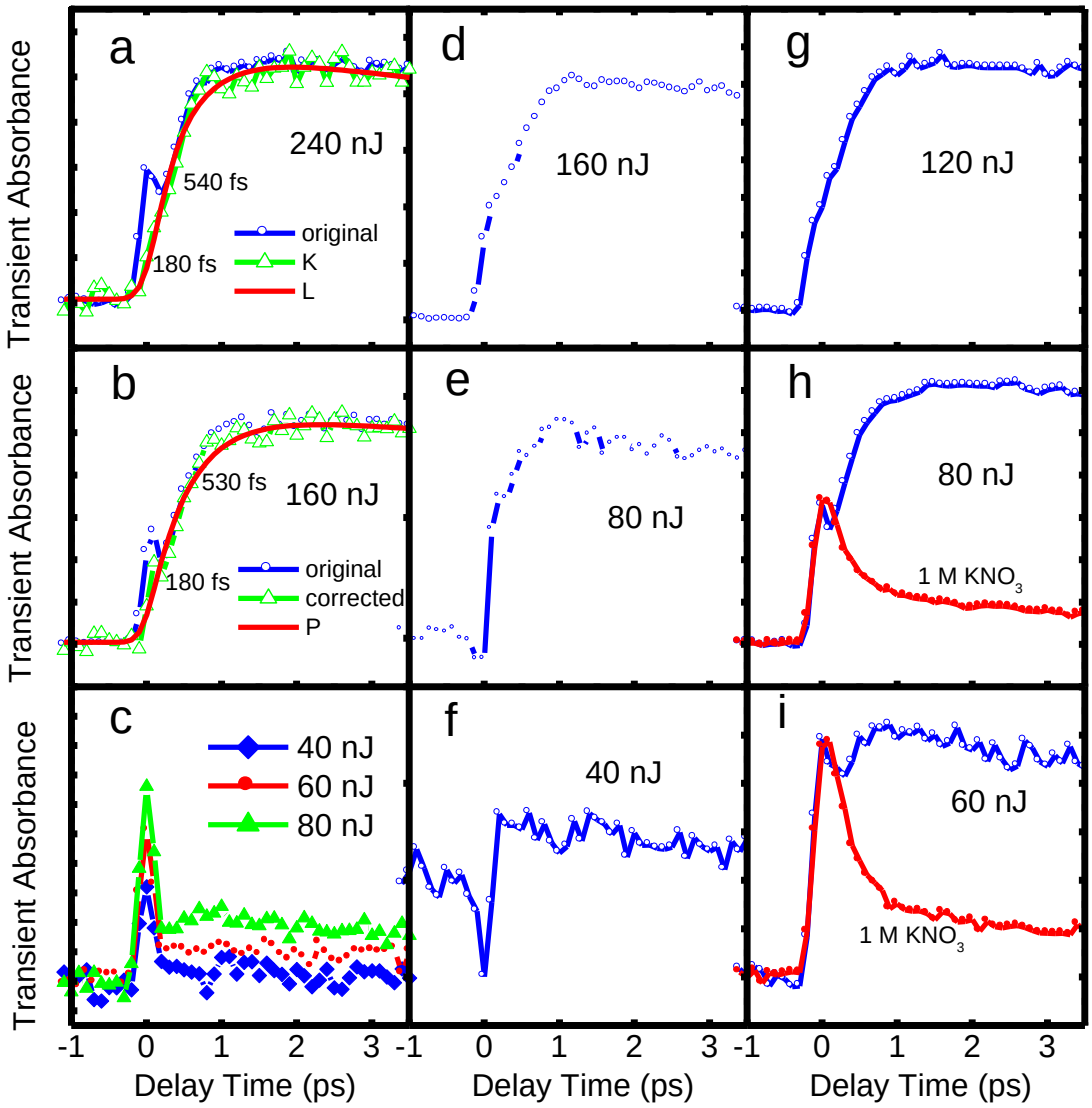
a
240 nJ
540 fs
180 fs
original
K
L
d
160 nJ
g
120 nJ
b
530 fs
160 nJ
180 fs
original
corrected
P
e
80 nJ
h
80 nJ
1 M KNO3
c
40 nJ
60 nJ
80 nJ
f
40 nJ
i
60 nJ
1 M KNO3
Transient Absorbance
Transient Absorbance
Transient Absorbance
-1 0 1 2 3
Delay Time (ps)
-1 0 1 2 3
Delay Time (ps)
-1 0 1 2 3
Delay Time (ps)

Figure 5.3.

Figure 5.3. Femtosecond transient absorption kinetic traces of the hydrated electron e_{hyd}^-, measured with experimental conditions similar to those for Fig. 5.2, but probed at 612 nm. Left column (*a*-*c*): the data were collected at the pump-probe overlap position moved from ~500 μm to 150 μm from the cell front surface without re-optimization of the electron signal, with various pump power (240-40 nJ/pulse); a linear dependence of the sharp peak intensity at delay zero on pump power under 80 nJ/pulse can be seen in *c*. In *a* and *b*, the corrected kinetic traces, after the artificial spike was linearly extrapolated from the lowest pump power (40 nJ/pulse) to the corresponding pump power and was subtracted from the original traces, are also shown, together with the best fits (solid lines) with the fitted rise times indicated. Center column (*d*-*f*): the data were collected with various pump power (160-40 nJ/pulse), at the pump-probe pulse spatial overlap position in water of ~500 μm from the cell front surface where the electron signal was optimized. Right column (*g*-*i*): the data were collected with various pump power (120-60 nJ/pulse), at the pump-probe overlap position moved from ~500 μm to 800 μm without re-optimization of the electron signal; the measured kinetic traces for the presence of 1 M KNO_3 in water with pump power at 80 and 60 nJ/pulse are also shown in *h* and *i*, respectively.

As a matter of fact, the narrow peak at delay time zero is not the electron signal but simply the coherence spike, which has previously been studied by Eisenthal et al. [277], Fleming et al. [278] and Kovalenko et al. [279]. This non-resonant coherence spike manifests itself especially in a high photon flux density and is especially well-known in fs pump-probe experiments using a supercontinuum probe [141, 279]. The spike has been explained as mainly due to conventional stimulated Raman scattering (SRS) or impulsive stimulated Raman scattering (ISRS) [141, 279]. SRS gives a sharp peak in the transient signal of the solvent if the difference between pump and probe frequencies matches a vibrational mode in the electronic ground state. In ISRS, in contrast, an ultrafast pump pulse excites low-frequency modes in the electronic ground state of the solvent, which lead to scattering of the probe light and thus give rise to a signal at any probe wavelength. It was first predicted by Nelson et al. [280] that ISRS should occur, without laser intensity threshold, when a sufficiently short laser pulse passes through many types of matter such as molecules and various solids. Scherer et al. [281] have shown that ISRS is actually the mechanism which induces coherent vibrational motion of molecules observed in either the transient grating geometry (TG-ISRS) or geometries employing only a single excitation beam, which can provide valuable information about the nature of molecular dynamics in neat liquids. It should be noted that the spike effect is dependent on relative polarizations of pump and probe pulses, but it can be significant even at perpendicular polarizations in pump-probe transient absorption kinetic traces, especially for ultrashort pulses [277].

In our experiments, three major observations give clear evidence of the narrow peak at delay zero being the coherence spike. First, a symmetric sharp peak, whose intensity has an excellent linear dependence on pump power, is observed at low pump power (Fig. 5.2f and Fig. 5.3c), at which the produced electron signal is negligible. Because of the quadratic

pump-power dependence of the signal of electrons generated by two-photon UV excitation, the coherence spike becomes less visible at high pump power, where the electron signal becomes dominant. The poorer linearity of the pump-power dependence of the spike intensity as the pump-probe spatial overlap point goes deeper into the water bulk (e.g., at 500-800 μm) can be well explained by the non-linear energy loss of the pump pulse during its penetration in the bulk. Second, the assignment of the narrow peak at delay time zero to the coherence spike is further confirmed by the experiments with addition of a strong precursor electron scavenger, KNO_3. It is clearly shown in Fig. 5.2i, Fig. 5.3h and Fig. 5.3i that at the concentration ~1 M of KNO_3, the electron signal is almost completely depleted, while the narrow peak intensity is almost unchanged. Third, as shown in Fig. 5.2i, the amplitude of the spike revealed by addition of 1 M KNO_3 electron scavenger into water at the pump power of 360 nJ/pulse is nearly the same as that linearly extrapolated from the naked spike measured at 140 nJ, i.e., as the spike at 140 nJ times 360/140. These facts give clear evidence that the narrow peak at delay zero is not the electron signal but solely the coherence spike. Although its presence complicates the extraction of electron hydration time scales from the kinetic traces, the coherence spike can be used as a means for direct, in-situ determinations of not only the delay time zero but the instrument temporal response, which are otherwise difficult to obtain in pump-probe experiments [245]. This can be achieved by measuring the position and the FWHM of the peak [279], since the coherence spike corresponds to the optimum temporal overlap between pump and probe pulses. A constant FWHM (~300 fs) of the spike is observed for a large penetration range (150-800 μm) of pump and probe pulses in water prior to their spatial overlap. This indicates that the group-velocity mismatch, as discussed by Lu et al. [245], has a minimal effect in the present experiments though a 5mm sample cell was used. This is because the pump-probe overlap point

never goes too deep (<1000 μm) in the bulk in order for a sufficient electron signal to be detected (limited by the energy loss of the pump-pulse penetration in water). Thus, the experimental results with water held in a 5mm sample cell should be the same as those obtained with a water jet of a few hundred μm diameter. Extrapolating the linear pump-power dependence of the spike intensity from the lowest pump power to high pump power, we can nearly completely remove the spike from the kinetic traces of e_{pre}^- and e_{hyd}^- measured at high pump power, as shown in the corrected kinetic traces of e_{pre}^- and e_{hyd}^- in Fig. 5.2g, Fig. 5.2h, Fig. 5.3a and Fig. 5.3b. The best fits to the corrected traces give a rise time of 150-182 fs and a decay time of 520-550 fs for e_{pre}^- (Fig. 5.2g and Fig. 5.2h). Similarly, we obtained two rise times of 180 fs and 530-540 fs for the corrected kinetic trace of e_{hyd}^- (Fig. 5.3a and Fig. 5.3b). After the removal of the spike, the kinetic traces of e_{pre}^- and e_{hyd}^- become independent of the pump power. Generally, these corrected kinetic traces are very close to those obtained with a low photon flux density shown in Fig. 5.1a and Fig. 5.1b. These results provide clear evidence that the spike is indeed responsible for the ultrashort rise or decay in the kinetic traces of e_{pre}^- and e_{hyd}^- observed here and it can be removed with careful measurements of the pure spike at low pump power. After the removal of the spike, the intrinsic lifetimes of two e_{pre}^- states are measured to be 180±30 fs and 545±30 fs in bulk water with a greater accuracy. These results agree well with some of the time scales reported in previous experiments where the sharp peak (spike) at delay zero was removed [141, 239], and are consistent with MD simulation results [216, 247-248].

After determining the intrinsic lifetimes of the two e_{pre}^- states, we now show an approach to reveal their physical nature. In chapter 4, we have shown that the nature, lifetimes and

reactivity of non-equilibrium e_{pre}^- states can be directly determined by real-time measurements of the transition states of their resonant electron transfer reactions with some quantum-state-specific probe molecules, namely, halopyrimidines (XdUs, X=Cl, Br and I). XdUs are an ideal probe for e_{pre}^- because their resonance energies for dissociative electron attachment in water are exactly around the binding energies of electronically excited e_{pre}^- states. Thus, any electronically excited e_{pre}^- states, if they exist, will be directly observed by real-time measurement of the transition state XdU^{*-} of the dissociative-electron-transfer (DET) resonant reaction: $e_{pre}^- + XdU \rightarrow XdU^{*-} \rightarrow X^- + dU^{\bullet}$. Just like the appearance kinetics of the hydrated electron, the rise kinetics of the XdU^{*-} signal corresponds to the decay kinetics of e_{pre}^-. The lowest-energy limits of DET of XdUs in water, leading to the formation of $CldU^{*-}$, $BrdU^{*-}$ and IdU^{*-}, were estimated to lie at –1.01, –1.24 and –1.42 eV, respectively, below the vacuum level [217]. The p-like excite state of e_{hyd}^- lies at ~–1.5 eV below the vacuum level, inferred from the absorption peak of e_{hyd}^- at 1.7 eV (~720 nm), which is believed as a transition from the s ground state at ~–3.2 eV to the p excited state in bulk water [238, 272]. DET is therefore expected to occur for all XdUs, CldU, BrdU and IdU, with the first weakly-bound e_{pre}^- state that has the energy slightly higher than the lowest p-like excited state of e_{hyd}^-. More specifically, a second DET channel can only occur for IdU with the p-like excited state when the energy-level broadening in the liquid is taken into account. Consequently, DET from electronically excited e_{pre}^- states to XdUs can occur with the expected efficiency: IdU>BrdU>CldU. This prediction is in good agreement with direct measurements of the reaction transition states XdU^{*-} which have an absorption peak at ~330 nm. Indeed, we have observed that the kinetic traces of $CldU^{*-}$

and BrdU*$^-$ show a single peak at ~0.55 ps and the fits to the data give a rise time of ~150 fs [See Chapter 4].

Transient absorption kinetic traces of IdU*$^-$ formed by DET of e_{pre}^- generated by two-320 nm photon excitation of water, measured with probe wavelengths around 330 nm (in the range of 325-335), are shown in Fig. 5.4. Indeed, two visible bumps are observed in the corrected kinetic traces of IdU*$^-$ after the spike was removed: the first peak appears at ~0.55 ps and the second is visible at ~1.0 ps. This observation immediately provides qualitative evidence of the existence of two e_{pre}^- states leading to the formation of IdU*$^-$. Furthermore, the quantitative fits to the data give two rise times and two decay times for each kinetic trace of IdU*$^-$ probed at wavelengths around 330 nm. Note that this fitting using a least-squares program is to achieve a minimum deviation between the experimental and fitted data for the whole time delay range from –2 ps to 12 ps, rather than to achieve the best fit just in the time delay range around the small bumps at 0.5-1.0 ps. Thus, the experimental data, though they have a reasonably good signal to noisy ratio, do not allow the fits to reproduce the tiny bumps. As shown in Fig. 5.4b, nevertheless, the best fits reproduce the whole kinetic trace curves fairly well. The two fitted rise times and two fitted decay times are respectively τ_1=161 ±30 fs, τ_2=545±30 fs, τ_3=1.81 ±0.20 ps and τ_4 fixed at 10 ns. Similar to the kinetic trace for BrdU*$^-$ [216-217], the τ_3 and τ_4 decay times correspond to the dissociative lifetime of IdU*$^-$ and the lifetime of the relaxed anion IdU$^-$, respectively. Here, the most interesting result is the two rise times (formation) of the transition state IdU*$^-$, resulting from two corresponding e_{pre}^- states. As mentioned above, the lowest-energy limit for DET with IdU lies at –1.42 eV, while the s ground

state of the hydrated electron is located at ~–3.2 eV. Thus, no 'hot' or 'cold' s-like ground e_{pre}^- states could lead to DET to IdU. As a result, it is now clearly revealed that both the first e_{pre}^- with a lifetime of ~180 fs and the second e_{pre}^- with a lifetime of ~545 fs must be electronically excited states of e_{hyd}^-. As shown in Fig. 5.4b, the extremely strong spike at delay zero slightly affects the rise of the electron signal even after the correction and unavoidably leads to a slight shortening in the fitted rise of the 180 fs component. But this effect should be negligible on the fitting leading to the 545 fs component, as the second bump at ~1.0 ps is far from the sharp spike. The results thus give a direct answer to a long-standing question of whether the "wet electron" of a ~540 fs lifetime is a p-like excited state or an s-like ground state of e_{hyd}^-. In other words, the present results provide the first direct evidence that the 545 fs process is the decay lifetime of the p-state that has a binding energy of ~1.5 eV. This conclusion disagrees with some reports in experiments [243-244] and simulations [254], but agrees with the mixed quantum-classical non-adiabatic dynamics simulations of the excited-state hydrated electron [244-245, 278] and with the excited-state model of the wet electron proposed in earlier experimental studies [141, 239].

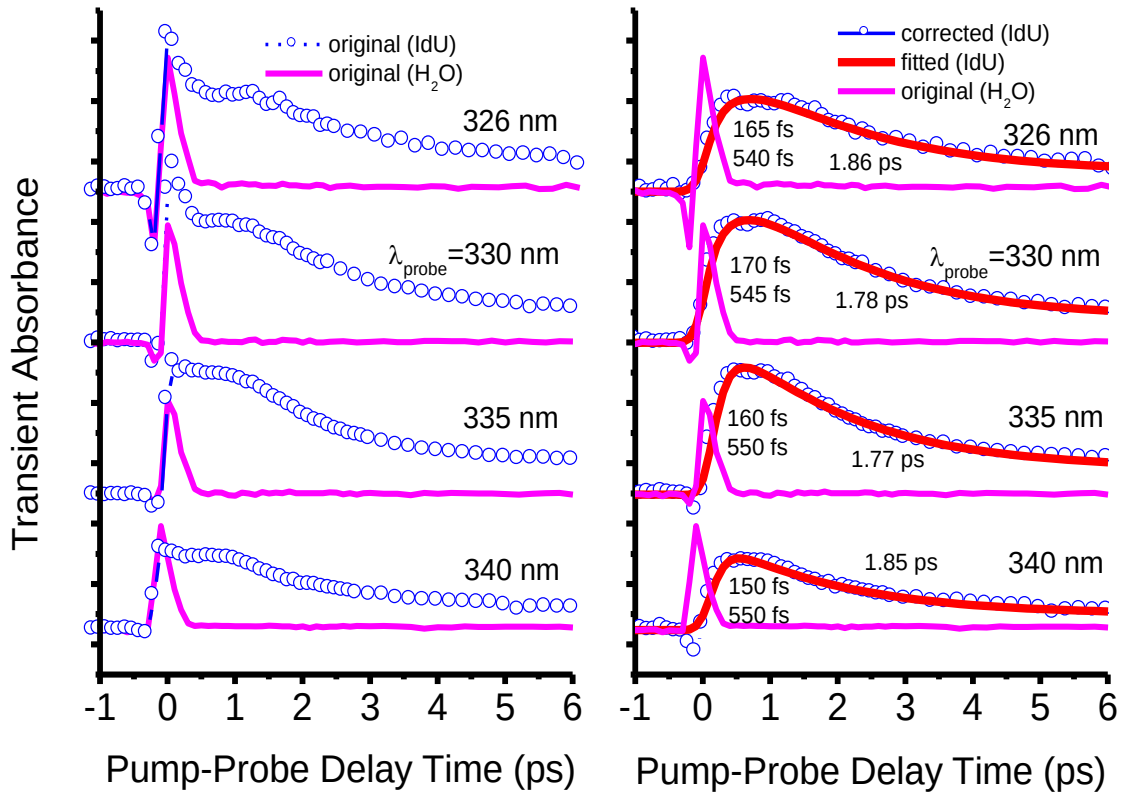

Figure 5.4. a: Femtosecond transient absorption kinetic traces of 3.6 mM IdU, pumped at 320 nm and probed at various wavelengths (326-340 nm), where the kinetic traces for the pure water, exhibiting a strong coherence spike at time zero, are also shown (fine dash lines). b: Corrected kinetic traces of IdU after the subtraction of the kinetic trace for the pure water from the traces shown in left column to remove the artificial coherence spike; the solid lines are the best fits to the corrected kinetic data (open circles) with a model of four-exponential functions which are convoluted with the instrument response function represented by a Gaussian function. The two rise times and one decay time for the corrected IdU^{*-} signal given by the best fits are also indicated.

5.4. Conclusion

We have shown that the existence of the coherence spike can significantly affect the measured dynamics of a transient species in ultrafast pump-probe spectroscopic measurements. This effect is most likely responsible for the long-standing significant discrepancies and controversies about electron hydration dynamics and about the nature of non-equilibrium e_{pre}^-. We have also shown that to obtain reliable and precise information on electron hydration dynamics from pump-probe measurements, special cautions must be taken to account for the coherence spike at delay zero. This hidden spike effect can result in a shortening of measured e_{pre}^- lifetimes from ~1 ps to almost zero fs, especially for a highly focused pump pulse. The spike is not the electron signal in nature and could thus be removed from the collected kinetic-trace data of e_{pre}^- and e_{hyd}^-. After this treatment, we have clearly shown that there are two intrinsic e_{pre}^- states that have lifetimes of 180±30 fs and 545±30 fs, respectively. Moreover, our direct, real-time measurements of the reaction transition state of e_{pre}^- with a probe molecule (IdU) have revealed that both the 180 fs and the 545 fs e_{pre}^- state are electronically excited states of e_{hyd}^-. More specifically, the latter (545 fs) is proved to be the decay lifetime of the p-state of e_{hyd}^-, the long-sought wet electron. These results not only resolve the outstanding discrepancies existing in the literature but provide new insights into electron hydration dynamics in bulk water. Such information is important for quantitative understanding and modeling of the role of non-equilibrium e_{pre}^- in electron-driven reactions in diverse systems from radiation chemistry and radical chemistry [246, 257-258, 276, 282-283], radiation biology [47], atmospheric ozone depletion [284], to the activation of radiosensitizers in cancer therapy [216-217]. It has clearly

been demonstrated that the reaction with non-equilibrium e_{pre}^-, rather than with the equilibrium e_{hyd}^-, is the major channel leading to breakups of environmentally and biologically important halogen-containing molecules under ionizing radiation [216-217, 285].

Chapter 6

Bond Breaks of Nucleotides by Dissociative Electron Transfer of Non-Equilibrium Prehydrated Electrons: A New Molecular Mechanism for Reductive DNA Damage

6.1. Introduction

A much deeper understanding of fundamental mechanisms of cancer biology and therapies can lead to improved clinical outcomes. Understanding the fundamental mechanisms and molecular pathways that induce DNA damage and cell death should lead to a clearer picture of the cause of cancers and benefit the development of improved strategies for cancer treatment. In fact, DNA damage is a central mechanism in the pathogenesis and treatment of human diseases notably cancer. In chapter 2, DNA damage induced by ionizing radiation has been reviewed. In the conventional context of radiobiology, it has long been believed that ·OH radical is the major culprit in causing DNA damage under ionizing radiation. However, there is still 30-65% 'non scavengable' double strand breaks (DSBs) [12, 124-131, 286], even when very high concentrations of ·OH scavengers up to 2M were used. The 'non scavengable' DNA damage has conventionally been attributed to direct action of radiation in the DNA [12, 124-131, 286]. However, this attribution is inconsistent with the observed enhancement *by orders of magnitude* of ionizing-radiation-induced damage of DNA in the presence of water solution, compared with

dry DNA [132]. From a general description in biology and medicine, *little is known about reductive DNA damage both in causing genetic mutations during oncogenesis and killing cancer cells during radiotherapy*.

With the advent of femtosecond (fs) laser spectroscopy, it has been found that there exist precursors to the fully hydrated electron, denoted as e_{pre}^-. e_{pre}^- is a novel electron species produced in radiolysis of water, which was first experimentally observed in 1987 [139]. Although experimental and theoretical studies once gave very diverse lifetimes and physical natures of e_{pre}^-, we have shown that they are electronically excited states and have lifetimes of ~180 and 540 fs after our finding and removal of the artifitial effect caused by the coherent spike, as discussed in Chapter 5. e_{pre}^- is a weakly bound electron at (–1.5 to –1.0 eV) [217, 287] and has the highest quantum yield, which is nearly double that of its ending product (e_{hyd}^-) [142] or the ·OH radical. There is evidence that e_{pre}^- can be attached to amino acids and nucleotides: Hunt and co-workers [256] obtained indirect evidence by monitoring the initial yield of e_{hyd}^- at 30 ps in picosecond radiolysis, while Gauduel et al. [257-258] observed ultrafast one-electron reduction of oxidized pyridine nucleotides and cystamine by e_{pre}^-. In general, however, the potential role of e_{pre}^- in inducing DNA damage is unknown, as evidenced by the fact that the potential DNA damage caused by e_{pre}^- is not even mentioned in current radiobiology [12, 100, 102, 123].

As shown and discussed in Chapter 4, we have applied our powerful fs time-resolved laser spectroscopy (fs-TRLS) to directly observe the dissociative electron transfer (DET) reaction of e_{pre}^- with halopyrimidines (XdUs) as potential radiosensitizers: $e_{pre}^- + XdU \rightarrow XdU^{*-} \rightarrow dU^{\bullet} + X^-$. The resultant $dU^{\bullet}$ radical can then cause DNA damage. Similarly, to reveal the role of e_{pre}^-

in inducing DNA damage, the reactions of e_{pre}^- with nucleotides (dXMP, X=A, G, C, and T), which are the basic units of DNA, can be directly observed in real time by using our fs-TRLS. The molecular structures of nucleotides are as shown in Fig. 6.1.

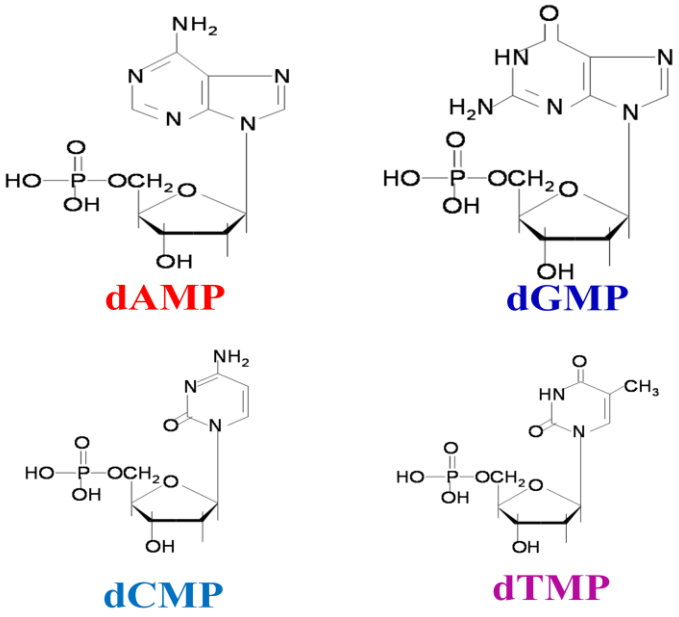

Figure 6.1. Molecular structure of nucleotides dXMP (X=A, G, C, and T) in free acid format.

6.2. Experiments

In this experiment, ultra pure water with a resistivity of > 18 MΩ/cm was used and guanine base, deoxyguanine, and nucleotides dXMP, X=A, G, C, and T obtained from Sigma- Aldrich were used as supplied. All the nucleotides were provided as sodium salts.

In transient absorbance experiments, certain sample concentrations were required. Since G and dG do not have good solubility in water and thier solubility can be enhanced by increased

solvent PH. a NaOH solution was used to obtain G and dG sample concentrations required in our experiments.

The standard methodology for pump-probe fs-TRLS transient absorption measurements has been described in Chapter 3. Similar to the observation of XdU^{*-} (X=Cl, Br and I) described in Chapter 4, a pump wavelength of 318 nm was used to generate excess electrons in water, and a probe wavelength at 330 nm was used to probe the intermediate state ($dXMP^{*-}$) of reaction of e_{pre}^- with a dXMP (X=A, G, C and T). As shown in Fig. 6.2, this is a key step in inducing DNA strand breaks. The fs-TRLS allows us to observe the DET reaction in real time. The formation and decay of the $dXMP^{*-}$ can be expressed in the following reaction:

$$e^-_{pre}\ (<0\ eV) + dXMP \rightarrow dXMP^{*-} \rightarrow \text{dissociation} \quad .....6.1$$

$$\text{or} \quad \rightarrow dXMP^-$$

where X denotes the DNA bases (A, T, G and C), and $dXMP^{*-}$ is a vibrationally-excited intermediate anion state. It is well-known that the electronic absorption spectrum of dXMP arises solely from the excitation of the π-electron system of the DNA base X, i.e., there is no UV absorption in the phosphate group and the sugar moiety. According to the results for halo-deoxyuridine anions ($CldU^{*-}$, $BrdU^{*-}$, and IdU^{*-}) [217], the electronic absorption of $dXMP^{*-}$ or its vibrationally-relaxed anion $dXMP^-$ is expected to have an UV absorption band in 300–350 nm, slightly red-shifting from the neutral counterpart. It is also known that the autodetachment of a molecular anion resonance occurs on timescales of 10^{-16} to 10^{-14} s and the vibrational relaxation times of molecules range from 0.1 to 1.0 picosecond (ps) [288], being 0.5-1.0 ps for nucleotides [289-290]. Here the detected real-time signal is the intensity of the electronic absorption, which is identical for both dissociative $dXMP^{*-}$ and non-dissociative

dXMP^{-}, independent of the vibrational states [216-217, 285]. Thus, the signal decay ≥1.0 ps simply reflects the dissociation of transient anion (dXMP*$^{-}$), that is, a flat signal indicates no dissociation but formation of a stable anion (dXMP^{-}) only [216-217, 285].

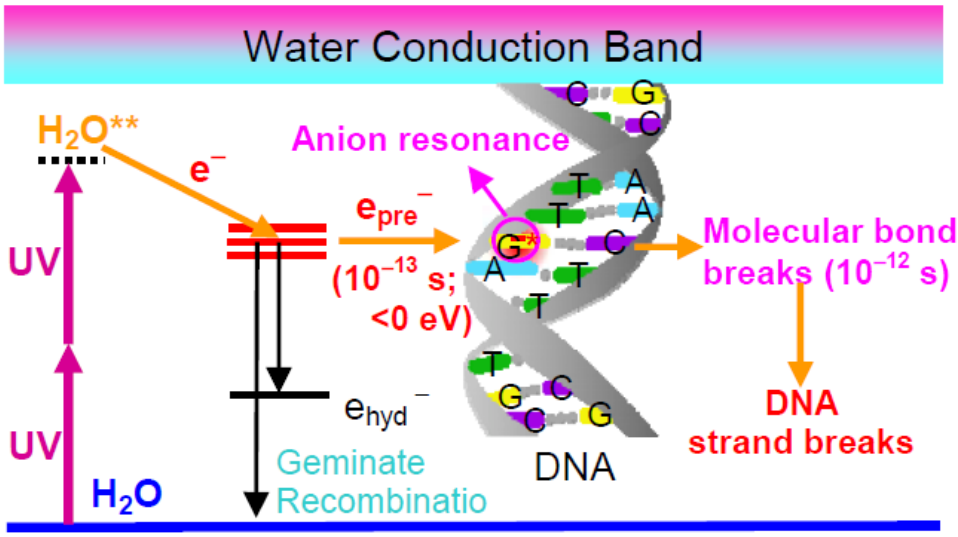

Figure 6.2. Two UV photon excitation of water leads to the formation of an electron localized at the p-like excited precursor states (e_{pre}^{-}), which then solvates to the equilibrated s-like hydrated state (e_{hyd}^{-}) . When DNA is around the e_{pre}^{-}, dissociative electron transfer (DET) can occur to form a transient molecular anion resonance that then leads to molecular bond breaks in DNA bases, followed by strand breaks of the DNA.

6.3. Results

The absorption spectrum of dXMPs is as shown in Fig. 6.3. All the four nucleotides have almost zero absorbance at wavelength ≧ 315 nm. To avoid possible absorption by any dXMP, a pump wavelength 318nm (~3.95 eV) was used to two-UV photon excite water molecules and generate e_{pre}^-. If we used pump wavelngth ≦ 315 nm, it would be difficult to tell whether the transient signal is from the excited dXMP* or from the reactions of dXMP with e_{pre}^-. The probe pulse with 330nm wavelength was used to observe the $dXMP^{*-}$ / $dXMP^-$ resulting from the reaction.

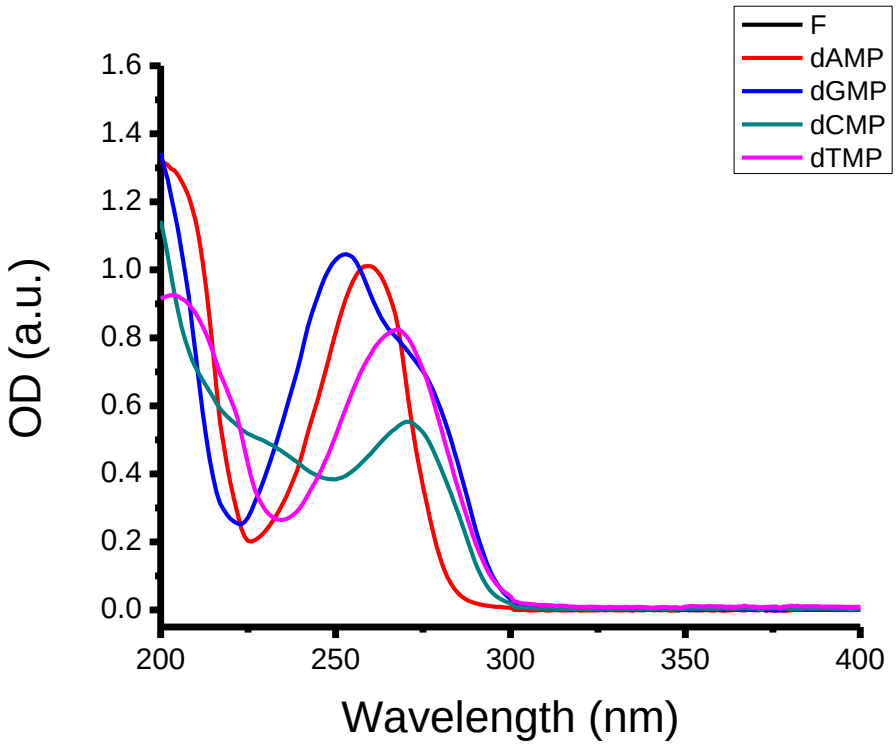

Figure 6.3. Static absorption spectrum of dXMP (X=A, G, C, and T) in pure water at room temperature.

The original transient absorbance kinetic traces of the nucleotide samples and the solvent H_2O are shown in Fig. 6.4. As mentioned in chapter 4, the absorption band of e_{hyd}^- peaks at 720 nm while it has a tail extending to the UV range even below 300 nm. The e_{hyd}^- signal was observable at probe wavelength 330 nm, as shown in Fig. 6.4. As a reult, the transient absorbance signal detected at 330 nm of the four nucleotide aqueous samples is composed of the $dXMP^{*-}$ / $dXMP^-$ signal and the e_{hyd}^- signal generated by radiolysis of water. To observe the real kinetic traces of $dXMP^{*-}$ / $dXMP^-$, the transient absorbance signal of the e_{hyd}^- signal has to be removed. This can easily be done by subtracting the signal of the pure water from those of nucleotide samples. The thus obtained real transient absorption kinetic traces of $dXMP^{*-}$/$dXMP^-$ are shown in Fig. 6.5.

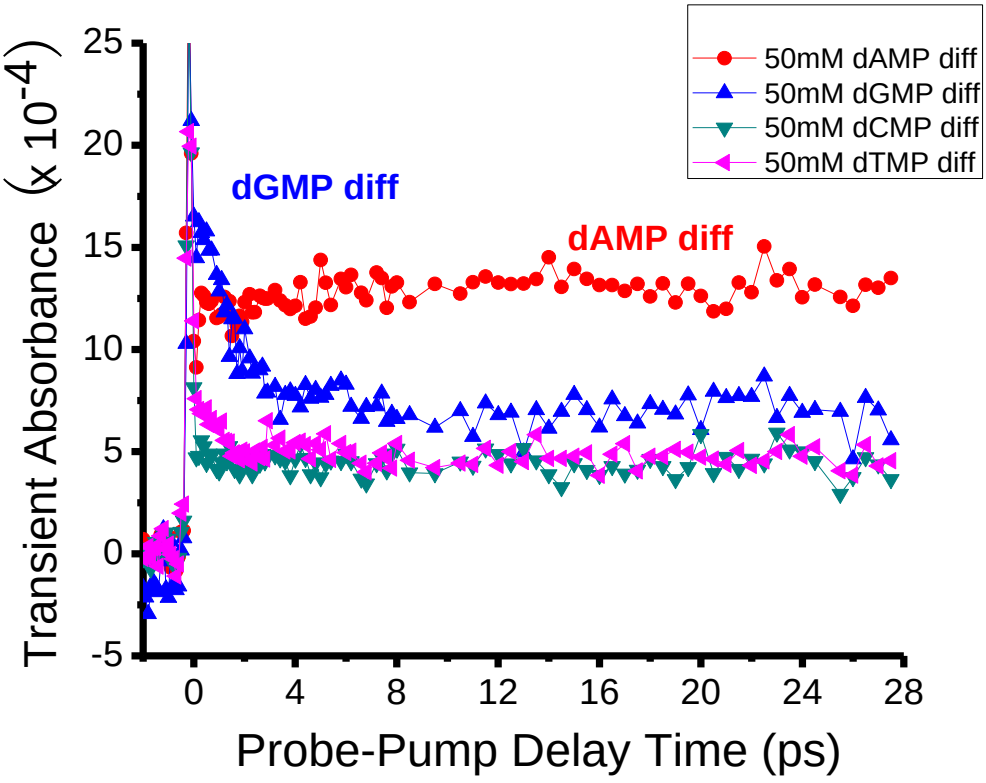

Figure 6.4. Femtosecond transient absorption kinetic traces of $dXMP^{*-}$ resulting from the DET reactions of e_{pre}^- with 50mM dAMP, dGMP, dCMP and dTMP in water, pumped at 318 nm and probed at 330 nm. Here, the sharp peak at time zero is the coherence "spike" of the pump and probe pulse.

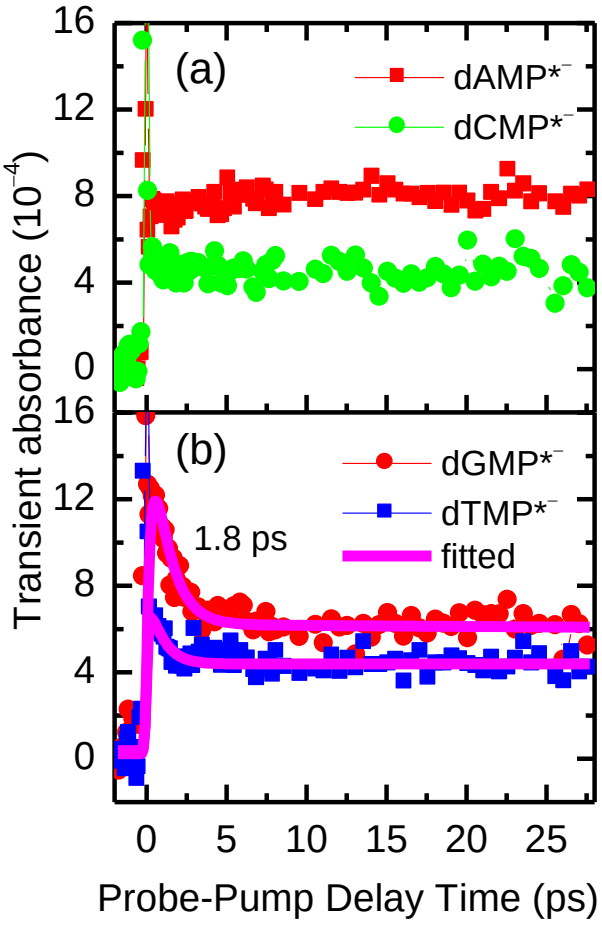

Figure 6.5. Corrected femtosecond transient absorption kinetic traces of dXMP*$^{-}$ resulting from the DET reactions of e^{-}_{pre} with (a) 50mM dAMP and dCMP; (b) dGMP and dTMP in water. All spectra were corrected after the subtraction of the spectrum for the solvent (H_2O), and the differences in absorption coefficients of dXMPs*$^{-}$ were corrected by those of neutral counterparts, which are 15.3 $\times$ 10^3, 9.3$\times10^3$, 10.2$\times10^3$ and 13.7$\times10^3$ $cm^{-1}M^{-1}$ for dAMP, dCMP, dTMP and dGMP respectively. Solid lines are the best fits to the experimental data, obtained by using a least-squares fitting program.

The fs transient absorption kinetic traces of $dXMP^{*-}$ resulting from the dissociative electron transfer (DET) reactions of dXMP with e_{pre}^- shown in Fig. 6.5 are quite interesting and surprising. First, it is interesting to observe that the formation of $dXMP^{*-}$ is complete within the lifetime (~500 fs) of e_{pre}^-. Our result shows that the electron transfer from water to nucleotides is ultrafast. Second, it is surprising to observe that purines dGMP and dAMP are more efficient in capturing e_{pre}^- than pyrimidines dTMP and dCMP. Interestingly, in previous experiments using ESR that does not have a capacity of real-time observation in the fs timescale [58, 61, 63-68, 291-306], it was shown that dCMP and dTMP would be efficient at capturing electrons, while dGMP and dAMP would tend to donate an electron and to form cations. Third, the results clearly indicate that e_{pre}^- can be attached to dAMP and dCMP to form stable anions $dAMP^-$ and $dCMP^-$ only, that is, no decay (dissociation) of $dAMP^{*-}$ and $dCMP^{*-}$ occurs. In contrast, DET of e_{pre}^- to dGMP is most efficient, forming a $dGMP^{*-}$ that dissociates rapidly within ~1.8 ps: about 60% of $dGMP^{*-}$ becomes dissociated and ~40% becomes a stable $dGMP^-$. Similarly, DET of e_{pre}^- to dTMP also occurs to form a $dTMP^{*-}$ that dissociates rapidly within two picoseconds, but only about 35% of $dTMP^{*-}$ becomes dissociated and 65% becomes a stable $dTMP^-$.

As shown in Fig. 6.1, each nucleotide consists of a phosphate group, a sugar moiety and a DNA base. However, there is no UV absorption in the phosphate group and the sugar moiety; the electron in dXMP must be captured by the DNA base. Fig. 6.5 shows that among the four nucleotides, dGMP is the most efficient at capturing e_{pre}^- and more than half of the transition state $dGMP^{*-}$ decays within 1.8 ps. Here, one might raise the question: Whether the decay

is due to the electron transfer from the base to the phosphate group or the sugar moiety or due to the direct dissociation of dGMP*$^-$? To address this possible question, we also studied the reactions of e_{pre}^- with base guanine (G), nucleoside deoxyguanine (dG) to compare them with that of dGMP. The molecular structures of G, dG, and dGMP are shown in Fig. 6.6. Unlike dGMP, G and dG have poor solubilities in water, so they were dissolved in 90 mM NaOH solutions. The absorbance spectra of G, dG, and dGMP are shown in Fig. 6.7, whereas the original and corrected transient absorption kinetic traces of G*$^-$, dG*$^-$ and dGMP*$^-$ resulting from the reactions of G, dG and dGMP with e_{pre}^- are plotted in Figs. 6.8 and 6.9, respectively

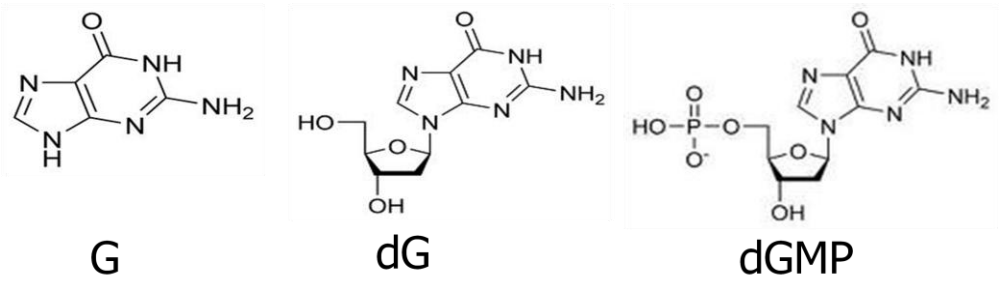

Figure 6.6. Molecular structure of G, dG, and dGMP

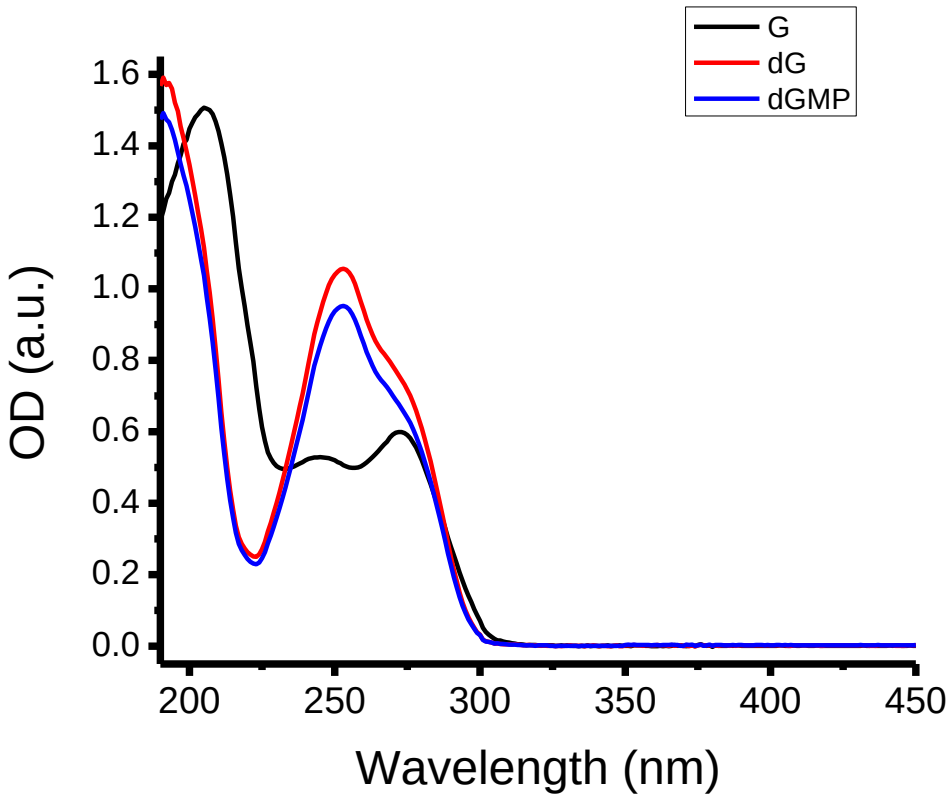

Figure 6.7. Static absorption spectra of G, dG, and dGMP

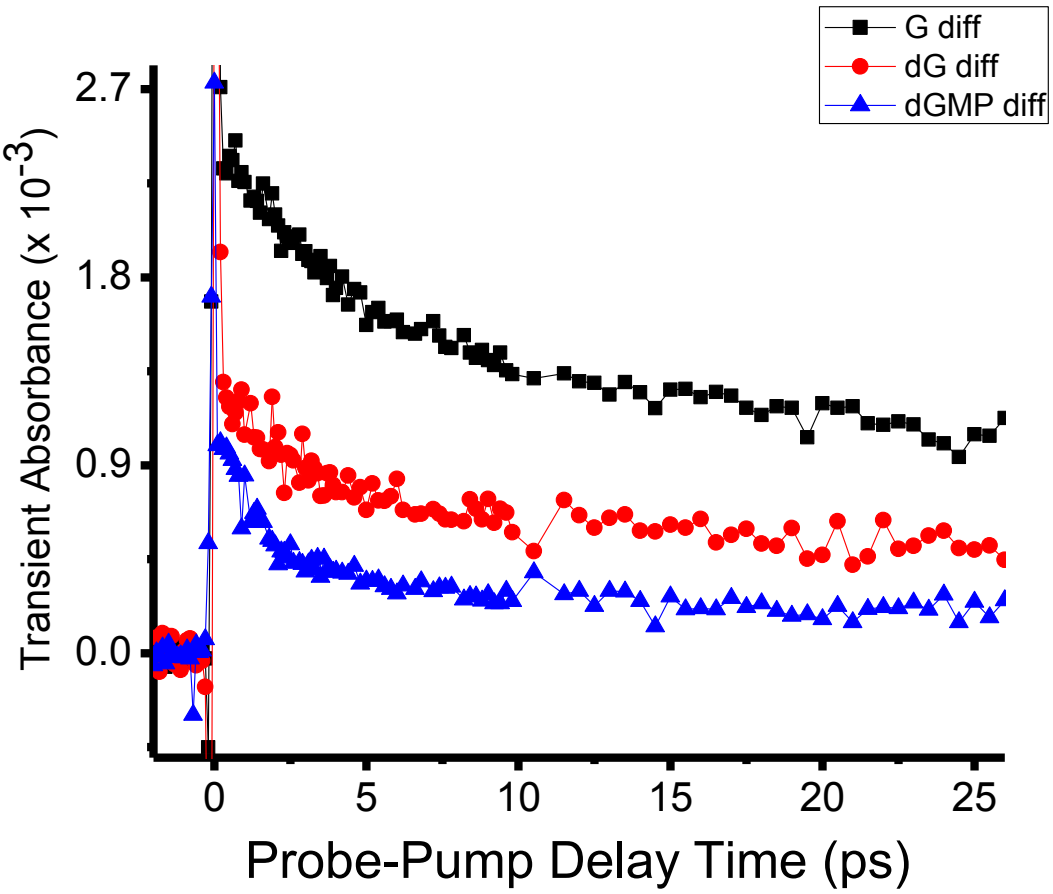

Figure 6.8. Femtosecond transient absorption kinetic traces of G, dG and dGMP*$^{-}$ resulting from the DET reactions of e_{pre}^{-} with 45.5 mM G dG and dGMP in 90 mM NaOH , pumped at 318 nm and probed at 330 nm. The sharp peak at time zero is the coherence "spike" observed due to a coherent pump-probe artifact.

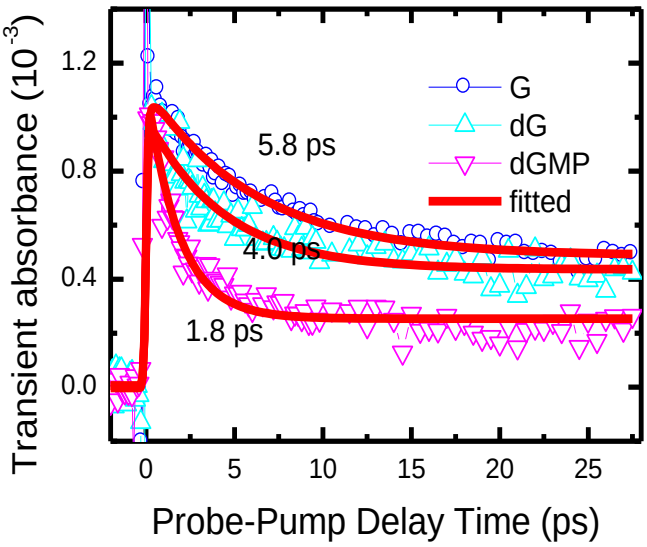

Figure 6.9. Corrected femtosecond transient absorption kinetic traces of G^{*-}, dG^{*-} and $dGMP^{*-}$ resulting from the DET reactions of e_{pre}^{-} with 45.5 mM G and dG and dGMP in 90 mM NaOH, pumped at 318 nm and probed at 330 nm. Here, the sharp peak at time zero is the coherence "spike" of the pump and probe pulse. All spectra were corrected after the subtraction of the spectrum for the solvent, and the differences in absorption coefficients of $dGMP^{*-}$, dG^{*-} and G^{*-} were corrected by those of neutral counterparts, which are 13.7×10^3, 17.1×10^3 and 30.4×10^3 $cm^{-1}M^{-1}$ for dGMP, dG and G respectively. Solid lines are the best fits to the experimental data, obtained by using a least-squares fitting program.

In the original kinetic traces shown in Fig. 6.8, G^{*-} has the highest transient absorbance signal; the intensities of the transient absorbance are in the order of: $G^{*-} > dG^{*-} > dGMP^{*-}$ with the same sample concentration. But this must be corrected by different absorption coefficients of G^{*-}, dG^{*-}, and $dGMP^{*-}$ at the probe wavelength of 330 nm, which are unknown. Thus, the transient absorbance signals of G^{*-}, dG^{*-}, and $dGMP^{*-}$ were approximately corrected by the absorbance coefficients of their neutral counterparts, which are 30.4, 17.1 and 13.7 $\times$ 10^3 M^{-1} cm^{-1} for G, dG, and dGMP, respectively. Moreover, the contribution of the solvent to the absorption signal has to be removed. Thus, the transient kinetic traces of G^{*-}, dG^{*-}, and $dGMP^{*-}$ were also corrected by subtracting the transient absorbance signal of the solvent from those of G, dG, and dGMP samples. After the two corrections, the real transient absorbance kinetic traces of G^{*-}, dG^{*-}, and $dGMP^{*-}$ are shown in Fig. 6.9.

The data in Fig. 6.9 show the following interesting observations: (1) It is clearly seen that the formation of G^{*-}, dG^{*-}, and $dGMP^{*-}$ is complete within the lifetime (~500 fs) of e_{pre}^-; (2) a clear decay of G^{*-} for the G base is seen, indicating that the direct dissociation of G^{*-} does occur; and (3) the lifetime of G^{*-} decreases in the order: G > dG > dGMP. This lifetime decrease is most likely due to the different environments around the G base in G, dG and dGMP molecules.

Finally, to study the possible influence of PH values on the transient absorption signal, we also detected the transient kinetic traces of dGMP and dAMP in different PH buffer solutions. The results are plotted in Figs 6.10 and 6.11, which show that the transient kinetic traces of

dGMP*$^-$ are independent of the PH values in the range from 4 to 9, and those of dAMP*$^-$ are independent of the PH values in the range from 6 to 9. dGMP and dAMP were directly purchased from Sigma. dGMP has better solubility than dAMP. At PH value lower than 6, dAMP compound cannot be completely dissolved to obtain the required concentration for transient absorption experiments. We did not measured the transient kinetic traces of dAMP*$^-$ at PH value lower than 6. Our results show that different PH values change neither the intensity nor lifetime of dGMP*$^-$ or dAMP*$^-$.

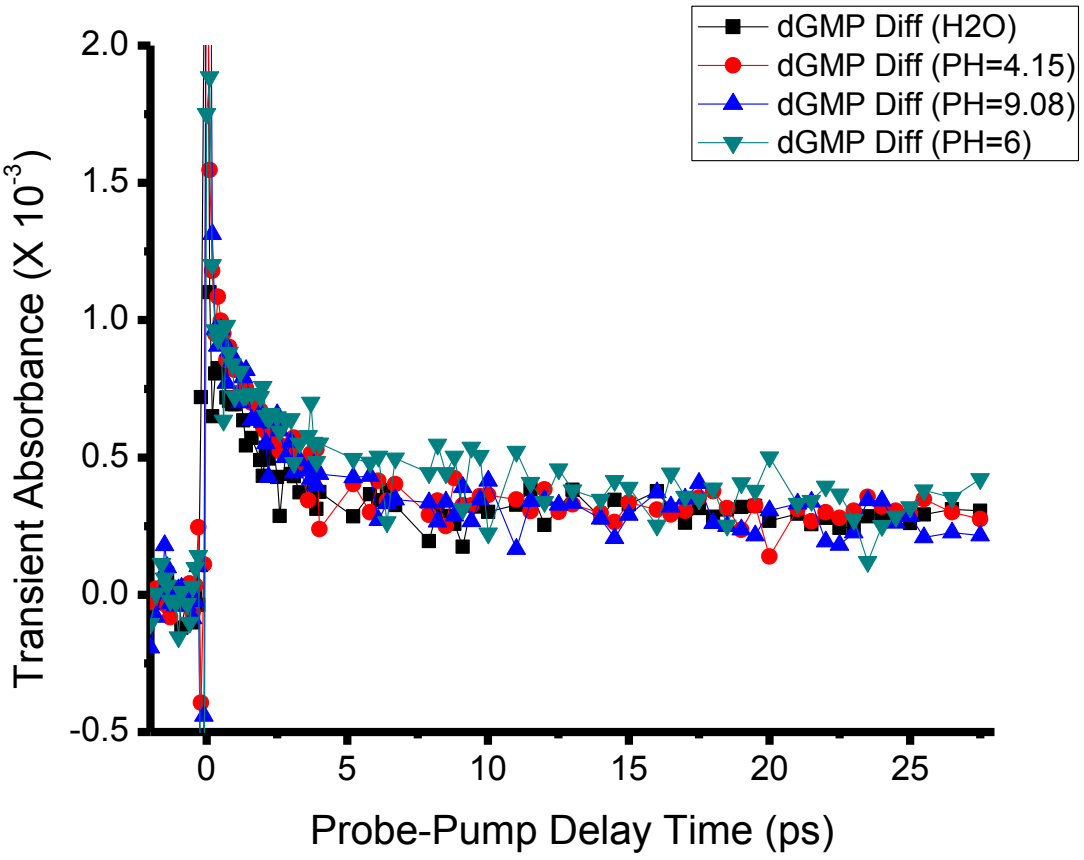

Figure 6.10. Corrected femtosecond transient absorption kinetic traces of dGMP*$^-$ resulting from the DET reactions of e_{pre}^- with 50mM dGMP in different PH buffer solutions, obtained with pump wavelength 318 nm, and probe wavelength 330 nm. Here, the sharp peak at time zero is the coherence "spike" of the pump and probe pulse. All traces were corrected by the subtraction of the trace for the solvent.

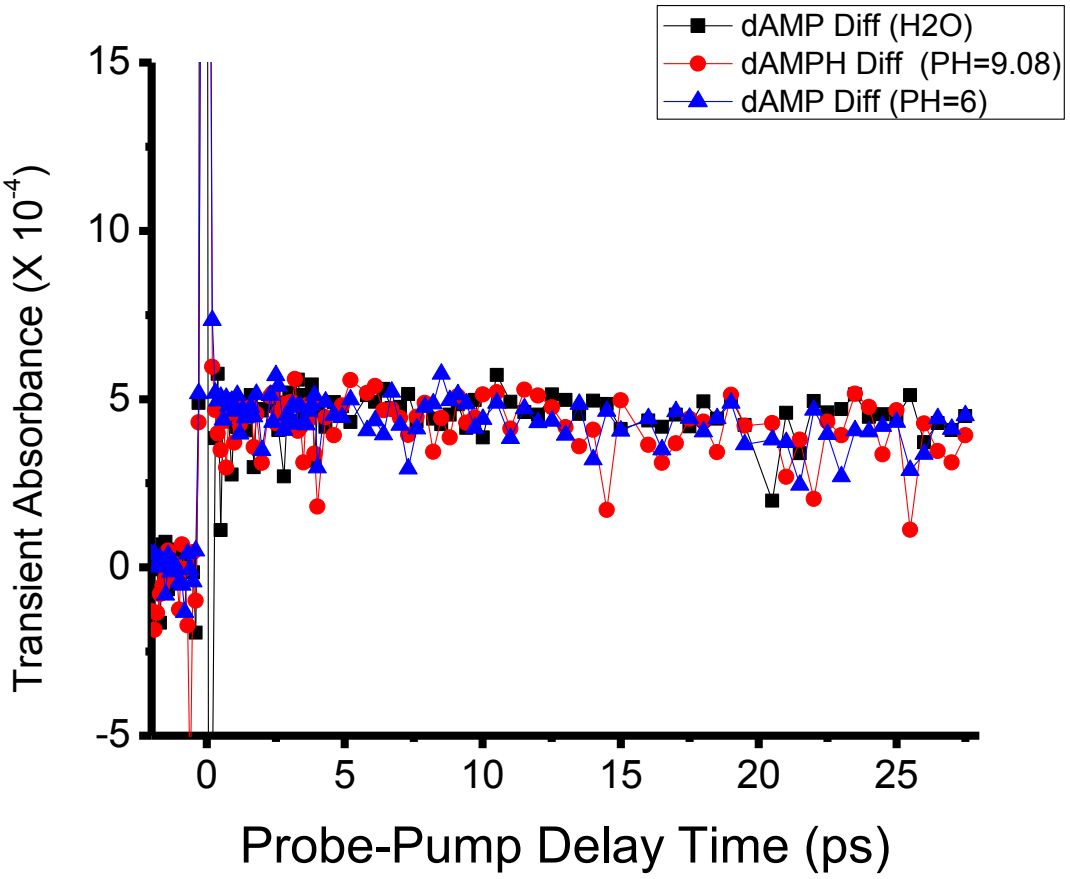

Figure 6.11. Corrected femtosecond transient absorption kinetic traces of $dAMP^{*-}$ resulting from the DET reactions of e_{pre}^- with 50mM dAMP in different PH buffer solutions, obtained with pump wavelength 318 nm, and probe wavelength 330 nm. Here, the sharp peak at time zero is the coherence "spike" of the pump and probe pulse. All traces were corrected by the subtraction of the trace for the solvent.

6.4. Discussion

As shown and discussed in Chapter 5, excess electrons produced by two-UV photon excitation of water molecules will rapidly be located in pre-existing traps within a few fs to form the e_{pre}^- states that have ultrashort lifetimes of less than 1.0 ps (~500 fs). The lifetimes of e_{pre}^- are much longer than those of free electrons in fs. The e_{pre}^- then becomes the well-bound e_{hyd}^- with a lifetime in μs. If the e_{hyd}^- had a significant contribution to the formation of $dXMP^{*-}$, the rising kinetics of the $dXMP^{*-}$ signal would not be complete within the first ps but would be observed in the timescale of μs corresponding to the lifetime of e_{hyd}^-. This is not the case, as revealed in the data shown in Figs 6.4, 6.5, 6.8, and 6.9. Instead, it is clearly seen that the formation of the $dXMPs^{*-}$ as well as G^{*-} and dG^{*-} is complete well within the ps timescale. Thus, it is obviously the ultrashort-lived e_{pre}^-, rather than the e_{hyd}^-, that reacts with dXMP and leads to the formation of $dXMP^{*-}$.

Once e_{pre}^- are captured by the DNA base in a nucleotide, what happens next? Our results in Fig. 6.5 show that $dGMP^{*-}$ and $dTMP^{*-}$ decay after they were formed, while dAMP and dCMP form stable anions. To obtained reliable information from the decay of $dGMP^{*-}$ and $dTMP^{*-}$, we have to clarify a few processes. First, it was previously reported that electron adducts of adenine nucleosides and nucleotides were protonated in water on the nitrogens (reaction rate $k \approx 1.4 \times 10^8\ s^{-1}$) [307-308] and on carbon 8 of the ring (reaction rate $k=3.6 \times 10^6\ s^{-1}$) [309-310]. From the reaction rate of protonation, however, one can deduce that the protonation occurs on the timescales ($\tau=1/k$) of nanosecond (ns) to μs. Thus the decay of G^{*-},

dG*$^-$, dGMP*$^-$ and dTMP*$^-$ within a few ps could not be due to the protonation reactions. In fact, no decay of the dAMP$^-$ signal was observed on the timescales of tens of ps. Moreover, the independence of the dGMP*$^-$ and dAMP*$^-$ signals of PH values, as shown in Figs. 4.10 and 4.11, also confirms that no protonation reactions were observed in our present fs transient absorption experiments.

Second, the electron transfer from the base to the sugar-phosphate backbone has been suggested in the literature, [91, 96, 310-312]. Thus one might suggest that the decay of dGMP*$^-$ be due to the electron transfer from the G*$^-$ to the sugar or phosphate group in dGMP. However, if effective intramolecular electron transfer from G*$^-$ to the sugar or phosphate group occurs, then similar ET would also occur for other base anions, especially A*$^-$ in dAMP*$^-$. This was not observed (Fig. 6.5). Moreover, Using BrdU / IdU as an electron acceptor, we have also observed that adenine is the most effective electron transporter among the four DNA bases after capture of an e_{pre}^- (see next Chapter), while no intramolecular ET from A*$^-$ to the sugar or phosphate group in dAMP*$^-$ was observed (Fig. 6.5).

Third, the transient absorption kinetic trace of G*$^-$ from the DET reaction of the pure G base with e_{pre}^- in Fig. 6.9 shows a decay of G*$^-$, giving clear evidence of *the direct dissociation of G*$^-$*. The decreasing lifetimes of G*$^-$ in the order of G>dG>dGMP can well be explained by the different environments around the G base in G, dG and dGMP molecules. Indeed, the absorption intensities of G*$^-$, dG*$^-$ and dGMP*$^-$ decrease in the same order as those of their neutral counterparts: G>dG>dGMP, leading to a nearly identical peak intensity after the correction as shown in Fig. 6.9.

All the above facts indicate that the suggestion of the intramolecular ET is *not* supported by our observed data. Instead, our observed data show that only T and especially G are vulnerable to DETs of e_{pre}^- leading to bond breaks, while the electron can be stably trapped at C and especially A to form stable anions. These results provide a molecular mechanism for e_{pre}^-— induced DNA strand breakage.

Our results are consistent with the experimental result by Ray et al. [313], showing that the capturing probability of ~1.0 eV free electrons by dry single-strand DNA oligomers increases with the increasing number of G bases included. Our results are also partially consistent with the recent observation of stable anionic states A^-, C^- and T^- (except G^-) in the gas phase by Bowen et al [314-315]. Our present results provide the *first real-time* observation of the DET-induced *dissociations* of G and T and the formation of all four stable anions (A^-, G^-, C^- and T^-) in *aqueous solution*.

Our results are also consistent with the theoretical results by Schaefer et al. [316], who studied the radicals generated by homolytic cleavage of an X-H bond from the guanine·cytosine (G C) base pair. They found that the lowest-energy base pair radical had the hydrogen atom removed from the guanine nitrogen atom that is used for the sugar phosphate linkage in DNA. In the biological system, the dissociation products of guanine (G) base further reacts with DNA molecules, either the sugar moiety, or other bases, causing DNA strand breaks and finally cell death.

It is interesting to compare our results about indirect DNA damage induced by DETs of weakly-bound e_{pre}^- produced by radiolysis of water with those for *direct* DNA damage by dissociative electron attachments (DEAs) of low-energy (0-20 eV) *free* kinetic electrons

generated by high-energy incident ionizing particles. There are essential differences between the DET process in water and the DEA with low energy free kinetic electron (0-20 eV) in the gas phase. For the latter process, when a free electron is resonant in kinetic energy with an anion molecule state, DEA can take place to form molecular fragments carrying the excess energy from the balance between the electron kinetic energy and the dissociation energy of the molecule anion. In 2000, Boudaïffa et al. [78] reported the first experimental result that DEAs of 3-20 eV free electrons cause strand breaks (SSBs and DSBs) of dry DNA in vacuum. Subsequently, Martin et al. [86] showed a higher yield of DNA SSBs at ~1 eV electrons but no yield of DSBs induced via DEA shape resonances of 0-4 eV free electrons. In 2005-2006, Illenberger et al. [87-88] reported experimental results for DEAs of near 0 eV electrons to gaseous DNA bases and the phosphate group. The experimental findings of Mark, Illenberger and co-workers [317-318] for the decomposition of D-ribose and thymidine by low-energy free kinetic electrons showed that migration of the excess electron from the anion of the nucleobase to DNA backbone is inhibited. But none of those experimental studies were performed in aqueous solutions.

Recent theoretical studies have searched for the possible effects of the aqueous environment on DEA-induced SSBs of DNA but reported very controversial results. Simons et al. [89] proposed that SSBs can effectively occur via formation of a π^* anion resonance at the DNA base after attachment of an excess electron of <1 eV if the DNA is stabilized by water solvation; the subsequent ET to the phosphodiester C-O bond results in the bond dissociation and a SSB. In contrast, Illenberger [317-318] and Sevilla [95] concluded that it is difficult for such an ET pathway to occur and will not cause DNA strand breaks in aqueous systems, while Schyman and Laaksonen [96] recently made an opposite conclusion for aqueous dGMP. Gu et al. [93-94] concluded that anions of pyrimidine nucleotides (dCMP and dTMP) would be more

electronically stable and thus more likely to cause DNA strand breaks. However, it is the bond break of dissociative transient anions that have ultrashort lifetimes of only a few ps that plays a crucial role in causing strand breaks of DNA. In fact, not a single theoretical model has predicted all essential features in our observed data: DETs only occur with dGMP and dTMP to cause DNA strand breaks, whereas each of dAMP and dCMP can only attach an electron to form a stable anion; the efficiency to form a stable anion is in the order of A>G>C~T. Thus, our experimental results have provided new challenges to the theoretical models.

The observed facts have indicated that water plays a dominant role in causing SSBs and DSBs of aqueous DNA under ionizing radiation [132]. But the water environment is unlikely to enhance DEAs of molecules at electron energies higher than 1.0 eV [91, 312]. In fact, Lu and Sanche [97-99] have observed that DEAs of many molecules to low-energy free electrons with energies above 1.0 eV, effective in the gas phase, are completely quenched when they are absorbed on H_2O ice due to the polar environment. As mentioned in Chapters 2 and 5, free electrons in water are rapidly trapped by surrounding H_2O molecules to form a weakly bound e_{pre}^- at around −1.5 eV. It is most likely that water has a protective effect on the DNA potentially damaged by DEA resonances at free electron energies above 1.0 eV. Instead, the DEA cross sections of the molecules to ~ 0 eV electrons were observed to be significantly enhanced by the presence of H_2O ice, which is due to the DET mechanism: the ~0 eV electron is first trapped to become an e_{pre}^- in the polar media, which is subsequently transferred to a molecule followed by its dissociation. As we have recently demonstrated for halopyrimidines [139, 216-217] and CCl_4 [285], the DEA resonances at near 0 eV electron energies in the gas phase shift to ~ −1.0 — −1.5 eV in water due to the polarization effect, in resonance with e_{pre}^- in energy, so that effective DETs of e_{pre}^- to these molecules were observed.

DSBs can be induced by the DET process of G or T. The bond dissociation induced by DET can result in SSBs on one strand of the DNA, and the dissociation products can then react further to break the other strand of the DNA. One e_{pre}^- can in this way produce multiply damaged sites, thus amplifying the complexity of DNA lesions as a single radiation track. Indeed, both SSBs and DSBs induced by e_{pre}^- of aqueous DNA under ionizing radiation were recently found by our group [220]. In that study, our fs-TRLS studies showed surprising but direct evidence that the so-called ·OH scavengers (iso-propanol and DMSO) widely used to study the effect of ·OH radicals in causing DNA damage can also scavenger e_{pre}^- as well. The observed decrease of DNA damage with the addition of iso-proponol and DMSO is not simply due to the scavenging of ·OH radicals only but is complicated by the scavenging of e_{pre}^- as well [220]. After taking this factor into account, we strikingly found that the yield of reductive DNA strand breaks induced by each e_{pre}^- is approximately twice the yield of oxidative DNA strand breaks induced by each ·OH radical [220].

6.5. Conclusion

In summary, we present the first real-time observation of dissociative electron transfer reactions of e_{pre}^- with DNA nucleotides in aqueous solutions. Our results show that purines (A and G) are more efficient at capturing e_{pre}^- than pyrimidines (C and T). Our data show that only T and especially G are vulnerable to DETs of e_{pre}^- leading to bond breaks, while the electron can be stably trapped at C and especially A to form stable anions. The results not only challenge the

conventional notion that damage to the genome by ionizing radiation is mainly induced by the oxidizing ·OH radical , but provide a deeper fundamental understanding of the molecular mechanism of the DNA damage caused by a reductive agent (e_{pre}^-). These findings can be applied to develop new strategies for more effective radiotherapies of disease such as cancer. The DET reaction pathway involving e_{pre}^- can be feasibly used to design drugs to cause DNA damage and kill tumour cells effectively. Furthermore, the direct observation of DNA base specific damage by DET of weakly bound electrons has a broad significance, as there are lots of weakly-bound electrons in biological systems. The resultant DNA strand breaks, if not repaired quickly, could cause genetic mutation and even serious diseases such as cancer. The oxidative damage at the guanine (G) base and its relation to human cancers have been well exploited. The present findings of the most fragile point at the G base and a new molecular mechanism of *reductive* DNA damage could also play a vital role in various diseases such as cancer and stroke. This work may therefore have general significance for a deep understanding of DNA damage and repair processes in biological systems and for developing effective therapies for various diseases such as cancer and stroke.

Chapter 7

Molecular Mechanisms of the DNA Sequence Selectivity of BrdU/IdU as Potential Radiosensitizers

7.1. Introduction

Direct, real-time observation of molecular reactions is of significant importance in diverse fields from chemistry and biology, environmental sciences to medicine. As introduced in Chapter 3, *femtosecond time-resolved laser spectroscopy* (fs-TRLS) is the most powerful, direct technique for real-time observation of molecular reactions. Its key strength lies in short duration laser flashes on a time scale at which reactions actually happen - femtoseconds (fs) (1fs = 10^{-15} second). Following the pioneering contribution of Zewail [210], its application to study chemical and biological systems led to the births of new subfields of science, called femtochemistry and femtobiology. Recently, Dr. Lu further proposed that integrating ultrafast laser techniques with biomedical methods to advance fundamental understandings and treatments of major human diseases might lead to the opening of a new transdisciplinary frontier called *femtomedicine* [47]. This is the remarkable opportunity afforded through real-time observation of biochemical reactions at the molecular level.

As mentioned in Chapter 4, replacement of thymidine in DNA by 5-bromouracil (BrU) or 5-iodouracil (IU) has long been observed to enhance DNA damage and cell death induced by ionizing radiolysis [168-169, 171, 174-177, 226-227] and UV photolysis [229-235], 5-Halo-2'-deoxyuridines, especially bromo-deoxyuridine (BrdU) and iododeoxyuridine (IdU), have been explored as potential sensitizers for radiotherapy of cancer. In addition, BrdU and IdU can be used as photosensitizers to induce DNA/RNA-protein crosslinking and be utilized to probe protein-nucleic acid interactions [319-320]. Because of their biological importance, BrdU (BrU) and IdU (IU) have been intensely studied. Despite their long research history for over 50 years, bromodeoxyuridine (BrdU) and iododeoxyuridine (IdU) have been tested in several Phase I - III clinical trials for radiotherapy of cancer but proven disappointing [181-183]. The failure of BrdU and IdU in clinicial trials is probably due to the fact that the reaction mechanism of BrdU/IdU on the molecular level was not well understood. For a long time, it has been speculated that BrdU reacted with the hydrated electron, leading to the formation of the transition state, $BrdU^{*-}$, which would then quickly dissociate into Br^- anion and a reactive $d U^{\bullet}$ radical, represented as: $BrdU + e_{hyd}^- \rightarrow BrdU^{*-} \rightarrow Br^- + d U^{\bullet}$. The reactive $d U^{\bullet}$ radicals then attack DNA by hydrogen abstraction and finally cause DNA strand breaks and cell death. This mechanism was first proposed by Adams in 1967 [262]. As described in Chapter 4, we have recently observed by using femtosecond time-resolved laser spectroscopy (fs-TRLS) that the $U^{\bullet}$ radical results from the UET reaction of CldU/BrdU/IdU with a precursor electron (e_{pre}^-) weakly-bound at about −1.5 eV, rather than with a long-lived e_{hyd}^- well-bound at −3.2 eV, in the aqueous phase [216-217, 287]. The reactions could be represented by the following two equations:

$$BrdU + e_{pre}^- \rightarrow BrdU^{*-} \rightarrow Br^- + dU^{\bullet} \quad \text{..... 7.1}$$

$$IdU + e_{pre}^{-} \rightarrow IdU^{*-} \rightarrow I^{-} + dU^{\bullet} \quad \text{..... 7.2}$$

One of the most important properties of BrdU / IdU in photo-/radio-sensitization is the dependence of their photosensitivity on the DNA sequence while its mechanism is unclear. In 1990, Saito, Sugiyama, and coworkers [267] reported that UV-induced strand damage in duplex DNA containing BrdU was highly dependent on the identity of the nucleotide bound to the 5'-phosphate of BrdU. They observed that duplex DNA containing the sequence 5'-dABrdU exhibits a significantly larger amount of UV (302nm)-induced strand damage than analogous duplexes containing either dG, dT, or dC in the place of dA. And they postulated a mechanism involving photoinduced single electron transfer (PSET) from neutral dA at the 5'-side to an adjacent BrdU in a specifically oriented complex formed in the duplex DNA. This proposed mechanism could be represented as:

$$dA + BrdU / IdU + h\nu \rightarrow dA^{+} + BrdU^{*-} \ / \ IdU^{*-} \quad \text{..... 7.3}$$

This mechanism was surprising, given that electron transfer from dG is more thermodynamically favourable [219, 323-328]. To account for this, Greenberg and coworkers [233] proposed that the contrathermodynamic sequence selectivity results from the confluence of at least three factors: photoinduced forward electron transfer, charge recombination, and electron migration within the DNA duplex. More recently, Sugiyama and co-workers [234-235] further showed efficient enhancements in photoinduced damage of BrU-substituted DNA at 5'-(G/C)AA^{Br}U^{Br}U-3' and 5'-(G/C)A^{Br}U^{Br}U-3' sequences under UV irradiation at 302 nm, and they proposed that the initial electron transfer would occur from G to the electron-deficient stacked ^{Br}U^{Br}U to produce the radical. The intervening A between G and ^{Br}U^{Br}U was considered to act as a bridge between the donor and acceptor and the intervening A may prevent rapid back electron transfer.

However, there is a significant difficulty in understanding the photo-induced forward single-electron transfer (PSET) mechanism. As shown in Fig. 6.3, all the four nucleotides have little absorbance at 302 nm. All the nucleotides were actually not excited under the irradiation of 302 nm. Ground state nucleotides cannot transfer electrons to BrdU, otherwise BrdU would have caused DNA damage without ionizing radiation. In fact, BrdU causes no damage to DNA without ionizing radiation or photon irradiation. However, the sequence selective phenomenon was observed when the DNA containing BrdU was irradiated at 302 nm [229, 233-235]. In those sequence selectivity experiments, the role of e_{pre}^-, which is a general product in ionizing radiation, was not taken into account. It was not clear whether e_{pre}^- were produced from two-photon ionization of water, which might occur with the UV light power of several mW used in those experiments [229-235], and subsequently captured by DNA bases.

As described in Chapter 6, we have demonstrated by femtosecond (fs) pump-probe (time-resolved) laser spectroscopy that nucleotides, especially dGMP and dAMP, are highly efficient at capturing pre-solvated electrons (e_{pre}^-). We have directly observed the dissociative electron transfer (DET) reactions leading to bond dissociations of G and T and the formation of all four stable anions (A^-, G^-, C^- and T^-) in aqueous nucleotides under UV irradiation [219]. We found that among four DNA bases, the weakly-bound e_{pre}^- (<0 eV) can be most effectively trapped at adenine to form a stable anion A^-, while G is most vulnerable to dissociative capture of e_{pre}^- leading to bond breakage. These results have provided a molecular mechanism for radiation-induced damage to DNA in an aqueous environment [329]. Since e_{pre}^- is a major species produced by ionizing radiation of biological systems [47], it is important to know if the

UET reaction involving e_{pre}^- will lead to a radiosensitivity dependence of BrdU/IdU on DNA sequence.

In the experiments presented in this Chapter, we employed fs-TRLS to demonstrate the likely DNA sequence dependence of the radiosensitivity of BrdU and IdU. We show a direct observation of the UET from nucleotide anions dAMP*$^-$ / dGMP*$^-$ to BrdU/IdU, leading to the formation of transient anion BrdU*$^-$/IdU*$^-$ that dissociates to produce the reactive uracilyl radical. As shown in Fig. 7.1, this UET mechanism can well explain the sequence selectivity.

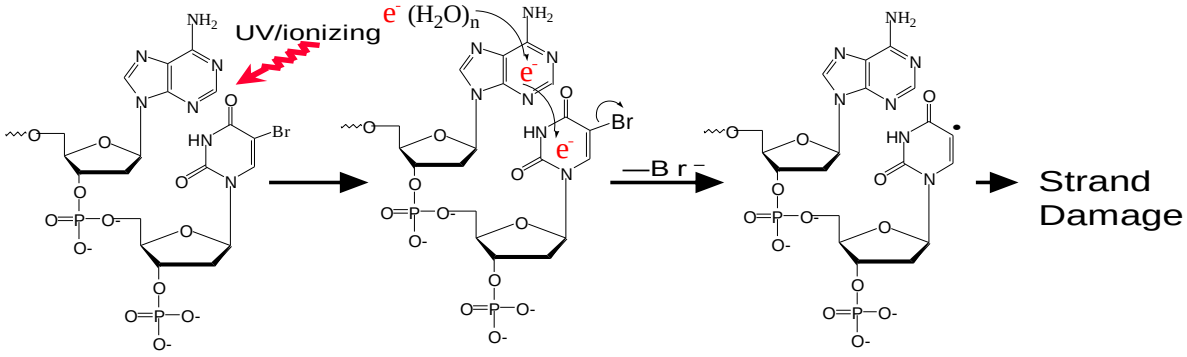

Figure 7.1. Ultrafast electron transfer (UET) to BrdU/IdU from a long-lived anion A^- formed by capture of a prehydrated electron due to radiolysis of water. The resultant transient anion BrdU*$^-$/IdU*$^-$ dissociates to produce the uracilyl radical that causes DNA damage

7.2. Experiments

In this experiment, ultra pure water with a resistivity of >18 MΩ/cm was used. Halopyrimidines and nucleotides(BrdU, IdU, dAMP, and dGMP) were obtained from Sigma-Aldrich and used as supplied.

The pump-probe fs laser spectroscopy methodology has been described in chapter 3. In the present experiments, weakly-bound prehydrated electrons (e_{pre}^-) were produced by two-photon excitation of water at 322 nm, and we monitored the formation of $BrdU^{*-}$/IdU^{*-} from ultrafast electron transfer (UET) of an e_{pre}^- in BrdU/IdU only or a nucleotide anion $dXMP^{*-}$ (X denotes the DNA base A or G) in BrdU/IdU+dXMP complexes. Here, a pump beam (120 fs, 40 μW) at 322 nm was focused into a diameter of ~0.5 mm to produce prehydrated electrons in water, while a probe beam at 333 nm detected the formation and dissociation of $BrdU^{*-}$/IdU^{*-} directly [216-217, 287]. There may exist free BrdU/IdU molecules in BrdU/IdU+dXMP mixtures, depending on the molecular ratio of dXMP to BrdU/IdU, but only UET in formed BrdU/IdU+dXMP hetero-dimers can be measured in fs-ps dynamics since ET reactions from diffusive free-molecule encounters would need much longer time scales (in μs). Since the bases A and G are much more efficient at capturing e_{pre}^- than C and T [219], and A and G are frequently considered for the sequence selectivity of BrdU/IdU, only the results about the effect of dAMP and dGMP are shown to demonstrate the UET mechanism.

7.3. Results and Discussion

The absorption spectra of BrdU and IdU are shown in Fig. 7.2. Both BrdU and IdU have almost zero absorption at wavelengths longer than 320 nm. Thus, all the BrdU/IdU, dXMP molecules would not be excited by the pump laser pulse. As mentioned in Chapters 2 and 4, essentially all the irradiation energy is absorbed by the water to yield the well-known primary radicals (e_{pre}^-, e_{hyd}^- and OH·) in moderately dilute (≤ 0.1 M) aqueous solutions [101].

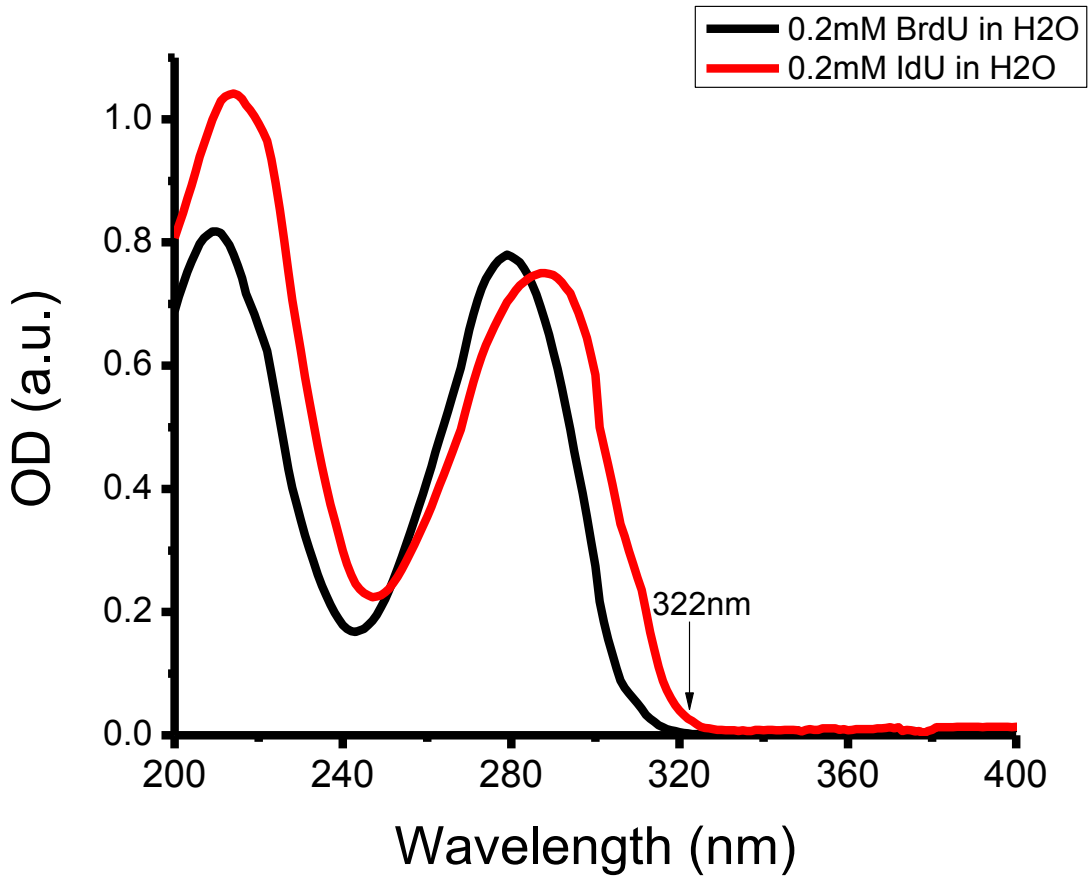

Figure 7.2. Absorbance spectra of BrdU and IdU in water at room temperature.

The results for the kinetic traces of BrdU*$^-$ formed for both BrdU only and BrdU+dXMP complexes are shown in Figs. 7.3 and 7.4. Here, the probe wavelength 333 nm was used to detect the transition state of BrdU*$^-$. At this wavelength, however, smaller yields of hydrated electrons and dAMP*$^-$/ dGMP*$^-$ were also detected [see Chapter 6]. To better compare the yields of BrdU^{*-} in the BrdU only sample and BrdU+dAMP/dGMP mixtures, e_{hyd}^- and/or dAMP*$^-$/ dGMP*$^-$ signal was substracted from those of corresponding samples. The kinetic trace for BrdU*$^-$ was obtained by substracting the kinetic trace of the solvent (H_2O) for the BrdU sample or the kinetic trace of dAMP/dGMP alone for the BrdU+dAMP/dGMP mixture. The kinetic trace after this substraction is for the pure BrdU*$^-$ signal. In this processing, a simplified assumption was made : the presence of BrdU / IdU would not cause any decrease in the yield of dAMP*$^-$/ dGMP*$^-$. Certainly, the real situation is that the presence of BrdU/IdU should somewhat reduce the yield of dAMP*$^-$/ dGMP*$^-$ relative to the case for pure dAMP/dGMP only because of the competition between dAMP/dGMP and BrdU/IdU in capturing e_{pre}^- and the UET from dAMP*$^-$/ dGMP*$^-$ to BrdU/IdU. The BrdU*$^-$ kinetic trace after the substraction is shown in Fig. 7.4.

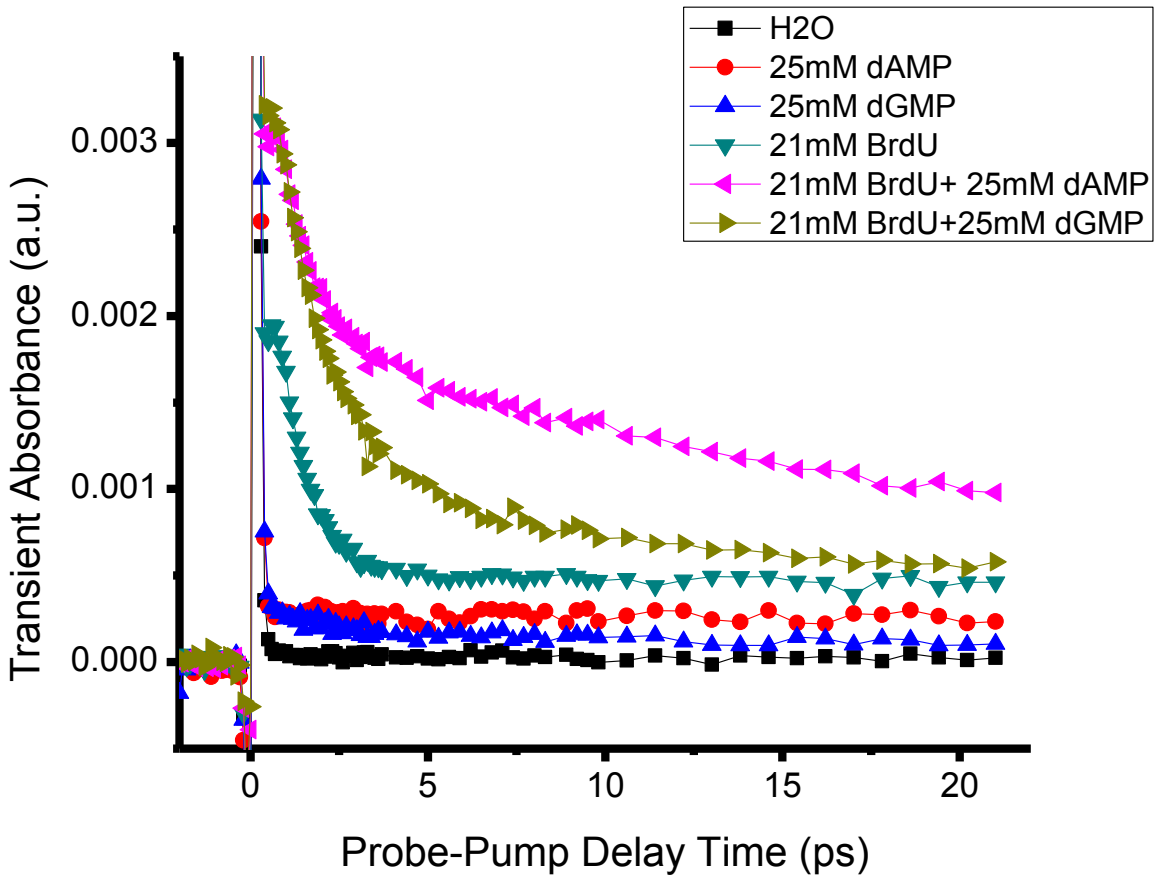

Figure 7.3. Femtosecond transient absorption kinetics trace of water only, 25 mM dAMP, 25 mM dGMP, 21 mM BrdU, 21 mM BrdU+25 mM dAMP mixture, and 21 mM BrdU+25 mM dGMP mixture. The pump and probe wavelengths were 322 nm and 333 nm respectively. The sharp peak at time zero is the coherence 'spike' of the pump and probe pulses.

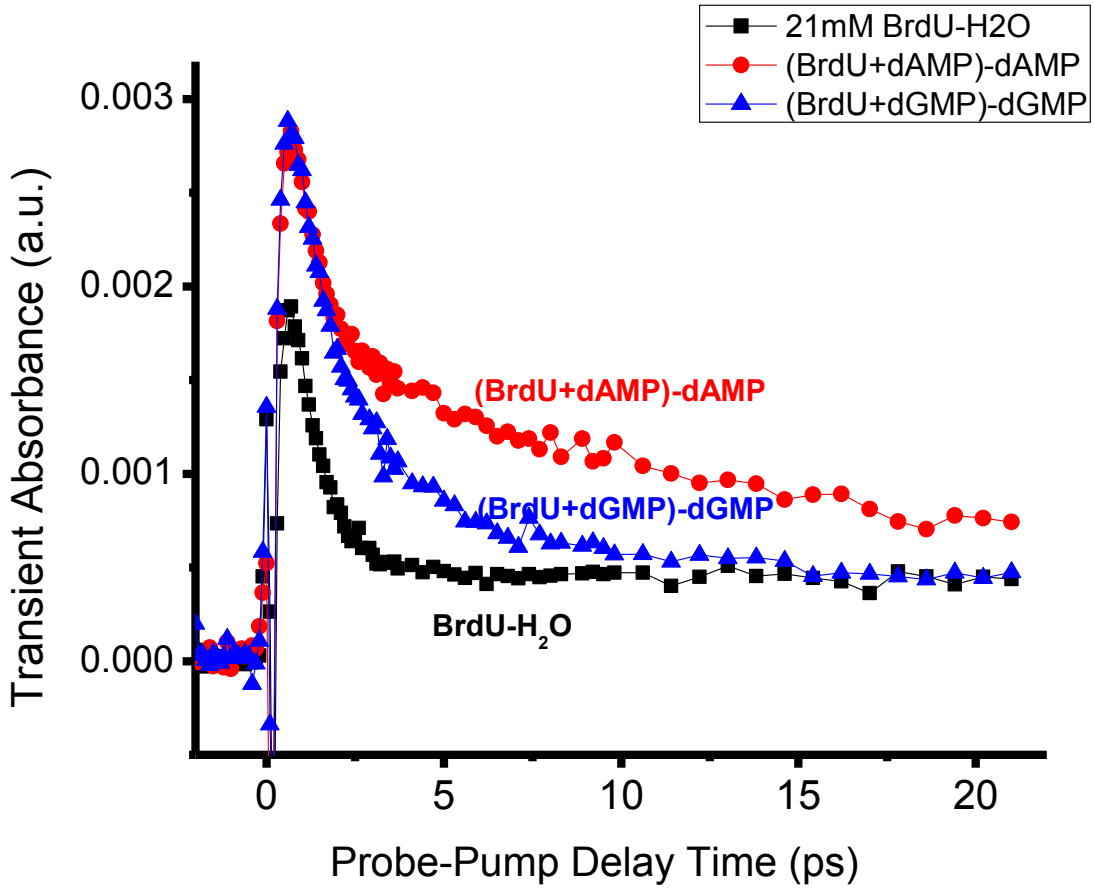

Figure 7.4. Femtosecond transient absorption kinetic traces of BrdU*$^{-}$ generated by UET to BrdU from dAMP*$^{-}$ and dGMP*$^{-}$ formed by capture of e_{pre}^{-} : (BrdU+dXMP) represents 21 mM BrdU + 25 mM dAMP / dGMP mixture. The pump and probe wavelenths were 322 nm and 333 nm, respectively. The sharp peak at time zero is the coherence 'spike' of the pump and probe pulses. The kinetic trace for BrdU was subtracted from that for the solvent (H_2O), while the kinetic trace for the BrdU + dAMP / dGMP mixture was subtracted from that of pure dAMP/dGMP alone.

To explain the result shown in Fig. 7.4, we need to consider the following processes. In the present experiments, the first step was to produce weakly-bound e_{pre}^- in aqueous BrdU+dAMP/dGMP complexes (Eq. 7.4a). As described in Chapter 4, we have previously demonstrated the direct UET between BrdU and e_{pre}^-, leading to the formation of $BrdU^{*-}$ (Eq. 7.4b) [216-217, 287]. And in Chapter 6, we have shown that e_{pre}^- can also be effectively transferred to dAMP or dGMP to form $dAMP^{*-}$or $dGMP^{*-}$ (Eq. 7.4c) [219]. But most of the formed $dGMP^{*-}$ quickly dissociates within the first five ps after its formation while $dAMP^{*-}$ does not dissociate but forms only a long-lived anion $dAMP^-$ (exhibits a flat kinetic trace line) [see Chapter 6] [219]. Thus, the ET between $dGMP^{*-}$ and BrdU can only occur effectively within the shorter lifetime of $dGMP^{*-}$, as is observed in Fig. 7.4. For the BrdU+dAMP complex, the effective ET from $dAMP^{*-}$ occurs on much longer time scales (up to ~30 ps), leading to a stronger enhancement in the total yield of $BrdU^{*-}$ (Eq. 7.4d). The processes, take BrdU as an example, can be expressed as:

$$H_2O + 2h\nu\ (UV) \rightarrow H_2O^* \rightarrow H_2O^+ + e_{pre}^- \quad \text{.....7.4a}$$

$$BrdU + e_{pre}^- \rightarrow BrdU^{*-} \quad \text{.....7.4b}$$

$$dAMP/dGMP + e_{pre}^- \rightarrow dAMP^{*-}/dGMP^{*-} \quad \text{.....7.4c}$$

$$dAMP^{*-}/dGMP^{*-} + BrdU \rightarrow dAMP/dGMP + BrdU^{*-} \quad \text{.....7.4d}$$

$$BrdU^{*-} \rightarrow Br^- + dU^{\bullet} \quad \text{..... 7.4e}$$

$$BrdU^{*-} \rightarrow BrdU^- \quad \text{..... 7.4f}$$

The enhancement of the yield (integration of the signal over time) of $BrdU^{*-}$ will lead to the increased yield of the $dU^{\bullet}$ radical (Eq. 7.4e), which will ultimately cause more DNA strand breakage. A small percentage of $BrdU^{*-}$ becomes stable $BrdU^{-}$ and exhibits the long-lived tails in Fig. 7.4 (Eq. 7.4f) [216].

In deducing the UET mechanism expressed in Eq. 7.4, we have also considered a very unlikely argument that instead of electron transfer (ET) from $dAMP^{*-}$/$dGMP^{*-}$ to BrdU, forming $BrdU^{*-}$, the ET from $BrdU^{*-}$ to dXMP (X=A, G) might occur and give rise to a larger $dXMP^{*-}$ yield for BrdU-dXMP mixtures than for pure dXMP. However, this argement can not stand for many well-known reasons. First, BrdU and IdU are well-known to be strong electron capturers (much stronger than any dXMP), which is why the replacment of dXMP by BrdU / IdU has been tested as a potential source of radiosensitizers and photosensitizers. Second, it has been well-observed that the lifetimes of $BrdU^{*-}$ / IdU^{*-} are less than 2 ps [216-217, 287], thus any enhancement of the $dXMP^{*-}$ yield must be observed within 2 ps. Moreover, the kinetic trace of $dAMP^{*-}$ once formed would exhibit only a flat line [219, Chapter 6]. Those expectations drastically differ from the observed results in Figs. 7.3 and 7.4. Thus the kinetic traces shown in Fig. 7.4 are actually the lower limit to the real yields of the formed $BrdU^{*-}$ from the BrdU-dXMP mixtures. That is, the true enhancement of the $BrdU^{*-}$ yield due to the UET from $dXMP^{*-}$ should be slightly higher than that shown in Fig. 7.4. Nevertheless, the results in Fig. 7.4 have clearly (visibly) demonstrated that the UET from $dXMP^{*-}$ to BrdU in BrdU+dXMP complexes leads to a significant enhancement in the yield of $BrdU^{*-}$, compared with the yield for the pure BrdU, and that the enhancement is stronger for BrdU+dAMP than for BrdU+dGMP complex.

Free BrdU / IdU molecules may exist in BrdU / IdU + dXMP mixtures, depending on the molecular ratio of dXMP to BrdU / IdU. Here, it should be noted that only electron transfer (UET) in *formed BrdU/IdU–dXMP heterodimers* can be measured in fs-ps dynamics because ET reactions from diffusive free-molecule encounters would need much longer time scales (μs). The $BrdU^{*-}$/IdU^{*-} yield enhancement is expected to rise as the part of BrdU/IdU in BrdU/IdU–dXMP dimers increases and to reach a maximum when all BrdU/IdU form dimers with dXMP. The latter can be made for the mixtures with dXMP in large excess. To examine this possibility, the kinetic traces of $BrdU^{*-}$ for BrdU+dXMP mixtures with various dXMP–BrdU molecular ratios (up to 10:1) were measured. Note that to satisfy the radiolysis condition that the majority of the radiation energy is adsorbed by the solvent (water), the highest concentration of dXMP must be kept below 100 mM ($\leq$ 0.1 M). This is also necessary to avoid forming clusters of dXMP and other measurement difficulties (e.g., a sudden large noise) if higher concentrations of dXMP are used. The kinetic traces of $BrdU^{*-}$ at different molecular ratios of dXMP to BrdU are shown in Fig. 7.5, which qualitatively shows that the higher the molecular ratio of dXMP to BrdU, the more significant enhancement of the $BrdU^{*-}$yield.

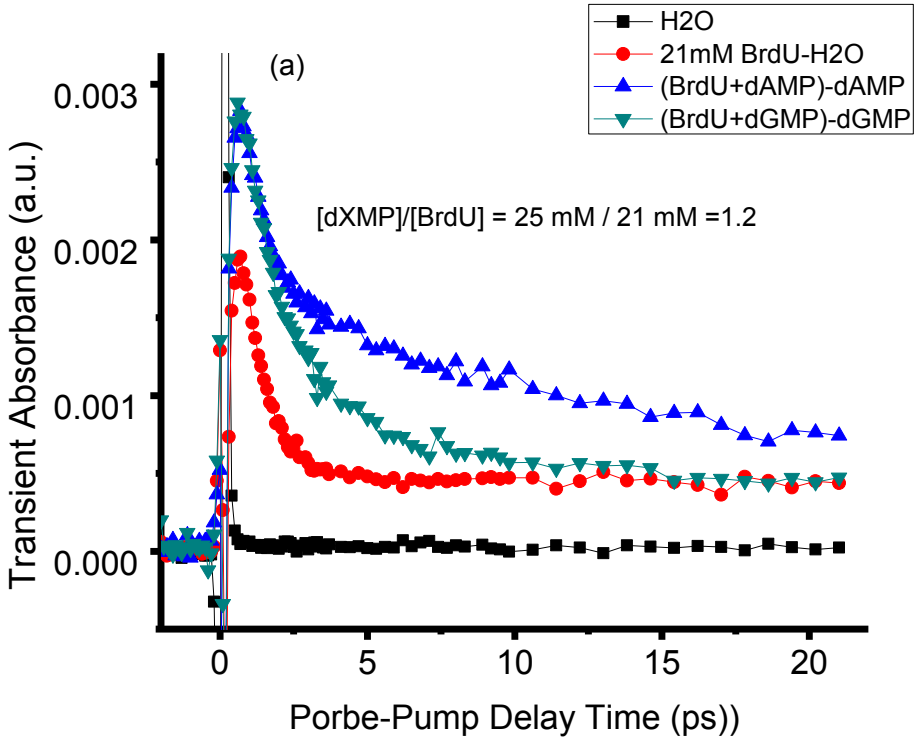
H2O
21mM BrdU-H2O
(BrdU+dAMP)-dAMP
(BrdU+dGMP)-dGMP
(a)
[dXMP]/[BrdU] = 25 mM / 21 mM =1.2
Transient Absorbance (a.u.)
0.003
0.002
0.001
0.000
0
5
10
15
20
Porbe-Pump Delay Time (ps))

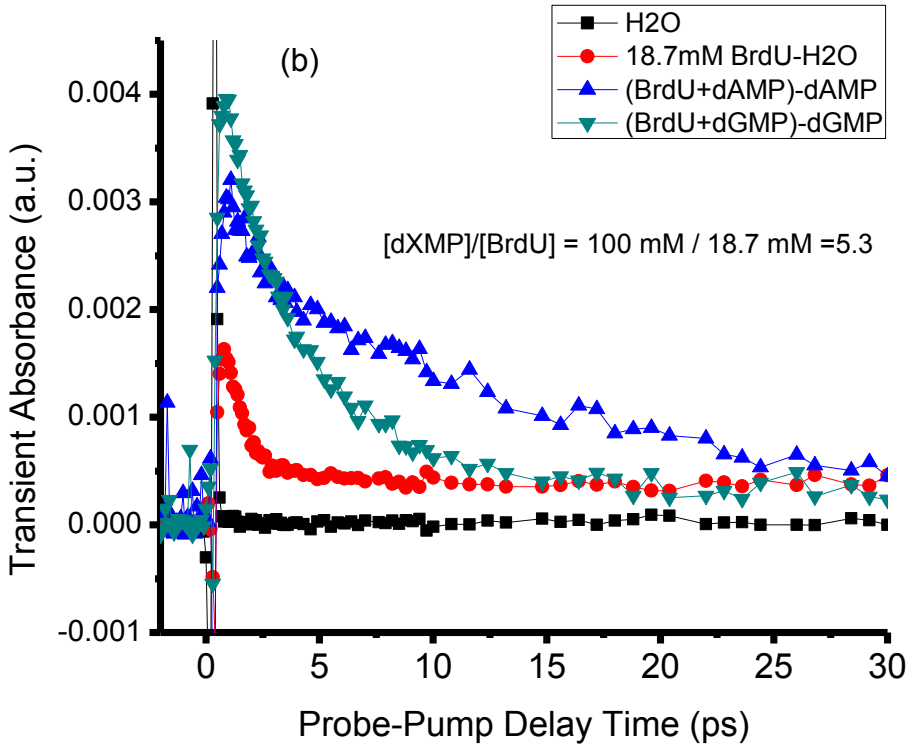
H2O
18.7mM BrdU-H2O
(BrdU+dAMP)-dAMP
(BrdU+dGMP)-dGMP
(b)
[dXMP]/[BrdU] = 100 mM / 18.7 mM =5.3
Transient Absorbance (a.u.)
0.004
0.003
0.002
0.001
0.000
-0.001
0
5
10
15
20
25
30
Probe-Pump Delay Time (ps)

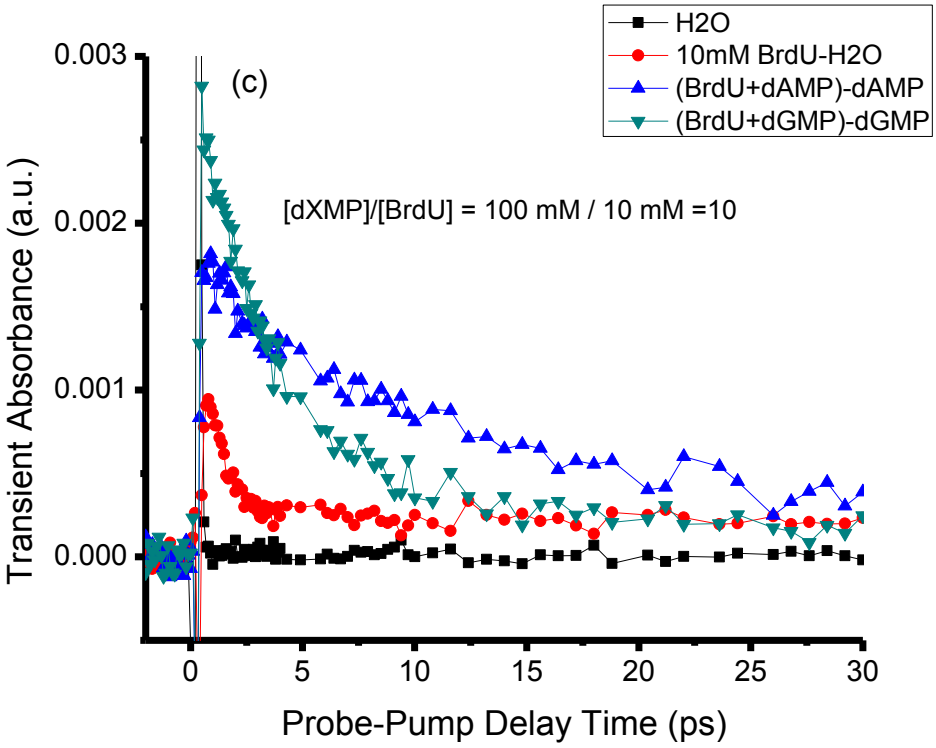

Figure 7.5. Femtosecond transient absorption kinetic traces of BrdU*$^{-}$ generated by UET to BrdU from dAMP*$^{-}$ and dGMP*$^{-}$ formed by capture of e_{pre}^{-} : (a) pure water, 21 mM BrdU, 21 mM BrdU + 25 mM dAMP/ dGMP mixture (dXMP/BrdU molecular ratio = 1.2:1); (b) pure water, 18.7 mM BrdU, 18.7 mM BrdU + 100 mM dAMP/ dGMP mixture (dXMP/BrdU molecular ratio = 5.3:1); (c) pure water, 10 mM BrdU, 10 mM BrdU + 100 mM dAMP/ dGMP mixture (dXMP/BrdU molecular ratio = 10:1). The pump and probe wavelenths were 322 nm and 333 nm, respectively. The sharp peak at time zero is the coherence 'spike' of the pump and probe pulses. The kinetic trace for BrdU was subtracted from that for the solvent (H_2O), while the kinetic traces for the BrdU + dAMP / dGMP mixtures were subtracted from that of pure dAMP/dGMP alone. Note that in obtaining various concentration ratios of BrdU/dXMP, the concentrations of the solute (dXMP or BrdU) must be kept ≤100 mM (0.1 M) ; otherwise the condition that the majority of the radiation energy is adsorbed by the solvent (water) would no longer be true.

To obtain a quantitative analysis, we define R as $BrdU^{*-}$ yield enhancement factor by:

R = (yield of $BrdU^{*-}$ in BrdU-dXMP mixture) / yield of $BrdU^{*-}$ in BrdU solution

It follows that the higher the molecular ratio of dXMP to BrdU, the higher the R value until R reaches a saturated value. In calculating the R values at various molecular ratios of dXMP to BrdU, the total yields (Y) of formed $BrdU^{*-}$ is obtained by integrating all the yield over the time window from 0.5 to 30 ps for the BrdU and BrdU+dXMP mixtures. The result is shown in Table 7.1 and Fig. 7.6.

Table 7.1 Yield of $BrdU^{*-}$ over time window from 0.5 ps to 30 ps and $BrdU^{*-}$ enhancement factor by dXMP (X=A, G).

Molecular Ratio of dXMP to BrdU	Total yield of $BrdU^{*-}$ over time window from 0.5 ps to 30 ps (a.u.)			Enhancement factor by dAMP $\mathbf{R_{dAMP}}$	Enhancement factor by dGMP $\mathbf{R_{dGMP}}$
	BrdU only sample	BrdU+dAMP mixture	BrdU+dGMP mixture		
0				**1**	**1**
1.2 (25 mM / 21 mM)	0.01089	0.02368	0.01577	**2.17**	**1.45**
5.3 (100 mM/18.7 mM)	0.01318	0.03625	0.02418	**2.75**	**1.83**
10 (100 mM/10 mM)	0.00766	0.02225	0.01527	**2.90**	**2.00**

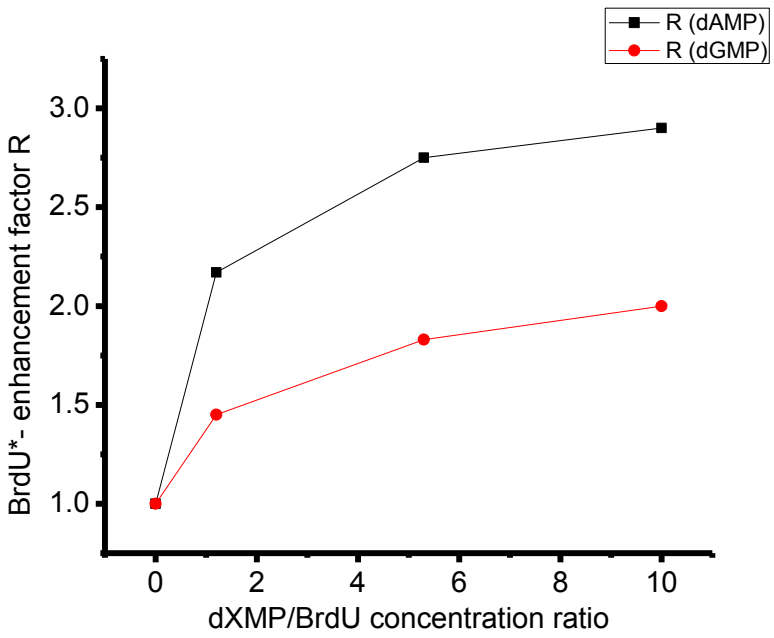

Figure 7.6. Enhancement factor of the $BrdU^{*-}$ yield for BrdU+dXMP mixtures as a function of the dXMP/BrdU molecular ratio (X=A, G).

Fig. 7.6 clearly shows that as dXMP/BrdU molecular ratio increased, both $BrdU^{*-}$ enhancement factors by dAMP and dGMP increased, confirming that ultrafast electron transfer only occurs between BrdU-dXMP heterodimers. The higher the molecular ratio of dXMP to BrdU, the higher percent of BrdU would become BrdU-dXMP heterodimers. When we made a slightly different definition of R in terms of the total yields (Y) of *dissociated* $BrdU^{*-}$ by integrating the *decaying* signal only over the time window of 0.5 to 30 ps for the samples of BrdU and BrdU+dXMP, even larger enhancement factors R were obtained [101]. As also shown in Fig. 7.6, with an identical molecular ratio of dXMP to BrdU, dAMP has significantly higher electron transfer efficiency than dGMP. This is reasonable, as most of the formed

dGMP*$^-$ quickly dissociates within the first five ps after its formation while dAMP*$^-$ does not dissociate but forms only a long-lived anion dAMP$^-$. Thus, the base A is a more effective promoter for the electron transfer reaction.

The integrated IdU*$^-$ yields in Fig. 7.7 over time window from 0.5 ps to 30 ps are shown in Table 7.2. Fig. 7.7 and Table 7.2 show that dAMP and dGMP have a similar enhancement effect on the yield of IdU*$^-$. dAMP enhances the IdU*$^-$ yield by 1.6 times, while dGMP by 1.5 times, for 2.8 mM IdU+46.5 mM dXMP mixtures. The enhancement factors for IdU*$^-$ are much lower than those of BrU*$^-$. This is reasonable because the direct UET reaction of IdU with e_{pre}^- is much stronger than that of BrdU. Our results are also consistant with the observation that much smaller sequence selectivity of photosensitivity was observed for similar duplex DNA containing IdU than for DNA containing BrdU [232-233].

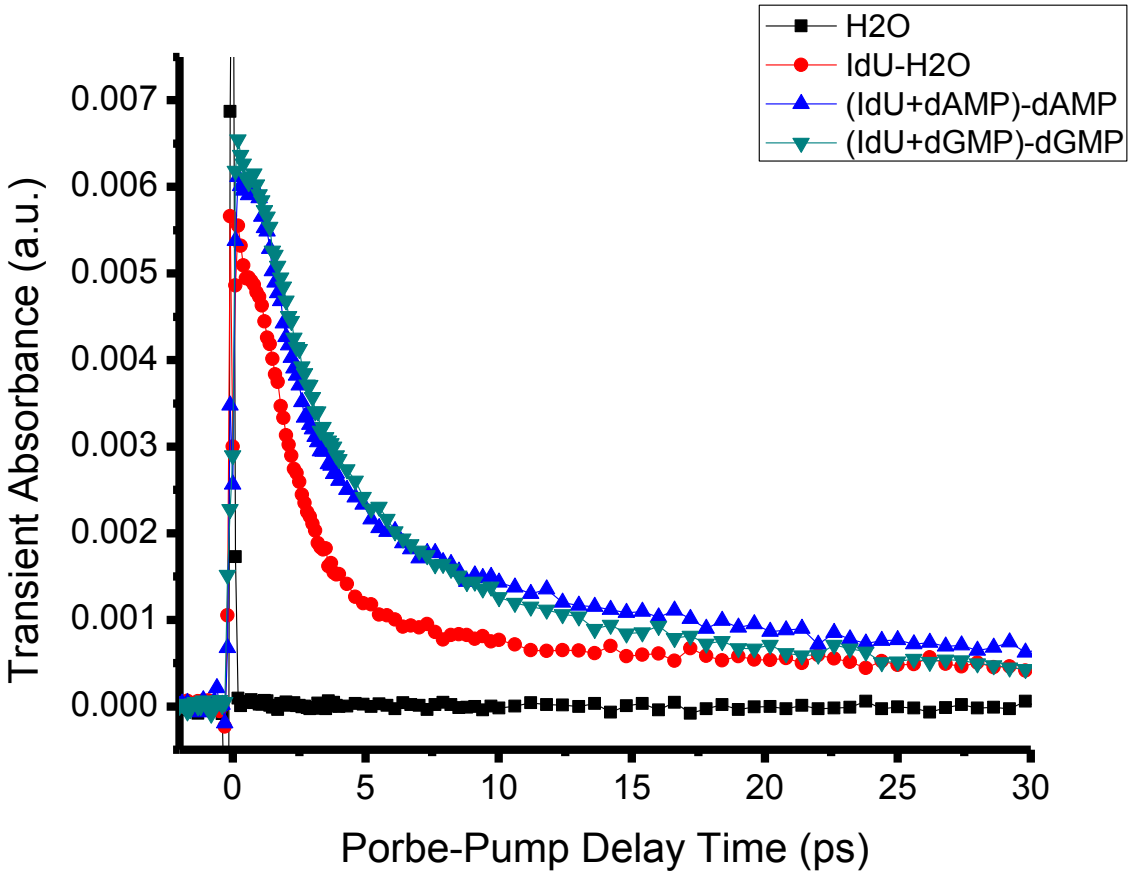

Figure 7.7. Femtosecond transient absorption kinetic traces of IdU^{*-} generated by UET to IdU from $dAMP^{*-}$ and $dGMP^{*-}$ formed by capture of e_{pre}^{-} : (IdU+dXMP) represents 2.8 mM IdU + 46.5 mM dAMP / dGMP mixture. The pump and probe wavelenths were 322 nm and 333 nm, respectively. The sharp peak at time zero is the coherence 'spike' of the pump and probe pulses. It is not completely removed after the substraction. The kinetic trace for IdU was subtracted from that for the solvent (H_2O), while the kinetic traces for the IdU + dAMP / dGMP mixtures were subtracted from that of pure dAMP/dGMP alone.

Table 7.2. Yield of IdU*$^-$ over time window from 0.5 ps to 30 ps and IdU*$^-$ enhancement factor by dXMP (X=A, G).

Total yield of IdU*$^-$ over time window from 0.5 ps to 30 ps (a.u.)			Enhancement factor by dAMP $\mathbf{R_{dAMP}}$	Enhancement factor by dGMP $\mathbf{R_{dGMP}}$
IdU only sample	IdU+dAMP mixture	IdU+dGMP mixture		
0.02773	0.04437	0.04164	**1.6**	**1.5**

Finally, it is also interesting to compare the present results with those of previous radiolysis studies by Nase et al. [321] using submicrosecond electron pulses of aqueous BrdU and nucleobase complexes. In those studies, the dU$^\bullet$ yield was attributed to ET from nucleobase electron adducts to BrU under irradiation, and it was proposed that ET from T and A electron adducts and their protonated forms to BrU occurs but that no ET to BrU occurs from the electron adduct of G, which was thought to serve as an ultimate electron sink in irradiated DNA. In contrast, our present real-time, direct observations by fs-TRLS [see Chapters 4 and 6] and the present results provide direct evidence that (1) the weakly bound e_{pre}^- can first be trapped at both A and G and then transferred to BrdU/IdU and (2) the base A is not only the main electron sink but also an efficient promoter for ET reactions, while G is the major site for DNA damage induced by ionizing radiation.

7.4. Conclusion

In summary, our results present the first real-time observation of UET from the anions of dAMP and dGMP to BrdU/ IdU in aqueous BrdU-dAMP/dGMP and IdU-dAMP/dGMP complexes under ionizing radiation. The results provide a molecular mechanism for the sequence selectivity of BrdU and IdU in radiosensitization. The capability of IdU for dissociative electron transfer of weakly bound e_{pre}^- is stronger than that of BrdU. Correspondingly, BrdU shows a more significant DNA sequence selectivity through UET from $dXMP^{*-}$ formed by attachment of e_{pre}^- generated by radiolysis of water. This new mechanistic insight into the mechanism of action of BrdU and IdU may provide clues to improve the halogen family as potential radiosensitizers and to develop more effective radiosensitizers for clinical applications.

Chapter 8

Development of New Radiosensitizers Based on Unique Molecular Mechanistic Understanding

8.1. Introduction

The modern drug discovery and development process has been proven to be an expensive and inefficient process. It generally takes about 20 years and approximately US $1.8 billion to develop a single new drug [40-41]. The identification of successful anticancer agents remains a somewhat empirical process [200]. There is a compelling need for a more fundamental and deeper understanding of the molecular mechanisms of action of anticancer drugs to design more appropriate drugs. In this Chapter, we will show the potential of utilizing our unique molecular understandings of the biological effect of ionizing radiation and the action of halopyrimidines to develop more effective radiosensitizers.

Applying the versatile femtosecond time-resolved laser spectroscopy (fs-TRLS), a powerful technique for real-time observation of molecular reactions, we have resolved the long existing controversies about the physical nature and lifetimes of a novel ultrashort-lived electron species (e_{pre}^-) generated in radiolysis of water (Chapter 5) and unraveled how it plays crucial roles in ionizing radiation induced DNA damage (Chapter 6) and in activating halopyrimidines

(BrdU and IdU) as hypoxic radiosensitizers (Chapters 4 and 7). Our group has also recently found a new molecular mechanism of cisplatin used in combination with radiotherapy, which involves the extremely effective dissociative electron transfer (DET) reaction of cisplatin with e_{pre}^- [45]. Our results show that compared with cisplatin, DET reactions of BrdU and IdU with e_{pre}^- are not strong enough so that they are not effective radiosensitizers. Thus, there is little chance for BrdU and IdU to be effective radiosensitizers for the clinical use.

Based on our mechanistic understandings at the molecular level of DNA damage induced by ionizing radiation and halopyrimidines as potential radiosensitizers, we are now identifying /designing and synthesizing new radiosensitizing drug candidates, one of which is labeled as Compound RS-1. In this chapter, through the femtomedicine approach integrating fs-TRLS with biomedical methods (DNA damage and cell death measurements), we studied the radiosensitizing efficacy of Compound RS-1 in comparison with existing halopyrimidines (BrdU and IdU) for the treatment of cancer cells. We tested the radiosensitizing effect of RS-1 by using some biomedical methods including DNA damage measurements by gel electrophoresis and cell viability/death assays with 3-(4,5-Dimethylthiazol-2-yl)-2,5-diphenyltetrazolium bromide (MTT).

8.2. Experiments

8.2.1. fs-TRLS measurements

The methodology and details for femtosecond pump-probe transient absorption spectroscopic measurements have been given in Chapters 3, 4 and 7. Briefly, a pump wavelength of 322 nm was used to generate e_{pre}^- in the aqueous sample solutions, while a probe wavelength of 333 nm was used to detect the transition state $[RS\text{-}1]^{*-}$ of the DET reaction of Compound RS-1 with e_{pre}^-: $e_{pre}^- + RS\text{-}1 \rightarrow [RS\text{-}1]^{*-} \rightarrow Br^- + radical$.

8.2.2. DNA damage and cell death measurements

DNA sample: Plasmid DNA [pGEM 3zf(-), 3197 kbp] was extracted from Escherichia Coli JM109 and purified using QIAprep Kit (Qiagen)

Cell lines and culture condition. The HeLa (ATCC#: CCL-2) cell line was obtained from the American Type Culture Collection (ATCC); fetal bovine serum (FBS) was obtained from Hyclone Laboratories (UT, USA). HeLa cells were cultivated with MEM (Hyclone) supplemented with 10% FBS, 100 units/mL penicillin G and 100 μg/mL streptomycin (Hyclone).

Agarose gel electrophoresis. The pump beam 318 nm, was used to produce radicals via two-photon excitation of water in DNA solutions. The laser beam was focused into a quartz

cuvette containing 3 μg of DNA in 200ul of water or drug solution in water. The solutions were stirred during radiation to produce uniform DNA damage throughout the samples. Aliquots equivalent to 100 ng DNA were removed from the cuvette in different irradiation time intervals. All aliquots were analyzed with a standard agarose gel electrophoresis method, namely, on 1% neutral TAE agarose gel in TAE running buffer. The gel was prestained with 0.5 μg/ml ethidium bromide. The image of the gel was taken on a FluorChem imaging station (Alpha Innotech) and exhibits various DNA topological forms, including supercoiled DNA (undamaged DNA), open circular DNA (single strand break, SSB), and linear form DNA (double strand break, DSB).

Cell viability assay by MTT. The radiosensitizing effect of Compound RS-01 on cell viability was determined by the MTT assay, one of the most commonly used cell viability assays [330]. The Vybrant MTT Cell Proliferation/viability Assay Kit purchased from Invitrogen was used per the manufacturer's protocol. Briefly, 5 mg MTT powder was dissolved in 1X phosphate buffer saline (PBS). 1 gram sodium dodecyl sulfate (SDS) was dissolved in 10 ml 0.01 M HCl solution to make stock SDS solution. Hela cells were seeded at a density of 5000 cells/well on 96-well plates (BD falcon, ON, Canada), and cultured in a humidified atmosphere (5% CO_2 + 95% room air) at 37 ℃. One day after seeding, the culture medium was changed to medium with different concentrations of drugs. The cells were incubated with different concentration of drugs for 24 hours, and then the plates were irradiated by different doses of X-ray, generated from the linear electron accelerator in the Grand River Regional Cancer Centre. After waiting a certain time after ionizing radiation, medium was changed to 90% MEM medium without phenol red +10% FBS. 10 μl 5mg/ml MTT solution was added to each well. The plates were kept in the 37 ℃ incubator for 4 hours. Then 100 μl stock SDS solution was added to each well to dissolve the formazan. Again the plates were kept in the 37℃ incubator for 4 – 18 hours. Then the

absorbance was read at 570 nm by a micro-plate reader. The radiosensitizing effect of Compound RS-1 on growth inhibition was assessed as percent cell viability where cells in control (with no irradiation and drug) were taken as 100% viable.

8.3. Results and Discussion

8.3.1. Static absorbance spectrum of compound RS-1

The absorption spectrum of compound RS-1 is shown in Fig. 8.1, which exhibits three absorption peaks at 210, 239 and 299nm. The absorption coefficient at 299 nm is determined to be 3.97×10^{5} $M^{-1}m^{-1}$, derived from the measured linear dependence of the absorbance as a function of RS-1 concentration.

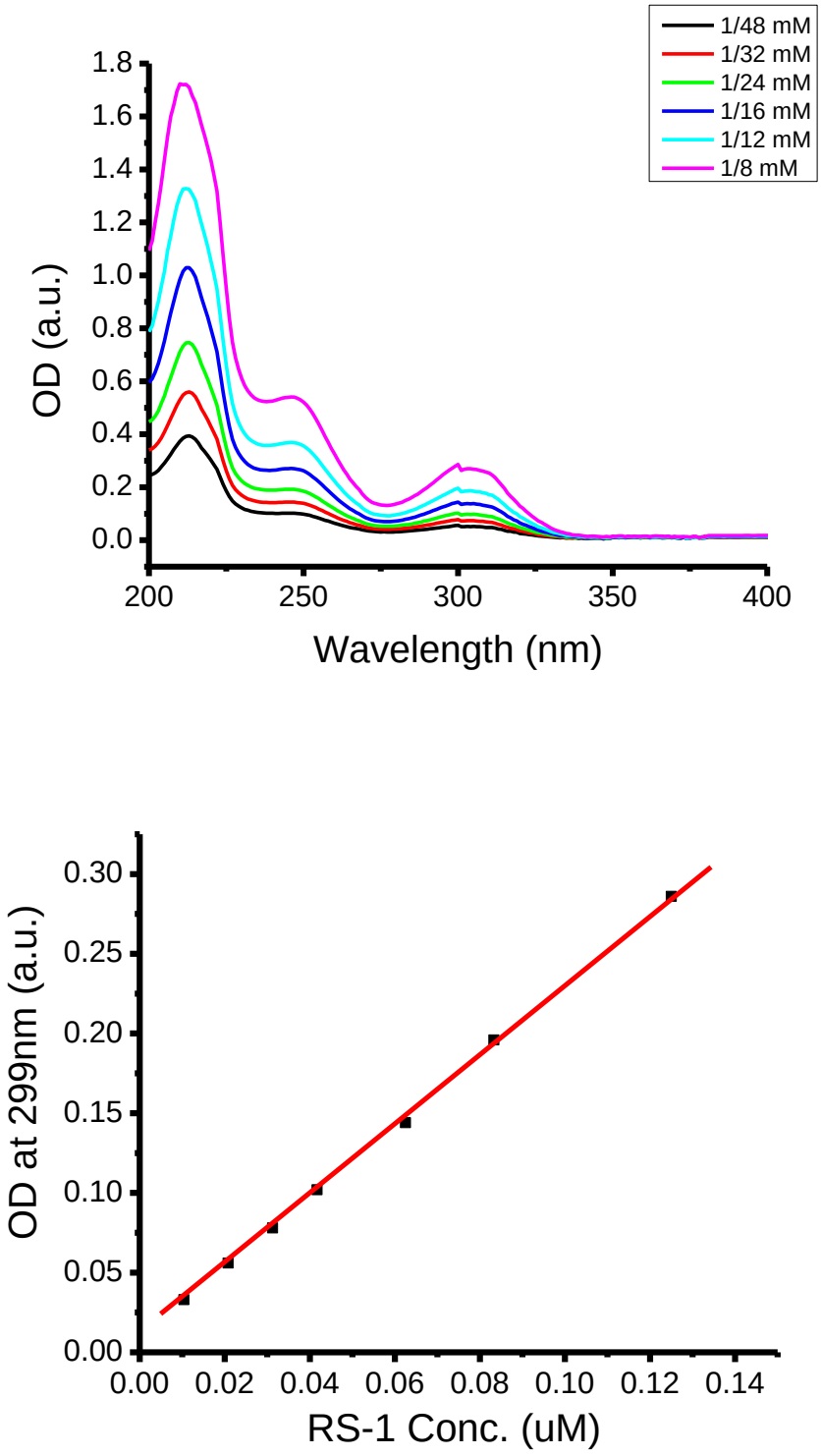

Figure 8.1. Absorbance of compound RS-1 in H_2O. Absorption spectrum of different concentrations and linear dependence of the absorbance at 299 nm.

8.3.2. fs-TRLS measurements

The transient kinetic trace of the RS-1 solution pumped at 322 nm and probed at 333 nm is shown in Fig. 8.2. A strong signal is instantaneously observed at near time zero with almost zero rising time. The decay of this dominant signal is quite rapid on a sub-picosecond time scale superposes on a slow component. The best fit to the data gives two decay lifetimes: the rapid decay with τ_1=~0.48 ps and the slower decay withτ_2=~6.0 ps. The strong signal at ~time zero is clearly due to the electronically excited state of RS-1. As shown in the static absorption spectrum (Fig. 8.1), Compound RS-1 has a small but visible absorption at 322 nm. When the pump wavelength was 266nm, the transient absorbance kinetic trace of BrdU probed at 330 nm had a similar sharp peak at near time zero, which had been attributed to the BrdU* state [216]. Thus the fast component can reasonably be explained as due to an excited state [RS-1]* resulting from the direct absorption at 322 nm by compound RS-1.

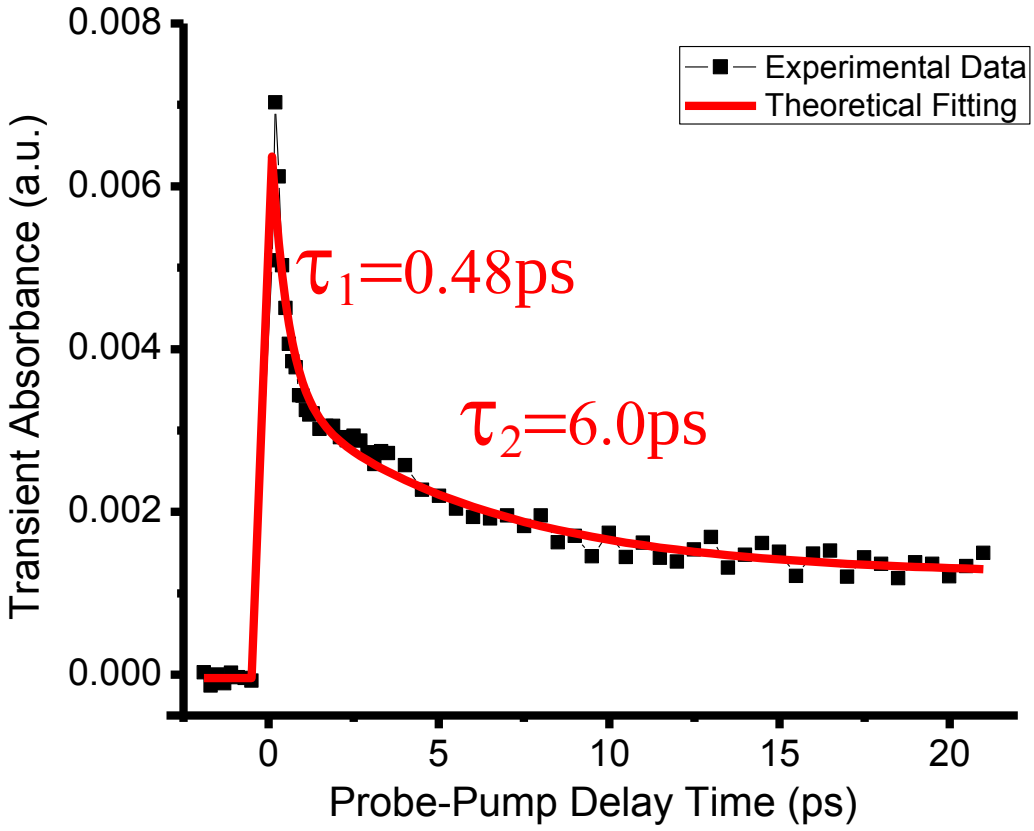

Figure 8.2. Femtosecond transient absorption kinetic traces of the excited state [RS-1]* and the transient state [RS-1]*$^{-}$ for RS-1 pumped at 322 nm and probed at 333 nm. The black squares are experimental data, while the red dots are the best fit to the experimental data. The data were corrected by the subtraction of the kinetic trace for the pure solvent.

The slower decay with τ_2=~6.0 ps is assigned to the transient state [RS-1]*$^-$ signal, because: 1) the halogenated molecule RS-1 is expected to be a strong electron scavenger; 2) the [RS-1]*$^-$ is expected to have a strong UV absorption in the wavelengths around 330 nm, a characteristic of the local C-Cl$^-$ bond. This has been observed for several halogenated molecules [216-218, 267]. The UV electronic absorption of a vibrationally excited AB*$^-$ state for the DET reaction of e_{pre}^- with a halogenated molecule AB should be identical to that of its vibrationally-relaxed anion AB$^-$ [217]. That is, the vibrational relaxation of a small molecule AB*$^-$, which occurs usually at time from 0.1 μs to 1 ps, is not reflected in the decay kinetics beyond 1 ps. Thus, the observed decay in transient absorption of AB*$^-$ reflects solely its dissociation lifetime. Similar to the BrdU*$^-$ and IdU*$^-$, the slower decay with τ_2=~6.0 ps is therefore assigned to be the dissociative lifetime of the transition state [RS-1]*$^-$, which dissociates into a Br$^-$ anion and a reactive neutral radical. We have also observed that the transient absorbance signal shows an excellent linear relationship on RS-1 concentration, indicating that it is a single molecule reaction.

It is worthwhile to compare RS-1 as a radiosensitizer candidate with IdU as the strongest radiosensitizer in the family of halopyrimidines in their DET reaction efficiencies with e_{pre}^- to produce reactive radical for inducing DNA damage and killing cancer cells. The fs-TRLS results of both RS-1 and IdU with an identical concentration are plotted together in Fig. 8.3. Interestingly, it is seen that the [RS-1]*$^-$ yield is much higher than that of IdU*$^-$. This indicates that the DET reaction of RS-1 with e_{pre}^- is much stronger than that of the strongest halopyrimidine IdU. This result shows the promise of RS-1 as an effective radiosensitizer.

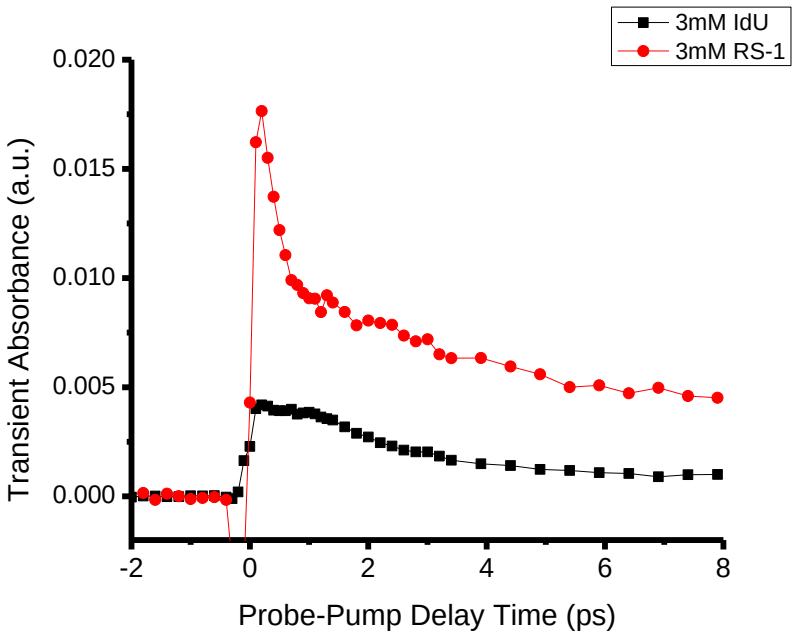

Figure 8.3. Femtosecond transient absorption kinetic traces of 3 mM IdU and 3 mM RS-1, pumped at 322 nm and probed at 333 nm. The data were corrected by the subtraction of the kinetic trace for the pure solvent.

8.3.3. DNA gel electrophoresis measurements

Although BrdU and IdU are potential hypoxic radiosensitizers, their incorporation into DNA is a prerequisite for radiosensitization of human tumors by the halogenated thymidine analogues, and the extent of radiosensitization correlates directly with the percentage of thymidine substitution in DNA [175, 331]. However, the incorporation of BrdU / IdU into DNA strands is actually mutation of the DNA. The treatment itself actually causes problems. Free BrdU and IdU (not incorporated into DNA) molecules show no radiosensitizing effects. To compare the radiosensitizing effect of compound RS-1 with halopyrimidines, we first tested the capabilities of IdU and RS-1 at inducing damage to plasmid DNA. The results are shown in Figs. 8.4, 8.5 and 8.6, as well as Tables 8.1 and 8.2.

Different DNA samples with /without the addition of 500 μM IdU were irradiated at 0, 3, 6, 9, 12, 15, 20, and 30 minute time intervals by UV laser pulses (185 μW, 318 nm). Fig. 8.4 shows that both the yields of SSB and DSB increased with UV irradiation time, while the amount of undamaged (SC) DNA decreased. If we compare the two lanes with 30-min UV irradiation time in Fig. 8.4 (a) and (b), it can even be seen that the percent of undamaged (SC) DNA was actually larger for the DNA mixed with 500 μM IdU than the DNA in pure water, that is, IdU somewhat protects DNA from UV irradiation.

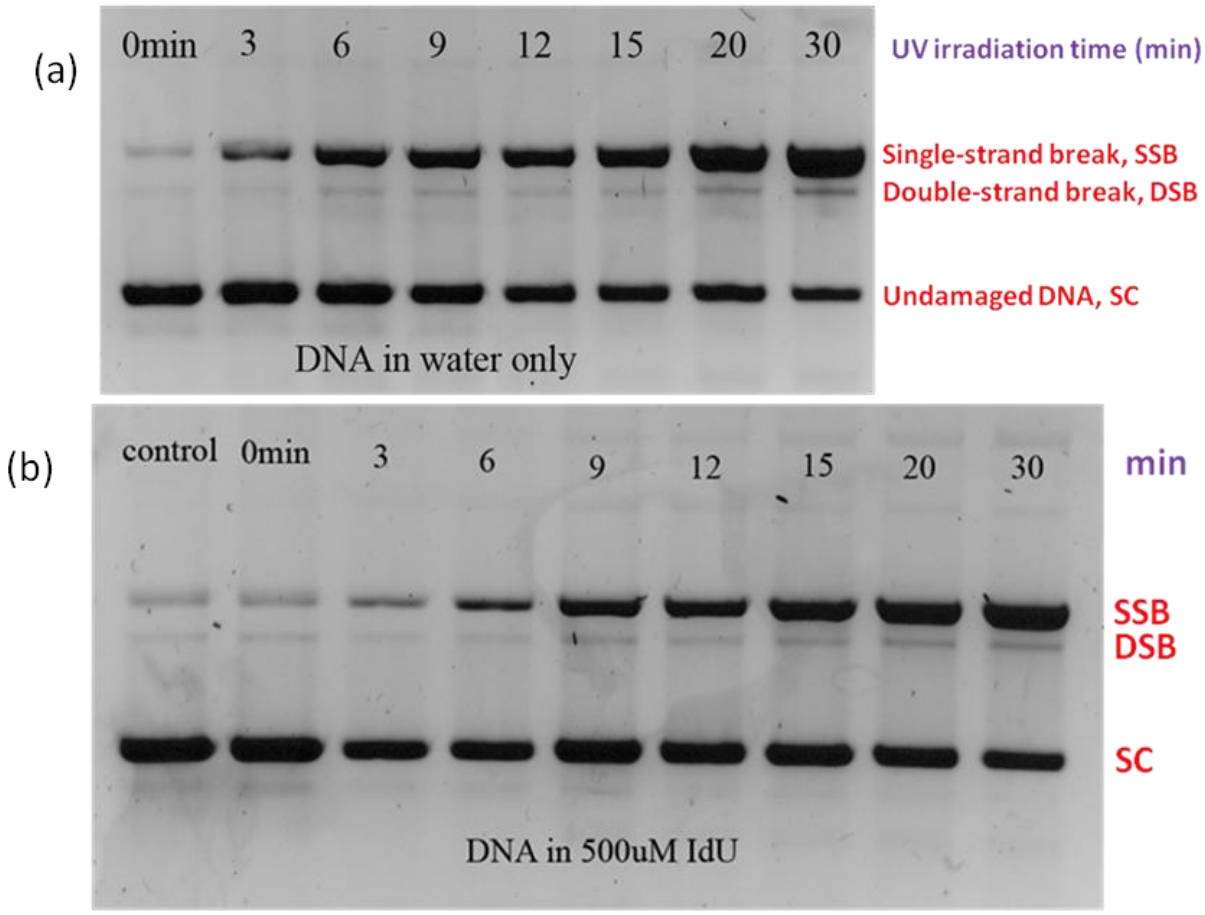

Figure 8.4. DNA gel electrophoretic results of plasmid DNA at different time intervals by fs UV laser pulses (185 μW, 318 nm). There was 100 ng DNA per lane. (a) DNA in water only; (b) DNA was incubated with 500 μM IdU.

Table 8.1. Percents of DNA strand breaks of DNA incubated without/with IdU, under 30-min UV laser irradiation (185 μW, 318 nm)

	H_2O only	500uM IdU
SSB	77.2 %	56.2%
DSB	4.0 %	4.7%
Undamaged DNA SC	18.8%	39.1%

Table 8.1 gives a quantitative analysis of the lanes with 30-min UV irradation shown in Fig. 8.4. Under UV irradiation (185 μW, 318 nm) for 30 min, the addition of 500 μM IdU into the DNA sample decreased the percentage of SSBs from 77.2% to 56.2%, while the percentage of DSBs remains almost the same. It appears puzzling since IdU is a well-known potential radiosensitizer. This could be due to two reasons: (1) IdU has a small but non-zero absorbance at 318 nm, as shown in Fig. 7.1 (Chapter 7). Some 318 nm UV photons were actually absorbed by IdU, causing the decreases of the yield of radicals arising from the radiolysis of water generated by the UV pulse. (2) Some of the e_{pre}^- generated by the UV pulse were scavenged by free IdU molecules in the solution. We have recently demonstrated that e_{pre}^- are effective in causing DNA strand breaks [219-220, Chapter 6]. When IdU is not incorporated into DNA, the $dU^\bullet$ radicals generated by the DET reaction of IdU with e_{pre}^- is not close enough to damage the DNA. The $dU^\bullet$ radicals interact with surrounding water molecules rather than the DNA, thus reducing the probability to cause DNA strand breaks when 500 μM IdU was added to the DNA solution.

DNA samples with/without compound RS-1 were irradiated by UV laser pulses (115 μW, 318 nm) at time intervals 0, 3, 6, 9, 12, 15, 20, and 30 min. The gel electrophoresis images are shown in Fig. 8.5, while their quantitative analysis results are given in Table 8.2. The values given in Table 8.2 are also shown in Fig. 8.6. For the DNA sample in pure water, the percentage of both SSBs and DSBs increase with UV irradiation time. Relatively significant amount of DSBs started to appear at the irradiation time of ~9 min. After the DNA sample was irradiated for 30 min, there were still ~30% of DNA remaining undamaged. With the presence of

250 μM RS-1, both SSBs and DSBs were significantly enhanced under the same UV irradiation time. For the latter case, Relatively significant amount of DSBs start to appear after the DNA sample was irradiated for 5 min only and all the plasmid DNA (supercoiled circular) were damaged after ~15 min irradiation. The DSB percentage increased by a factor of about 2.6 at 30 min irradiation, compared with the DNA sample in pure water. Thus, the presence of compound RS-1 significantly enhances DNA strand breaks under 2-photon ionizing irradiation. These results clearly show that compound RS-1 has a better efficiency than BrdU and IdU in inducing DNA damage.

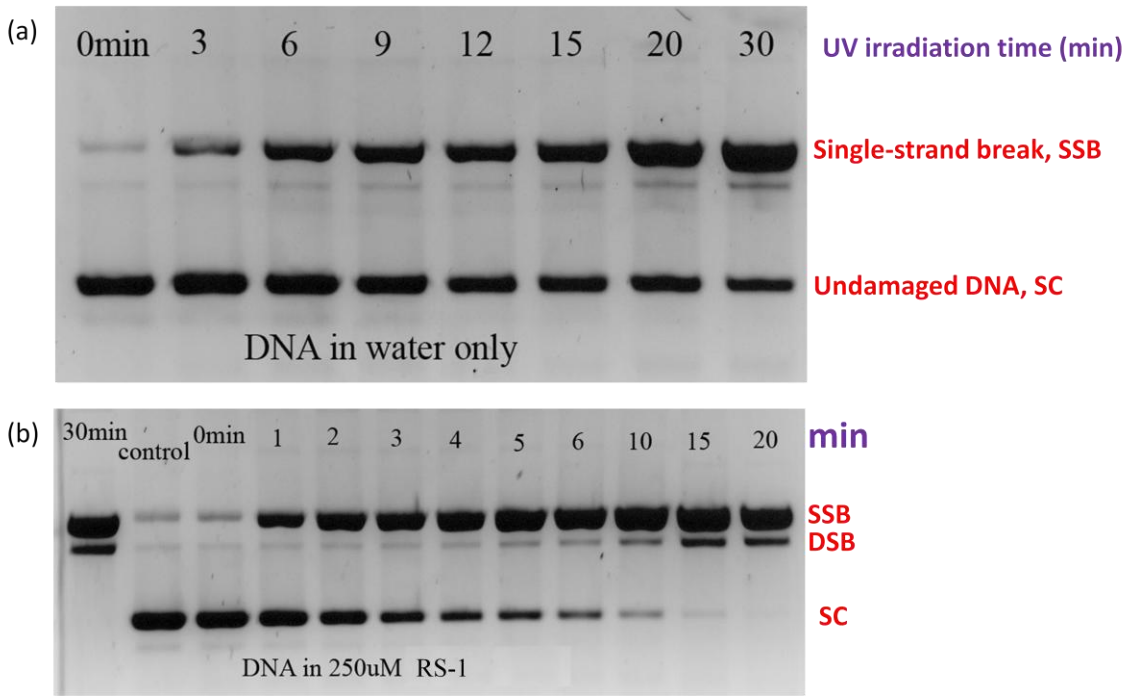

Figure 8.5. DNA gel electrophoresis results of plasmid DNA at different time intervals by UV laser pulses (185 μW, 318 nm). There was 100 ng DNA/lane. (a) DNA in water only; (b) DNA incubated with 250 μM compound RS-1.

Table 8.2. Percentage of strand breaks of the DNA without/with the addition of compound RS-1, for different time intervals of UV laser pulses (185 μW, 318 nm)

irradiation time (min)	SSB (%)		DSB (%)		SC (%)	
	H_2O	250 μM RS-1	H_2O	250 μM RS-1	H_2O	250 μM RS-1
0	6.1	6.7	0	0	93.9	93.3
1		38.8		0		61.2
2		57.5		0		42.5
3	22.2	70.1	0	0	77.8	29.9
4		79		0		21
5		82		3.1		14.9
6	37.8	86.1	0	3.3	62.2	10.6
9	44.4		2.5		53.1	
10		92.1		5.5		2.5
15	54.5	87.9	3.3	12.1	42.2	0
20	60.6	86.6	4.2	13.4	35.1	0
30	65.3	82.6	6.6	17.4	28.1	0

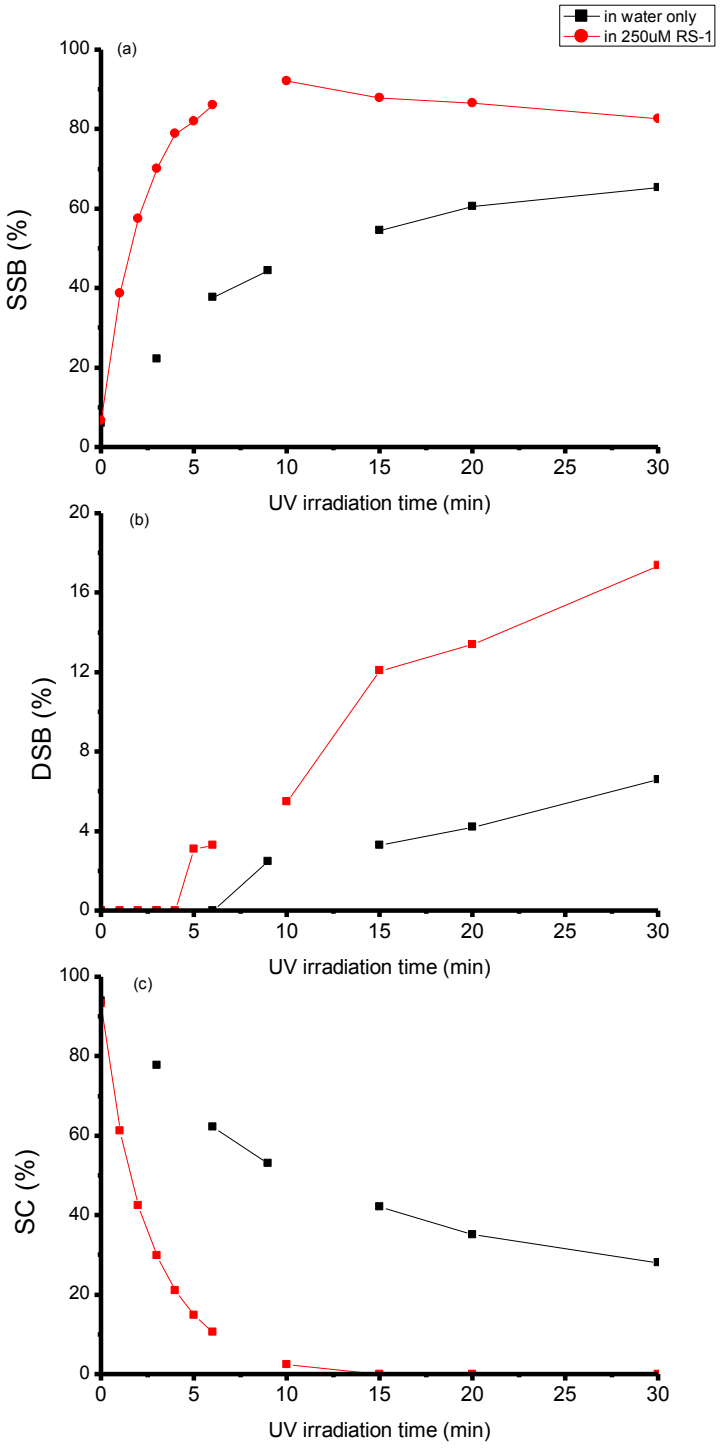

Figure 8.6. Comparison of SSB, DSB, and SC for DNA samples without / with compound RS-1. The black curves represent DNA in water only. The red curves represent DNA in 250 μM RS-1 solution.

8.3.4. Cell viability test

We used the MTT assay to test whether compound RS-1 is more efficient than halopyrimidines in enhancing the radiosensitivity of cancer cells under ionizing radiation. The MTT-based assay relies upon the cellular reduction of tetrazolium salts to their intensely colored formazans. In the MTT results, higher absorbance indicates higher viable cell numbers.

The cytotoxicity (MTT-assay) results for HeLa cells incubated with IdU at various concentrations (0-500 μM) for 24 hr and then exposed to various x-ray doses (0, 20, 40 Gy) are shown in Fig. 8.7. First, without x-ray irradiation (for the zero Gy group), the cell viability (survival rate) showed a IdU dose dependence: about 40% of the treated cells were killed at very high IdU concentrations up to 500 μM. Second, without IdU treatment (at zero IdU concentration), the initial x-ray irradiation up to 20 Gy killed the cells effectively: approximately 70% of the cells were killed, but higher radiation doses up to 40 Gy did not increase the cell killing. The latter indicates that the cells have some degree of resistance to ionizing radiation. Third, the irradiation of the IdU-treated cells with a given x-ray dose (either 20 or 40 Gy) did not show a dependence of the cell survival/viability on IdU concentration in 0-500 μM; the treatment of IdU even increased the cell viability by about 30%. This result seems surprising, but is actually consistant with our DNA gel electrophoresis results in Fig. 8.4 and Table 8.1. IdU decreased DNA strand breaks when it is not incorporated into the DNA. This can be explained by the fact that IdU is a strong electron scavenger. When not incorporated into DNA, it scavenged the e_{pre}^-, which are critical in causing DNA damage [219-220]. The $dU^\bullet$ radicals generated are too far away to abstract a H atom from the DNA (to cause DNA damage). Our test

result in Fig. 8.7 confirms the ineffectiveness of IdU as a radiosensitizer, consistent with the result in recent clinical trials [183].

(a)

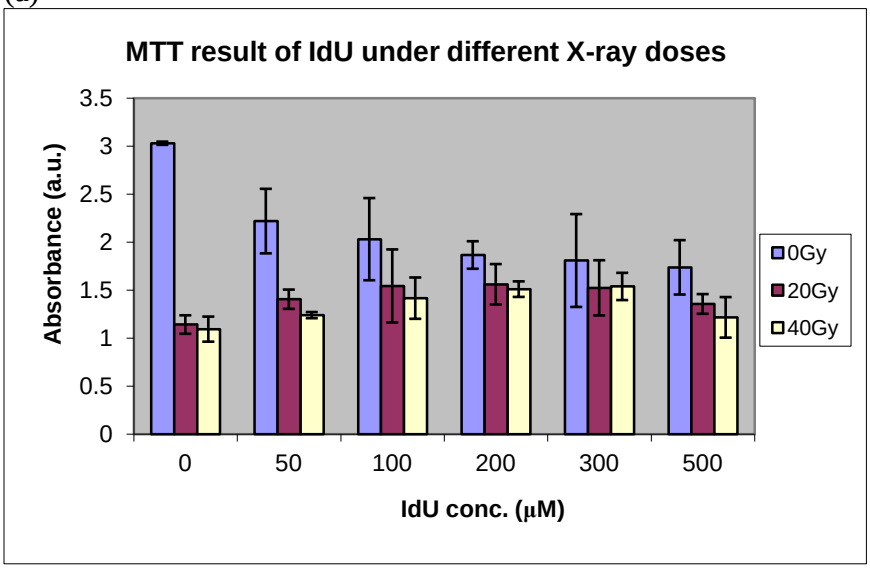

(b)

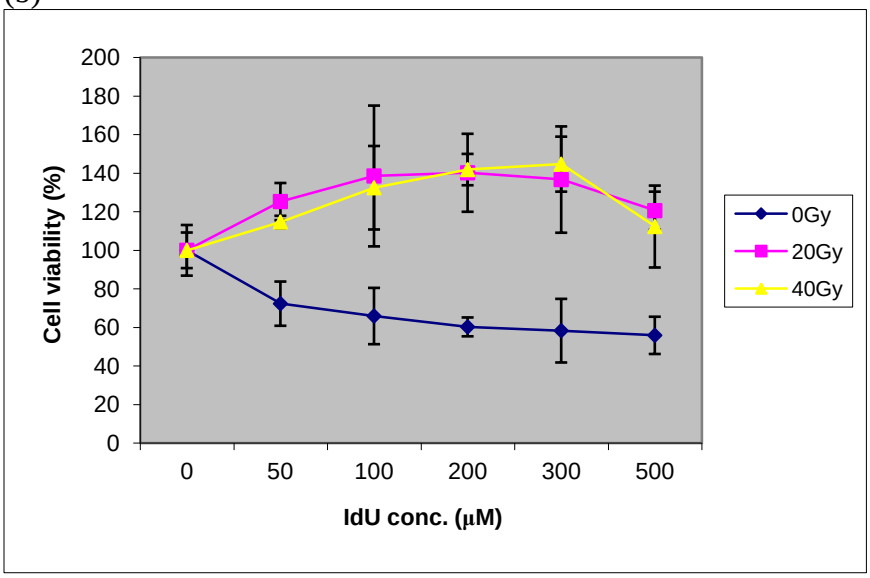

Figure 8.7. Cytotoxicity of IdU at different concentrations and different doses of X-ray irradiation, determined using the MTT assay on Hela cells: (a) Original MTT data. (b) Absorbances of MTT results were converted into percentages of cell viability. The three sets with 0 μM IdU (irradiated by 0, 20, and 40 Gy X-ray) were all normalized to 100% cell viability.

Fig. 8.8 shows the radiosensitizing effect of compound RS-1 for HeLa cells incubated with RS-1 at various concentrations (0-100 μM) for 24 hr and then exposed to various x-ray doses (0, 10, 20 Gy). RS-1 shows some cytotoxic effect on HeLa cells even without ionizing radiation: the percentage of cell viability exhibited a dependence on RS-1 concentration and was reduced from 100% to 45% when RS-1 concentrations were increased from zero to 100 μM. When RS-1 concentration was zero, 10 Gy X-ray decreased cell viability from 100% to 73%, while 20 Gy X-ray decreased cell viability from 100% to 70%. The latter is consistent with the result shown in Fig. 8.7. Interestingly, at a given x-ray dose (either 10 or 20 Gy), the treatment of RS-1 largely reduced the cell viability, which showed a dependence on RS-1 concentration. At the high RS-1 concentration of 100 μM, the x-ray induced cell killing was enhanced by a factor of approximately 5 (100% : 20%). This result is consistent with our gel electrophoresis results shown in Figs. 8.5 and 8.6 and Table 8.2. All of these results show that compound RS-1 has significant radiosensitizing effects, which are much stronger than IdU.

(a)

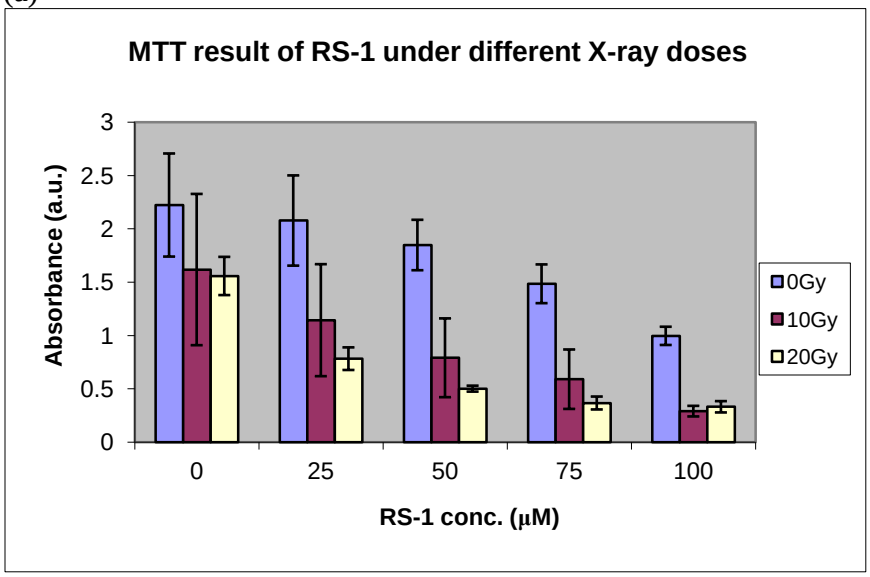

(b)

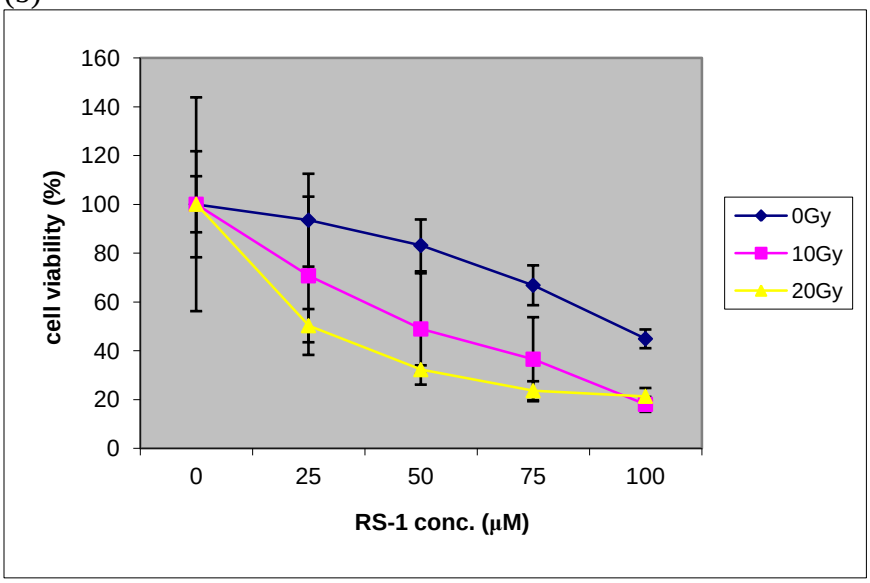

Figure 8.8. Cytotoxicity of compound RS-1 at different concentrations and after different doses of X-ray irradiation, determined using the MTT assay on HeLa cells: (a) Original MTT data. (b) Absorbances of MTT results were converted into percentages of cell viability. The three sets with 0 μM RS-1 (irradiated by 0, 10, and 20 Gy X-ray) were normalized to 100% cell viability.

8.4. Conclusion

The DET reaction of e_{pre}^- with compound RS-1 has been directly observed by our fs-TRLS measurements. RS-1 shows a much higher DET reaction efficacy than IdU (and certainly BrdU and CldU). It was therefore expected that RS-1 will have a much better radiosensitizing effect than halopyrimidines. Indeed our measurements of DNA damage by gel electrophoresis and cell viability by the MTT assay have confirmed that RS-1 can largely enhance the radiosensitivity of the treated human cervical cancer (HeLa) cells to x-ray (ionizing) radiation. It is clearly demonstrated that RS-1 has a much better radiosensitizing effect than IdU.

Chapter 9

Conclusions and Future Work

Direct, real-time observation of molecular reactions is of significant importance in various fields from chemistry, biology, environmental sciences to medicine. *Femtosecond time-resolved laser spectroscopy* (fs-TRLS) has been demonstrated to be a very powerful, direct technique for real-time observation of molecular reactions. It has the capability of observing reactions that actually happenon the ultrashort time scale - femtoseconds. Since the late 1980s, its application to study chemical and biological systems led to the births of new subfields of science, called femtochemistry and femtobiology. Recently, *femtomedicine* has been proposed as a new transdisciplinary frontier to integrate ultrafast laser techniques with biomedical methods for advances in fundamental understandings and treatments of major human diseases. These studies enabled through real-time observation of biochemical reactions at the molecular level may open many opportunities in biomedical fundamental research and clinical applications. For example, the femtomedicine approach is promising to advance the radiotherapy of cancer by obtaining new understandings of radiation-induced DNA damage and the mechanisms of action of existing radiosensitizers. *This thesis presents a molecular-mechanism-based drug discovery project to develop novel drugs for effective radiotherapy of cancer through the emerging* ***femtomedicine*** *approach*. Its ultimate goal is to develop more effective radiosensitizers, based on our unique molecular understandings of ionizing radiation induced DNA damage and halopyrimidines as a family of potential radiosensitizers.

The conclusions of this thesis include the following:

(1) Our careful, high-quality femtosecond time-resolved laser spectroscopic measurements have revealed the universal existence of the coherence spike hidden in ultrafast pump-probe transient absorption spectroscopic results. Our results have resolved the long-standing controversies about the physical nature and lifetimes of ultrashort-lived prehydrated electron (e_{pre}^-), a novel electron species produced in radiolysis of water. We show that the spike effect could result in a shortening of measured e_{pre}^- lifetimes from ~1 ps to almost zero fs. Furthermore, after removal of this spike effect, we found that there are two intrinsic e_{pre}^- states that have lifetimes of 180±30 fs and 545±30 fs, respectively. Moreover, our direct, real-time measurements of the transition state of the dissociative electron transfer (DET) reaction e_{pre}^- with a probe molecule (IdU) have revealed that both the 180 fs and the 545 fs e_{pre}^- state are electronically excited states of the hydrated electron (e_{hyd}^-). The latter is proved to be the decay lifetime of the p-state of e_{hyd}^-, the long-sought wet electron. These results have not only resolved the large discrepancies existing in the literature but provided new insights into electron hydration dynamics in bulk water. Such information is important for quantitative understanding and modeling of the role of non-equilibrium e_{pre}^- in electron-driven reactions in diverse environmental and biological systems, from radiation chemistry and radiation biology to atmospheric ozone depletion.

(2) We obtained the first real-time observation of dissociative electron transfer (DET) reactions of e_{pre}^- with DNA nucleotides in aqueous solutions. Our results show that purines (A and G) are more efficient at capturing e_{pre}^- than pyrimidines (C and T). More interestingly, our observed data show that only T and especially G are vulnerable to DETs of e_{pre}^- leading to

bond breaks, while the electron can be stably trapped at C and especially A to form stable anions. The results not only challenge the conventional notion that damage to the genome by ionizing radiation is mainly induced by the oxidizing ·OH radical, but provide a deeper fundamental understanding of the molecular mechanism of the DNA damage caused by a reductive agent (e_{pre}^-). These findings can be applied to develop new strategies for more effective radiotherapies of disease such as cancer. Furthermore, the direct observation of DNA base specific damage by DET of weakly bound electrons has a broad significance, as there are sources of weakly-bound electrons in biological systems. The resultant DNA strand breaks, if not repaired quickly, could cause genetic mutation and even serious diseases such as cancer. The oxidative damage at the guanine (G) base and its relation to human cancers have been well exploited. The present findings of the most fragile point at the G base and a new molecular mechanism of *reductive* DNA damage could also play a vital role in various disease such as cancer and stroke.

(3) Our results of femtosecond time-resolved laser spectroscopic studies of the molecular mechanism of action of halopyrimidines (XdUs, X=F, Cl, Br and I) as potential hypoxic radiosensitizers have clearly shown that it is the ultrashort-lived e_{pre}^-, rather than the long-lived e_{hyd}^-, that is responsible for DET reactions to XdUs. This reaction leads to the formation of the reactive dU·radical, which can attack DNA by hydrogen abstraction and finally cause DNA strand breaks and cancer cell death. The DET reaction is therefore a key step in the mechanism of action of these pro-drugs in radiotherapy of cancer. Our results have challenged a long accepted mechanism that long-lived e_{hyd}^- would be responsible for the radical formation from halogenated molecules. Furthermore, we found that the DET reaction efficacy leading to the formation of the reactive dU·radical is in the order of FdU

<< CldU < BrdU < IdU. Thus, only BrdU and IdU could be explored as potential radiosensitizers, in agreement with the results of bioactivity tests and clinical trials. Moreover, as a more general conclusion, our results demonstrate that despite their ultrashort lifetimes in femtoseconds, nonequilibrium e_{pre}^- can play a crucial role in many ET reactions occurring in aqueous environments, especially for chlorine-, bromine- and iodine-containing molecules, which also have important impacts on the Earth's environment.

(4) Our fs-TRLS studies have demonstrated the DET reactions of BrdU/ IdU with $dAMP^{*-}$ and $dGMP^{*-}$ formed by attachment of e_{pre}^- generated by radiolysis of water in aqueous BrdU-dAMP/dGMP and IdU-dAMP/dGMP complexes under ionizing radiation. The results have provided a molecular mechanism for the DNA sequence selectivity of BrdU and IdU in radiosensitization. This new mechanistic insight into the interaction of BrdU and IdU with DNA provides clues to improve the halogen family as potential radiosensitizers and to develop more effective radiosensitizers for clinical applications.

(5) Comparing with our observed results of the DET reaction of cisplatin with e_{pre}^- generated in radiotherapy, we found that the DET reactions of BrdU and IdU with e_{pre}^- are much weaker so that they are hardly effective radiosensitizers. Thus, there is little chance for BrdU and IdU to be effective radiosensitizers for clinical use. Instead, development of other compounds to enhance the radiosensitivity of cancer cells is suggested.

(6) Based on our molecular mechanistic understandings of DNA damage induced by ionizing radiation and halopyrimidines as potential radiosensitizers, we are now developing more effective new radiosensitizing drug candidates through the femtomedicine approach integrating fs-TRLS with biomedical methods. We have performed a fs-TRLS study of the

DET reaction of a candidate compound (RS-1) with e_{pre}^-, and found that the DET reaction of e_{pre}^- with RS-1 is much stronger than that of IdU (and certainly BrdU and CldU). Moreover, we have tested the radiosensitizing effect of RS-1 against human cervical cancer (HeLa) cells exposed to various doses of x-ray irradiation through DNA damage measurements by gel electrophoresis and cell viability/death assays by MTT. Our results have confirmed that RS-1 can largely enhance the radiosensitivity of treated human cervical cancer (HeLa) cells to x-ray (ionizing) radiation. It is clearly demonstrated that RS-1 has a much better radiosensitizing effect than IdU. Although these are just preliminary results, our results have shown the high potential of utilizing our unique molecular understandings of the biological effect of ionizing radiation and the action of halopyrimidines to develop more effective radiosensitizers.

In summary, our studies have demonstrated the potential of *femtomedicine* as an exciting new frontier to bring breakthroughs in understanding fundamental biological processes and to provide an efficient and economical strategy for development of new anticancer drugs. Further tests of RS-1 and other compounds in cancer cell lines and animal cancer models will be needed in the future.

REFERENCES:

[1] http://www.cancer.gov/cancertopics/understandingcancer/cancer

[2] Roger J. B. King, and Mike W. Robins, 'Cancer Biology', Third edition (2006).

[3] G. M. Cooper, 'The Cancer Book' (1993).

[4] M. Blasco, C. J. Norbert, et.al, 'The Molecular Biology of Cancer', edited by Stella Pelengaris and Michael Khan (2006).

[5] http://training.seer.cancer.gov/disease/categories/classification.htm

[6] http://www.center4cancer.com/categories-cancer.php

[7] http://www.cancer.gov/cancertopics/cancerlibrary/what-is-cancer

[8] http://www.ons.org/Publications/Books/Excerpts/INPU0597intro

[9] http://www.ncbi.nlm.nih.gov/books/NBK9963/

[10] P. Vaupel, 'Tumour microenvironmental physiology and its implications for radiation oncology', Semin. Radiat. Oncol. 14, 198 (2004).

[11] I. F. Tannock, 'Tumour physiology and drug resistance', Cancer Metastasis Rev. 20, 123 (2001).

[12] S. Lehnert, 'Biomolecular Action of Ionizing Radiation', Taylor & Francis, Boca Raton (2007).

[13] D. Fukumura, D. G. Duda, L. L. Munn, and R. K. Jain, 'Tumor microvasculature and microenvironment: novel insights through intravital imaging in pre-clinical models', Microcirculation 17(3), 206-225 (2010).

[14] D. Fukumura, and R. K. Jain, 'Tumor microenvironment abnormalities: causes, consequences, and strategies to normalize', J. cellular Biochemistry 101, 937 (2007).

[15] A. J. Leu, D. A. Berk, A. Lymboussaki, K. Alitalo and P. K. Jain, 'Absence of functional lymphatics within a murine sarcoma: a molecular and functional evaluation', Cancer Res. 60, 4324 (2000).

[16] T. P. Padera, A. Kadambi, E. di Tomaso, et. al., 'Lymophatic metastasis in the absence of functional intratumour lymphatics', Science 296, 1883 (2002).

[17] R. K. Jain, 'Physiological barriers to delivery of monoclonal antibodies and other macromolecules in tumours', Cancer Res. 50, 814 (1990).

[18] C. J. Koch, 'Measurement of absolute oxygen levels in cells and tissues using oxygen sensors and 2-nitroimidazole EF5', Methods Enzymol. 352, 3 (2002).

[19] P. Vaupel, K. Schlenger, C. Knoop and M. Hockel, 'Oxygenation of human tumours: evaluation of tissue oxygen distribution in breast cancers by computerized O_2 tension measurements', Cancer Res. 51, 3316 (1991).

[20] F. Kallinowski, R. Zander, M. Hockel and P. Vaupel, 'Tumour tissue oxygenation as evaluated by computerized-pO_2-histography', Int. J. Radiat. Oncol. Biol. Phys. 19, 953 (1990).

[21] H. Izumi, T. Torigoe, H. Ishiguchi, et al. 'Cellular PH regulations: potentially promising molecular targets for cancer chemotherapy', Cancer Res. 56, 1194 (1996).

[22] D. M. Prescott, H. C. Charles, J. M. Poulson et al. 'The relationship between intracellular and extracellular pH in spontaneous canine tumours', Clin. Cancer Res. 6, 2501 (2000).

[23] Malin Dollinger, Ernest H. Rosenbaum, and Greg Cable, 'Everyone's Guide to Cancer Therapy', Kansas City, MO: Andrews and McMeel (1991).

[24] Paras N. Prasad, 'Introduction to Biophotonics', Hoboken, N.J.: Wiley-Interscience (2003).

[25] R. Clairns, I. Papandreou and N. Denko, 'Overcoming Physiologic Barriers to Cancer Treatment by Molecularly Targeting the Tumour Microenvironemnt', Mol. Cancer Res. 4(2), 61 (2006).

[26] R. K. Jain, 'Transport of molecules in the tumour interstitium: a review', Cancer Res., 47, 3039 (1987).

[27] B. D. Curti, W. J. Urba, W. G. Alvord, et al., 'Interstitial pressure of subcutaneous nodules in melanoma and lymphoma patients: changes during treatment', Cancer Res. 53, 2204 (1993).

[28] L. E. Gerweck, S. V. Kozin and S. J. Stocks, 'The PH partition theory predicts the accumulation and toxicity of doxorubicin in normal and low-PH adapted cells', Br. J. Cancer 79, 838 (1999).

[29] S. Koch, F. Mayer, F. Honecker, M. Schittenhelm and C. Bokemeyer, 'Efficacy of cytotoxic agents used in the treatment of testicular germ cell tumours under normoxic and hypoxic conditions in vitro', Br. J. Cancer 89, 2133 (2003).

[30] S. L. Green, R. A. Freiberg and A. J. Giaccia, 'p21 (Cip1) and p27 (Kip1) regulate cell cycle re-entry after hypoxic stress but are not necessary for hypoxia-induced arrest', Mol. Cell Biol. 21, 1196 (2001).

[31] J. K. Mohindra and A. M. Rauth, 'Increased cell killing by metronidazole and nitrofurazone of hypoxic compared to aerobic mammalian cells', Cancer Res. 36, 930 (1976).

[32] A. Fyles, M. Milosevic, D. Hedley, et al., 'Tumour hypoxia has independent predictor impact only in patients with node-negative cervix cancer', J. Clin. Oncol. 20, 680 (2002).

[33] D. M. Brizel, S. P. Scully, J. M. Harrelson, et al., 'Tumour oxygenation predicts for the likelihood of distant metastases in human soft tissue sarcoma', Cancer Res. 56, 941 (1996).

[34] M. Nordsmark and J. Overgaard, 'Tumour hypoxia is independent of hemoglobin and prognostic for loco-regional tumour control after primary radiotherapy in advanced head and neck cancer', Acta Oncol. 43, 396 (2004).

[35] W. U. Shipley, J. A. Stanley, V. D. Courtenay and S. B. Field, 'Repair of radiation damage in Lewis lung carcinoma cells following in situ treatment with fast neutrons and γ-rays', Cancer Res. 35, 932 (1975).

[36] J. Dougherty, C. J. Gomer, B. W. Henderson et. al, 'Review: photodynamic therapy', J. Natl. Cancer. Inst. 90, 889 (1998).

[37] W. Sneader, 'Drug Discovery: a history', John Wiley & Sons. Ltd. pp: 1-5 (2005).

[38] 'Lead generation approaches in drug discovery', Edited by Z. Rankovic and R. Morphy, Wiley A join wiley & sons, inc. publication (2010).

[39] B. D. Anson, J. Ma and J.-Q. He, 'Identifying cardiotoxic compounds', Genet. Eng. & Biotechnol. News 29(9), 34 (2009).

[40] B. H. Littman and R. Krishna, 'Translational medicine and drug discovery', Cambridge University Press, pp: 329, (2011).

[41] S. M. Paul, D. S. Mytelka, C. T. Dunwiddie, C. C. Persinger, B. H. Munos, S. R. Lindborg and A. L. Schacht, 'How to improve R&D productivity: the pharmace Futical industry's grand challenge', Nat. Rev. Drug Discov. 9(3), 203(2010).

[42] I. Reedijk, 'New clues for platinum antitumor chemistry: Kinetically controlled metal binding to DNA', Proc. Natl. Acad. Sci. USA 100, 3611 (2003).

[43] M. A. Fuertes, C. Alonso, J. M. Perez, 'Biochemical modulation of cisplatin mechanisms of action: enhancement of antitumor activity and circumvention of drug resistance', Chem. Rev. 103, 645 (2003).

[44] D. Wang and S. Lippard, 'Cellular Processing of platinum anticancer drugs', Nature review: drug discovery 4, 307 (2005).

[45] Q.-B. Lu, 'Molecular Reaction Mechanisms of Combination Treatments of Low-Dose Cisplatin with Radiotherapy and Photodynamic Therapy', J. Med. Chem. 50, 2601 (2007).

[46] Q.-B. Lu, S. Kalantari and C.-R. Wang, 'Electron Transfer Reaction Mechanism of Cisplatin with DNA at the Molecular Level', Mol. Pharmaceutics 4, 624 (2007).

[47] Q.-B. Lu, 'Effects of Ultrashort-Lived Prehydrated Electrons in Radiation Biology and Their Applications for Radiotherapy of Cancer', Reviews in Mutation. Research 704, 190 (2010).

[48] D. J. Pizzarello and R. L. Witcofski, 'Basic Radiation Biology', Philadelphia: Lea & Febiger, (1967).

[49] E. L. Alpen, 'Radiation Biophysics', San Diego: Academic Press, p103 (1990).

[50] A. Cole, 'The study of radiosensitive structures with low voltage electron beams' in 'Cellular Radiation Biology', Baltimore: Williams and Wilkins, pp. 267-271 (1965).

[51] T. R. Munro, 'The relative radiosensitivity of the nucleus and cytoplasm of Chinese hamster fibroblasts', Radiat. Res. 42, 451 (1970).

[52] R. Datta, A. Cole and S. Robinson, 'Use of track-end alpha particles from 241Am to study radiosensitive sites in CHO cells', Radiat. Res. 65, 139 (1976).

[53] A. Cole, R. E. Meyn, R. Chen, P. M. Corry and W. Hittelman, 'mechanism of cell injury', in 'Radiation Biology In Cancer Research', edited by R. E. Meyn and H. R. Withers, New York: Raven Press, pp. 33-58 (1980).

[54] A. Graslund, A. Ehrenberg, A. Rupprecht and G. Strom, 'Ionic base radicals in γ-irradiated DNA', Biochim. Biophys. Acta 254, 172 (1971).

[55] A. Graslund, A. Ehrenberg, A. Rupprecht and G. Strom, 'Ionic base radicals in γ-irradiated oriented non-deuterated and fully deuterated DNA', Int. J. Radiat. Biol. 28, 313 (1975).

[56] A. Graslund, A. Ehrenberg, A. Rupprecht and G. Strom, 'Free-radical formation in γ-irradiated oriented DNA containing electron-affinic radiosensitizers', Int. J. Radiat. Biol. 31, 145 (1977).

[57] J. Huttermann, K. Voit, H. Oloff, W. Kohnlein, A. Graslund and A. Rupprecht, 'Specific formation of electron gain and loss centers in X-irradiated oriented fibres of DNA at low temperatures', Faraday Discuss. Chem. Soc. 78, 135 (1984).

[58] S. Gregoli, M. Olast and A. Bertinchamps, 'Radiolytic pathways in γ-irradiated DNA: influence of chemical and conformational factors', Radiat. Res. 89, 238 (1982).

[59] P. J. Boon, P. M. Cullis and M. C. R. Symons, 'Effects of ionizing radiation on deoxyribonucleic acid and related systems. Part I. the role of oxygen', J. Chem. Soc. Perkin Trans. 2, 1393 (1984).

[60] M. D. Sevilla, J. B. D'Arcy, K. W. Morehouse and M. L. Englehardt, 'Antigenicity of DNA induced by photo addition of 8-methoxypsoralen', Photochem. Photobiol. 28, 37 (1978).

[61] M. D. Sevilla, D. Becker, M. Yan and S. R. Summerfield, 'Relative abundance of primary ion radicals in γ-irradiated DNA: Cytosine vs Thymine anions and guanine vs adenine cations', J. Phys. Chem. 95, 3409 (1991).

[62] M. Yan, D. Becker, S. Summerfield, P. Renke and M. D. Sevilla, 'Relative abundance of primary ion radicals in γ-irradiated DNA at low temperatures. 2. Single- vs double-stranded DNA', J. Phys. Chem. 96, 1983 (1992).

[63] J. Huttermann, A. Scharffer and G. Kraft, 'Free radicals induced in solid DNA by heavy ion bombardment', Adv. Space Res. 9(10), 35 (1989).

[64] J. Huttermann and A. Scharffer, 'Heavy-ion-induced free radical formation in solid DNA constituents: quantitative and structural aspects', Int. J. Radiat. Appl. Instrum. Part A 40, 915 (1989).

[65] A. Scharffer, J. Huttermann and G. Kraft, 'Direct radiation action of heavy ions as studied by ESR-spectroscopy', Adv. Space Res. 12(2), 45 (1992).

[66] A. Scharffer, J. Huttermann and G. Kraft, 'Free radicals from polycrystalline pyrimidines and purines upon heavy ion bombardment at low temperatures; an electron spin resonance study', Int. J. Radiat. Biol. 63, 139 (1993).

[67] D. Becker, Y. Razskazovskii, M. U. Callaghan and M. D. Sevilla, 'Electron spin resonance of DNA irradiated with a heavy-ion beam ($^{16}O^{8+}$): Evidence for damage to the deoxyribose phosphate backbone', Radiat. Res. 146, 361 (1996).

[68] W. Wang, M. Yan, D. Becker and M. D. Sevilla, 'The influence of hydration on the absolute yields of primary ionic free radicals in γ-irradiated DNA at 77K. II. Individual radical yields', Radiat. Res. 137, 2 (1994).

[69] C. Tronche, B. K. Goodman and M. M. Greenberg, 'DNA damage induced via independent generation of the radical resulting from formal hydrogen abstraction from the C1'-position of a nucleotide', Chem. Biol. 5, 263 (1998).

[70] W. K. Pogozelski and T. D. Tullius, 'Oxidative strand scission of nucleic acids: route initiated by hydrogen abstraction from the sugar moiety', Chem. Rev. 98, 1089 (1998).

[71] Y. Razskazovskii, M. Roginskaya and M. D. Sevilla, 'Modification of the reductive pathway in gamma-irradiated DNA by electron scavengers: Targeting the sugar-phosphate backbone', Radiat. Res. 149, 422 (1998).

[72] L. I. Shukla, R. Pazdro, J. Huang, C. Devreugd, D. Becker and M. D. Sevilla, 'The formation of DNA sugar radicals from photoexcitation of guanine cation radicals', Radiat. Res. 161, 582 (2004).

[73] B. Weiland and J. Huttermann, 'Free radicals from lyophilized 'dry' DNA bombarded with heavy ions as studied by electron spin resonance spectroscopy', Int. J. Radiat. Biol. 75, 1169 (1999).

[74] M. G. Debije and W. A. Bernhard, 'Electron paramagnetic resonance evidence for C3' sugar radical in cryatalline d(CTCTCGAGAG) X-irradiated at 4K', Radiat. Res. 155, 687 (2001).

[75] D. Becker, A. Bryant-Friedrich, C. Trzasko and M. D. Sevilla, 'Electron spin resonance study of DNA irradiated with an argon-ion beam: evidence for formation of sugar phosphate backbone radicals', Radiat. Res. 160, 174 (2003).

[76] L. I. Shukla, R. Pazdro, D. Becker and M. D. Sevilla, 'Sugar radicals in DNA: Isolation of neutral radicals in gamma-irradiated DNA by hole and electron scavenging', Radiat. Res. 163, 591 (2005).

[77] H. S. W. Massey, ‘Negative Ions’, Cambridge Univ. Press, London (1976).

[78] B. Boudaiffa, P. Cloutier, D. Hunting, M. A. Huels and L. Sanche, ‘Resonant Formation of DNA Strand Breaks by Low-energy (3-20eV) Electrons’, Science, 287, 1658 (2000).

[79] B. D. Michael and P. O'Neill, ‘A Sting in the Tail of Electron Tracks’, Science 287, 1603 (2000).

[80] D. T. Goodhead and H. Nikjoo, ‘Track structure analysis of ultrasoft X-rays compared to high- and low-LET radiations’, Int. J. Radiat. Biol. 55, 513 (1989).

[81] H. Nikjoo, D. T. Goodhead, D. E. Charlton and H. G. Paretzke, ‘Energy deposition in cylindrical volume by monoenergetic electrons 10 eV – 100 keV’, Int. J. Radiat. Biol. 60, 739 (1991).

[82] D. T. Goodhead and D. J. Brenner, ‘Estimation of a single property of low LET radiation which correlates with biological effectiveness’, Phys. Med. Biol. 28, 485 (1983).

[83] H. Nikjoo, D. T. Goodhead and H. G. Paretzke, ‘Energy deposition in small cylindrical targets by ultrasoft x-rays’, Phys. Med. Biol. 34, 691 (1989).

[84] H. Nikjoo, P. O’Neil, D. T. Goodhead and M. Terrissol, ‘Computational modelling of low-energy electron-induced DNA damage by early physical and chemical events’, Int. J.Radiat. Biol. 71, 467(1997).

[85] S. W. Botchway, D. L. Stevens, M. A. Hill, T. J. Jenner and P. O’Neil, ‘Induction and rejoining of DNA double-strand breaks in Chinese hamster V79-4 cells irradiated with characteristic Aluminum K and Copper L ultrasoft C rays’, Radiat. Res. 148, 317 (1998).

[86] F. Martin, P. D. Burrow, Z. Cai, P. Cloutier, D. Hunting and L. Sanche, ‘DNA Strand Breaks Induced by 0-4 eV Electrons: The Role of Shape Resonances’, Phys. Rev. Lett. 93, 068101 (2004).

[87] C. König, J. Kopyra, I. Bald and E. Illenberger, 'Dissociative Electron Attachment to Phosphoric Acid Esters: The Direct Mechanism for Single Strand Breaks in DNA', Phys. Rev. Lett. 97, 018105 (2006).

[88] H. Abdoul-Carime, J. Langer, M. A. Huels and E. Illenberger, 'Decomposition of purine nucleobases by very low energy electrons', Eur. Phys. J. D35, 399 (2005).

[89] R. Barrios, P. Shurski and J. Simons, 'Mechanism for Damage to DNA by Low-Energy Electrons', J. Phys. Chem. B106, 7991 (2002).

[90] J. Berdys, I. Anusiewicz, P. Skurski and J. Simons, 'Damage to Model DNA Fragments from Very Low-Energy (<1 eV) Electrons', J. Am. Chem. Soc. 126, 6441(2004).

[91] J. Simons, 'How Do Low-Energy (0.1-2 eV) Electrons Cause DNA-Strand Breaks?', Acc. Chem. Res. 39, 772 (2006).

[92] X. Bao, J. Wang, J. Gu and J. Leszczynski, 'DNA strand breaks induced by near-zero-electronvolt electron attachment to pyrimidine nucleotides', Proc. Natl. Acad. Sci. USA 103, 5658 (2006).

[93] J. Gu, Y. Xie and H. F. Schaefer III, 'Near 0 eV Electrons Attach to Nucleotides', J. Am. Chem. Soc. 128, 1250 (2006).

[94] J. Gu, Y. Xie and H. F. Schaefer III, 'Electron attachment to DNA single strands: gas phase and aqueous solution', Nucl. Acid. Res. 35, 5165 (2007).

[95] A. Kumar and M. D. Sevilla, 'Low-Energy Electron Attachment to 5'-Thymidine Monophosphate: Modeling Single Strand Breaks Through Dissociative Electron Attachment', J. Phys. Chem. B111, 5464 (2007).

[96] P. Schyman and A. Laasksonen, 'On the Effect of Low-Energy Electron Induced DNA Strand Break in Aqueous Solution: A Theoretical Study Indicating Guanine as a Weak Link in DNA'. J. Am. Chem. Soc. 130, 12254 (2008).

[97] Q.-B. Lu and L. Sanche, 'Enhanced dissociative electron attachment to CF_2Cl_2 by transfer of electrons in precursors to the solvated state in water and ammonia ice', Phys. Rev. B63, 153403 (2001).

[98] Q.-B. Lu and L. Sanche, 'Large enhancement in dissociative electron attachment to HCl adsorbed on H_2O ice via transfer of presolvated electron', J. Chem. Phys. 115, 5711 (2001).

[99] Q.-B. Lu and L. Sanche, 'Enhancement in dissociative electron attachment to CF4 Chlorofluorocarbons and hydrochlorofluorocarbons adsorbed on H_2O ice', J. Chem. Phys. 120, 2434 (2004).

[100] 'Radiation Chemistry: Principles and Applications', Edited by Farhataziz and Michael A. J. Rodgers, VCH Publishers (1987).

[101] G. V. Buxton, C. L. Greenstock, W. P. Helman, and A. B. Ross, 'Critical reviews of rate constants for reactions of hydrated electrons, hydrogen atoms and hydroxyl radicals (OH/ O^-) in aqueous solution', J. Phys. Chem. Ref. Data 17, 513 (1988)

[102] C von Sonntag, 'The Chemical Basis of Radiation Biology', London: Taylor & Francis (1987).

[103] P. O'Neil and D. Schulte-Frohlinde, 'Evidence for formation of a $(TlOH)^+$ complex', J. Chem. Soc. Chem. Commun. 387 (1975).

[104] K. D. Asmus, M. Bonifacic, P. Toffel, P. O'Neil, D. Schulte-Frohlinde and S. Steenken, 'On the hydrolysis of Ag^{II}, Tl^{II}, Sn^{III} and Cu^{III}', J. Chem. Soc. Faraday Trans. I74, 1820 (1978).

[105] G. V. Buxton, 'Radiation chemistry of metal-ions in aqueous splution', Coord. Chem. Rev. 22, 195 (1977).

[106] M. N.Schuchmann and C. von Sonntag, 'Radiation Chemistry of carbohydrates, Part 14 Hydroxyl radical-induced oxidation of D-glucose in oxygenated aqueous solution', J. Chem. Soc. Perkin Trans. II1958 (1977).

[107] E. J. Hart and M. Anbar, 'The Hydrated Electron', New York: Wiley-Interscience (1970).

[108] S. Fujita and S. Steenken, 'Pattern of OH radical addition to uracil and methyl- and carboxyl-substituted uracils. Electron transfer of OH adducts with N,N,N',N'-tetramethyl-p-phenylenediamine and tetranitromethane', J. Am. Chem. Soc. 103, 2540 (1981).

[109] D. K. Hazra and S. Steenken, 'Pattern of OH radical addition to cytosine and 1-, 3-, 5- and 6-substituted cytosines. Electron transfer and dehydration reactions of the OH adducts', J. Am. Chem. Soc. 105, 4380 (1983).

[110] 'DNA and free radicals', edited by B. Halliwell and O. I. Aruoma, Ellis Horwood Limited, pp19-40 (1993).

[111] A. Hissung, and C. von Sonntag, 'The reaction of solvated electrons with cytosine, 5-methylcytosine and 2'-deoxycytidine in aqueous solutions. The reaction of the electron adduct intermediates with water, p-nitroacetophenone and oxygen. A pulse spectroscopic and pulse conductometric study', Int. J. Radiat. Biol., 35, 449 (1979)

[112] S. Das, D. J. Deeble, M. N. Schuchmann, and C. von Sonntag, 'Pulse radiolytic studies on uracil and uracil derivatives. Protonation of their electron adducts at oxygen and carbon', Int. J. Radiat. Biol., 46, 7 (1984)

[113] H. M. Novais, and S. Steenken, 'ESR studies of electron and hydrogen adducts of thymine and uracil and their derivatives and of 4,6-dihydroxyprimidines in aqueous solution. Comparison with data from solid state. The protonation at carbon of the electron adducts', J. Am. Chem. Soc. 108, 1 (1986)

[114] S. Nishimoto, H. Ide, T. Wada and T. Kagiya, 'Radiation-induced hydroxylation of thymine promoted by electron-affinic compounds', Int. J. Radiat. Biol. 44, 585 (1983).

[115] E. A. Furlong, T. J. Jorgenson and W. D. Henner, 'Production of dihydrothymine stereoisomers in DNA by gamma-radiation', Biochemistry 25, 4344 (1986).

[116] S. Boiteux, E. Gajewski, J. Laval and M. Dizdaroglu, 'Substrate specificity of the Escherichia coli Fpg protein (formamidopyrimidine – DNA glycosylase): excision of purine

lesions in DNA produced by ionizing radiation or photosensitization', Biochemistry 31, 106 (1992).

[117] A. Bonicel, N. Mariaggi, E. Hughes and R. Teoule, 'In vitro gamma irradiation of DNA: identification of radiation-induced chemical modification of the adenine moiety', Radiat. Res. 83, 19 (1980).

[118] C. J. Chetsanga and C. Grigorian, 'A dose-response study on opening of imidazole ring of adenine in DNA by ionizing radiation', Int. J. Radiat. Biol. 44, 321 (1983).

[119] H. Kasai, P. F. Crain, Y. Kuchino et. al, 'Formation of 8-hydroxyguanine moiety in cellular DNA by agents producing oxygen radicals and evidence for its repair', Carcinogenesis 7, 1849 (1986).

[120] M. Dizdaroglu, 'Formation of an 8-hydroxyguanine moiety in deoxyribonucleic acid on gamma-irradiation in aqueous solution', Biochemistry 24, 4476 (1985).

[121] S. Shibutani, M. Takeshita and A. P. Grollman, 'Insertion of specific bases during DNA synthesis past the oxidation-damaged base 8-oxodG', Nature 349, 431 (1991).

[122] T. R. O'Conner, S. Boiteux and J. Laval, 'Ring-opened 7-methylguanine residues in DNA are a block to in vivo DNA synthesis', Nucleic Acids Res. 16, 5879 (1988).

[123] E. J. Hall and A. J. Giaccia, 'Radiobiology for the Radiologist', 6th Ed., Lippincott Williams & Wilkins (2006).

[124] F. J. Nabben, H. A. van der Stroom and H. Loman, 'Inactivation of biologically active DNA by isopropanol and formate radicals', Int. J. Radiat. Biol. 43, 495 (1983).

[125] R. Roots and S. Okada, 'Protection of DNA molecules of cultured mammalian cells from radiation-induced single-strand scissions by various alcohols and SH compounds', Int. J. Radiat. Biol. 21(4), 329 (1972).

[126] K. van Rijn, T. Mayer, J. Block, J. B. Verberne and H. Loman, 'Reaction rate of ·OH radicals with ϕX174 DNA: influence of salt and scavenger', Int. J. Radiat. Biol., 47, 309 (1985).

[127] A. P. Reuvers, C. L. Greenstock, J. Borsa and J. D. Chapman, 'Studies on the mechanism of chemical radioprotection by Dimethyl Sulphoxide', Int. J. Radiat. Biol. 24(5), 533 (1973).

[128] C. M. deLara, T. J. Jenner, K. M. S. Townsend, S. J. Marsden and P. O'Neil, 'The effect of dimethyl sulfoxide on the induction of DNA double-strand breaks in V79-4 mammalian cells by alpha particles', Radiat. Res. 144, 43 (1995).

[129] J. Block, L. H. Luthjens and A. L. M. Roos, 'The radiosensitivity of bacteriophage DNA in aqueous solution', Radiat. Res. 30, 468 (1967).

[130] K. D. Held, R. W. Synek and E. L. Powers, 'Radiation sensitivity of transforming DNA', Int. J. Radiat. Biol. 33, 317 (1978).

[131] K. D. Held and E. L. Powers, 'Protection of transforming DNA from x-irradiation-induced damage by OH scavengers', Int. J. Radiat. Biol. 36, 665 (1979).

[132] T. Ito, S. C. Baker, C. D. Stickley, J. G. Peak and M. J. Peak, 'Dependence of the yield of strand breaks induced by γ-ray in DNA on the physical conditions of exposure: water content and temperature', Int. J. Radiat. Biol. 63, 289 (1993).

[133] E. S. Henle, Y. Luo, W. Gassman and S. Linn, 'Fe^{2+}, Fe^{3+} and oxygen react with DNA-derived radicals formed during iron-mediated Fenton reactions', J. Biol. Chem. 271, 21167 (1996).

[134] Y. Luo, E. S. Henle and S. Linn, 'Oxidative damage to DNA constitutes by iron-mediated Fenton reactions. The deoxycytidine family', J. Biol. Chem. 271, 21167 (1996).

[135] M. Dizdaroglu, 'Oxidative damage to DNA in mammalian chromatin', Mutat. Res. 275, 331 (1992).

[136] T. Lindahl, 'DNA glycosylases, endonucleases for apurinin / apyrimidinic sites and base excision repair', Prog. Nucleic. Acid. Res. Mol. Biol. 22, 135 (1979).

[137] K. B. Beckman and B. N. Ames, 'Oxidative decay of DNA', J. Biol. Chem. 272, 19633 (1997).

[138] J. F. Ward, 'Biochemistry of DNA lesions', Radiat. Res. 104, S103 (1985).

[139] A. Migus, Y. Gauduel, J. L. Martin and A. Antonetti, 'Excess electrons in liquid water: first evidence of a prehydrated state with femtosecond lifetime', Phys. Rev. Lett. 58, 1559 (1987).

[140] M. Assel, R. Laenen and A. Laubereau, 'Dynamics of excited solvated electrons in aqueous solution monitored with femtosecond-time and polarization resolution' J. Phys. Chem. A102, 2256 (1998).

[141] M. Assel, R. Laenen and A. Laubereau, 'Retrapping and solvation dynamics after femtosecond UV excitation of the solvated electron in water', J. Chem. Phys. 111(15), 6869 (1999).

[142] R. Laenen, T. Roth and A. Laubereau, 'Novel precursors of solvated electrons in water: evidence for a charge transfer process', Phys. Rev. Lett. 85 (1), 50 (2000).

[143] J. Bernier, E. J. Hall and A. Giaccia, 'Radiation Oncology: a century of achievements', Nat. Rev. Cancer, 4, 737 (2004).

[144] T. Y. Seiwert, J. K. Salama and E. E. Vokes, 'The concurrent chemoradiation paradigm-general principles', Nat. Clin. Pract. Oncol. 4, 86 (2007).

[145] P. Bischoff, A. Altmeyer and F. Dumont, 'Radiosensitizing agents for the radiotherapy of cancer: advances in traditional and hypoxia targeted radiosensitizers', Expert. Opin. Ther. Petents 19(5), 643 (2009).

[146] P. Wardman, 'Chemical radiosensitizers for use in radiotherapy', Clin. Oncol. 19, 397 (2007).

[147] D. S. Shewach and T. S. Lawrence, 'Antimetabolite radiosensitizers', J. Clin. Oncol. 25, 4043 (2007).

[148] H. Kazuno, Y. Shimamoto, H. Tsujimoto, et. al, 'Mechanism of action of a new antitumour ribonucleoside. 1-(3-C-ethynyl-beta-D-ribo-pentofuranosyl)cytosine (ECyd, TAS-106), differs from that of 5-fluorouracil.', Oncol. Rep. 17, 1453 (2007).

[149] M. J. Cariveau, M. Stackhouse, X. L. Cui et. al, 'Clofarabine acts as radiosensitizer in vitro and in vivo by interfering with DNA damage response', Int. J. Radiat. Oncol. Biol. Phys. 70, 213 (2008).

[150] C. A. Barker, W. E. Burgan, D. J. Carter, et. al. 'In vitro and in vivo Radiosensitization induced by the ribonucleotide reductase inhibitor triapine (3-aminopyridine-2-carboxaldehyde-thiosemicarbazone)', Clin. Cancer Res. 12, 2912 (2006).

[151] P. Anderson, D. Aguilera, M. Pearson, et. al., 'Outpatient chemotherapy plus radiotherapy in sarcomas: improving cancer control with radiosensitizing agents', Cancer Control 15, 38(2008).

[152] L. Kelland, 'The resurgence of platinum-based cancer chemotherapy', Nat. Rev. Cancer 7, 573 (2007).

[153] Y. Pommier, 'Topoisomerase I inhibitors: camptothecins and beyond', Nat. Rev. Cancer 6, 789 (2006).

[154] P. Fumoleau, B. Coudert, N. Isambert, et al., 'Novel tubulin-targeting agents: anticancer activity and pharmacologic profile of epothilones and related analogues', Ann. Oncol. 18 (suppl 5), v9 (2007).

[155] J. M. Brown, 'Tumour hypoxia in cancer therapy', Methods Enzymol. 435, 297 (2007).

[156] M. Bache, M. Kappler, H. M. Said, et. al. 'Detection and specific targeting of hypoxic regions within solid tumours: current preclinical and clinical strategies', Curr. Med. Chem. 15, 322 (2008).

[157] M. Lennartz, T. Coquerelle and V. Hagen, 'Effects of oxygen on DNA strand breaks in irradiated thymocytes', Int. J. Radiat. Biol. 24, 621 (1973).

[158] H. G. Modig, M. Edgren and L. Revesz, 'Dual effect of oxygen on the induction and repair of single-strand breaks in the DNA of X-irradiated mammalian cells', Int. J. Radiat. Biol. 26, 341 (1974).

[159] I. R. Radford, 'The level of induced DNA double-strand breakage correlates with cell killing after X-irradiation', Int. J. Radiat. Biol. 48, 45 (1985).

[160] I. R. Radford, 'Evidence for a general relationship between the induced level of DNA double-strand breakage and cell-killing after X-irradiation of mammalian cells', Int. J. Radiat. Biol. 49, 611(1986).

[161] S. J. Whitaker and T. J. McMillan, 'Oxygen effects for DNA double-strand break induction determined by pulse-field gel electrophoresis', Int. J. Radiat. Biol. 61, 29(1992).

[162] J. Overgaard, 'Hypoxic radiosensitization: adored and ignored', J. Clin. Oncol. 25, 4066 (2007).

[163] G. L. Semenza, 'Evaluation of HIF-1 inhibitors as anticancer agents', Drug Discov. Today 12, 853 (2007).

[164] G. Melillo, 'Targeting hypoxia cell signalling for cancer therapy', Cancer Metastasis rev. 26, 341 (2007).

[165] N. C. Denko, 'hypoxia, HIF-1 and glucose metabolism in the solid tumour', Nat. Rev. Cancer 8, 705 (2008).

[166] M. W. Dewhirst, Y. Cao and B. Moeller, 'Cycling hypoxia and free radicals regulate angiogenesis and radiotherapy response', Nat. Rev. Cancer 8, 425 (2008).

[167] S. R. Mckeown, R. L. Cowen and K. J. Williams, 'Bioreductive drugs: from concept to clinic', Clin. Oncol. 19, 427 (2007).

[168] W. C. Dewey and R. M. Humphrey, 'Increase in radiosensitivity to ionizing radiation related to replacement of thymidine in mammalian cells with 5-bromodeoxyuridine', Radiat. Res. 26(4), 538 (1965).

[169] G. P. Raaphorst, J. A. Vadasz and E. I. Azzam, 'Thermal sensitivity and radiosensitization in V79 cells after BrdUrd and IdUrd incorporation', Radiat. Res. 98(1), 167 (1984).

[170] G. Iliakis, S. Kurtzman, G. Pantelias and R. Okayasu, 'Mechanism of Radiosensitization by halogenated pyrimidines: effect of BrdU on radiation induction of DNA and chromosome damage and its correlation with cell killing', Radiat. Res. 119(2), 286 (1989).

[171] L. L. Ling and J. F. Ward, 'Radiosensitization of Chinese hamster V79 cells by bromodeoxyuridine substitution of thymidine: enhancement of radiation-induced toxicity and DNA strand break production by monofilar and bifilar substitution', Radiat. Res. 121(1), 76 (1990).

[172] T. S. Lawrence, M. A. Davis, J. Maybaum, P. L. Stetson and W. D. Ensminger, 'The effect of single versus double-strand substitution on halogenated pyrimidine-induced Radiosensitization and DNA strand breakage in human tumor cells', Radiat. Res. 123(2), 192 (1990).

[173] G. Iliakis, G. Pantelias and S. Kurtzman, 'Mechanism of Radiosensitization by halogenated pyrimidines: effect of BrdU on cell killing and interphase chromosome breakage in radiation-sensitive cells', Radiat. Res. 125(1), 56 (1991).

[174] J. B. Mitchell, T. J. Kinsella, A. Russo, S. McPherson, J. Rowland, B. H. Smith, P. L. Kornblith and E. Glatstein, 'Radiosensitization of hematopoietic precursor cells (CFUc) in glioblastoma patients receiving intermittent intravenous infusion of bromodeoxyuridine (BUdR)', Int. J. Radiat. Oncol. Biol. Phys. 9(4), 457 (1983).

[175] T. J. Kinsella, P. P. Dobson, J. B. Mitchell and A. J. Fornace, 'Enhancement of X ray induced DNA damage by pre-treatment with halogenated pyrimidine analogs', Int. J. Radiat. Oncol. Biol. Phys. 13(5), 733 (1987).

[176] D. Larson, W. J. Bodell, C. Ling, T. L. Phillips, M. Schell, D. Shrieve and T. Troxel, 'Auger electron contribution to bromodeoxyuridine cellular radiosensitization', Int. J. Radiat. Oncol. Biol. Phys. 16(1), 171 (1989).

[177] R. B. Tishler and C. R. Geard, ‘Correlation of sensitizer enhancement ratio with bromodeoxyuridine concentration and exposure time in human cervical carcinoma cells treated with low dose rate irradiation’, Int. J. Radiat. Oncol. Biol. Phys. 22(3), 495 (1992).

[178] H. Nagasawa, Y. Uto, K. L. Kirk and H. Hori, ‘Design of hypoxia-targeting drugs as new cancer chemotherapeutics’, Biol. Pharm. Bull. 29, 2335 (2006).

[179] C. Sugie, Y. Shibamoto, M. Ito, H. Ogino, H. Suzuki, Y. Uto, H. Nagasawa and H. Hori, ‘Reevaluation of the radiosensitizing effects of sanazole and nimorazole in vitro and in vivo’, J. Radiat. Res. 46, 453 (2005).

[180] W. Dobrowsky, N. G. Huigol, R. S. Jayatilake, N. I. A. Kizilbash, S. Okkan, V. T. Kagiya and H. Tatsuzaki, ‘AK-2123 (Sanazol) as a radiation sensitizer in the treatment of stage III cervical cancer: results if an IAEA multicentre randomised trial’, Radiotherapy and Oncology 82, 24 (2007).

[181] J. F. Vander, M. C. Kincaid, T. J. Hegarty, M. Page, D. Averill, L. Junck and H. S. Greenberg, ‘The ocular effects of intracarotid bromodeoxyuridine and radiation therapy in the treatment of malignant glioma’, Ophthalmology 97, 352(1990).

[182] A. H. Epstein, J. A. Cook, T. Goffman and E. Glatstein, ‘Tumour radiosensitization with the halogenated pyrimidines 5'-bromo- and 5'-iododeoxyuridine’, Br. J. Radiat. Suppl. 24, 209(1992).

[183] M. D. Prados et al. ‘A phase 3 randomized study of radiotherapy plus procarbazine, CCNU and vincristine (PCV) with or without BUdR for the treatment of anaplastic astrocytoma: a preliminary report of RTOG 9404’, Int. J. Radiat. Oncol. Biol. Phys. 45, 1109(1999).

[184] G. E. Adams, ‘Hypoxia-mediated drugs for radiation and chemotherapy’, Cancer 48, 696 (1981).

[185] M Saunders and S. Dische, ‘Clinical results of hypoxic cell Radiosensitization from hyperbaric oxygen to accelerated radiotherapy, carbogen and nicotinamide’, Br. J. Cancer, Suppl. 27, S271 (1996).

[186] J. Overgaard, ‘Clinical evaluation of nitroimidazoles as modifiers of hypoxia in solid tumours’, Oncol. Res. 6 (10-11), 509 (1994).

[187] C. N. Coleman, A. T. Turrisi, ‘Radiation and chemotherapy sensitizers and protectors’, Crit. Rev. Oncol. Hematol. 10, 225 (1990).

[188] C. N. Coleman, T. H. Wasserman, R. C. Urtasun, J. Halsey, L. Noll, S. Hancock and T. L. Phillips, ‘Final report of the phase I trial of the hypoxic cell radiosensitizer SR 2508 (etanidazole) radiation therapy oncology group 83-03’, Int. J. Radiat. Oncol. Biol. Phys. 18, 389 (1990).

[189] J. Overgaard and M. R. Horsman, ‘Modification of hypoxia-induced radioresistance in tumors by the use of oxygen and sensitizers’, Semi. Radiat. Oncol. 6, 10 (1996).

[190] C. J. Koch, P. R. Oprysko, A. L. Shuman, W.T. Jenkins, G. Brandt and S. M. Evans, ‘Rdiosensitization of hypoxic tumor cells by dodecafluoropentane: a gas-phase perfluorochemical emulsion’, Cancer Res. 62, 3626 (2002).

[191] J. M. Brown, ‘SR 4233 (tirapazamine): a new anticancer drug exploiting hypoxia in solid tumours’, Br. J. Cancer 67, 1163 (1993).

[192] M. J. Done and J. M. Brown, ‘Tumour-specific, schedule dependent interaction between tirapazamine (SR 4233) and cisplatin’, Oncol. Res. 6 (10-11), 509 (1994).

[193] J. Treat, E. Johnson, C. Langer, et. al, ‘Tirapazamine with Cisplatin in patients with advanced non-small-cell lung cancer: a phase II study’, J. Clin. Oncol. 16(11), 3524 (1998).

[194] D. Rischin, L. Peters, B. O’Sullivan et. al, ‘Tirapazamine, cisplatin and radiation versus cisplatin and radiation for advanced squamous cell carcinoma of the head and neck (TROG 02.02, HeadSTART): a phase III trial of the Trans-Tasman Radiation Oncology Group’, J. Clin. Oncol. 28(18), 2989 (2010).

[195] S. B. Reddy and S. K. Williamson, ‘Tirapazamine: a novel agent targeting hypoxic tumour cells.’, Expert Opin. Inverting drugs 18, 77 (2007).

[196] W. A. Denny, ‘Hypoxia-activated anticancer drugs’, Expert Opin. Ther Patents 15, 635 (2005).

[197] M. P. Hay, G. J. Atwell, W. R. Wilson, et. al, 'Structure-activity relationships for 4-nitrobenzyl carbamates of 5-aminobenze indoline minor groove alkylating agents as prodrugs for GDEPT in conjunction with E. Coli nitroreductase', J. Med. Chem. 46, 2456 (2003).

[198] A. V. Patterson, D. M. Ferry, S. J. Edmunds et al. 'Mechanism of action and preclinical antitumour activity of the novel hypoxia-activated DNA cross-linking agent PR-104', Clin. Cancer Res. 13, 3922 (2007).

[199] K. O. Hicks, H. Myint, A. V. Patterson, et. al, 'Oxygen-dependence and extravascular transport of hypoxia-activated prodrugs: comparison of the dinitrobenzamide mustard PR-104A and tirapazamine', Int. J. Radiat. Oncol. Biol Phys. 69, 560 (2007).

[200] J. B. Gibbs, 'Mechanism-Based Target Identification and Drug Discovery in Cancer Research', Science 287, 1969(2000).

[201] C.-R. Wang, 'Real-time observation of molecular reaction mechanism of halopyrimidines as radio-/photosensitizing drugs using time-resolved femtosecond laser spectroscopy', University of Waterloo MSc thesis (2007).

[202] A. D. McNaught and A. Wilkinson, 'IUPAC Compendium of Chemical Terminology (Gold book), 2nd edn, Blackwell Science, Cambrige, UK pp. 464 (1997).

[203] J. H. Espenson, 'Chemical Kinetics and Reaction Mechanisms', 2nd edn, McGraw-Hill Series in Advanced Chemistry (1995).

[204] J. March, 'Advanced organic chemistry: reactions, mechanisms, and structure', 3rd ed. Wiley (1985).

[205] R. S. Berry, S. A. Rice, and J. Ross, 'Physical Chemistry', 2nd ed, Oxford: Oxford University Press (2000)

[206] 'Arrhenius equation', IUPAC gold book (http://goldbook.iupac.org/A00446.html)

[207] http://en.wikipedia.org/wiki/Transition_state_theory

[208] K. J. Laldler, and M. C. King, 'The development of transition-state theory', J. Phys. Chem. 87, 2657 (1983)

[209] J. C. Polanyi and A. H. Zewail, 'Direct observation of the transition state', Acc. Chem. Res. 28, 119 (1995)

[210] A. H. Zewail, 'Femtochemistry: atomic-scale dynamics of the chemical bond using ultrafast lasers' (Nobel Lecture), Angew. Chem. Int. Ed. 39, 2586 (2000).

[211] 'Press Release: The 1999 Nobel Prize in Chemistry', Nobelprize.org. http://nobelprize.org/nobel_prizes/chemistry/laureates/1999/press.html.

[212] V. Sundström, 'Femtobiology', Annu. Rev. Phys. Chem. 59, 53 (2008).

[213] Q.-B. Lu, 'Effects of Ultrashort-Lived Prehydrated Electrons in Radiation Biology and Their Applications for Radiotherapy of Cancer', Reviews in Mutation Research 704, 190 (2010).

[214] Q.-B. Lu, 'Molecular Reaction Mechanisms of Combination Treatments of Low-Dose Cisplatin with Radiotherapy and Photodynamic Therapy', J. Med. Chem. 50, 2601 (2007).

[215] Q.-B. Lu, S. Kalantari and C.-R. Wang, 'Electron Transfer Reaction Mechanism of Cisplatin with DNA at the Molecular Level', Mol. Pharmaceutics 4, 624 (2007).

[216] C.-R. Wang, A. Hu and Q.-B. Lu, 'Direct observation of the transition state of ultrafast electron transfer reaction of a radiosensitizing drug bromodeoxyuridine', J. Chem. Phys. 124, 241102 (2006).

[217] C.-R. Wang and Q.-B. Lu, 'Real-Time Observation of a Molecular Reaction Mechanism of Aqueous 5-Halo-2'-deoxyuridines under UV/Ionizing Radiation', Angew. Chem. Intl. Ed. 46, 6316 (2007).

[218] C.-R. Wang and Q.-B. Lu, Molecular Mechanism of the DNA Sequence Selectivity of 5-Halo-2'-Deoxyuridines as Potential Radiosensitizers, J. Am. Chem. Soc. 132, 14710 (2010).

[219] C.-R. Wang, J. Nguyen and Q.-B. Lu, 'Bond Breaks of Nucleotides by Dissociative Electron Transfer of Nonequilibrium Prehydrated Electrons', J. Am. Chem. Soc. 131, 11320 (2009).

[220] J. Nguyen, Y. Ma, T. Luo, R. G. Bristow, D. A. Jaffray and Q.-B. Lu, 'Direct Observation of Ultrafast Electron Transfer Reactions Unravels High Effectiveness of Reductive DNA Damage', Proc. Natl. Acad. Sci. USA. 108, 11778 (2011).

[221] T. Luo, J. Yu, J. Nguyen, C.-R. Wang, R. G. Bristow, D. A. Jaffray, X. Z. Zhou, K. P. Lu and Q.-B. Lu, 'Electron-Transfer Based Combination Therapy of Cisplatin with Tetramethyl-p-Phenylenediamine for Ovarian, Cervical and Lung Cancers', Proc. Natl. Acad. Sci. USA (PNAS), Published online before print June 8, 2012, doi: 10.1073/pnas.1203451109, (2012).

[222] Soren Pedersen, 'Development and applications of techniques in laser femtochemistry', California Institute of Technology PhD thesis (1996)

[223] http://www.biochem.arizona.edu/classes/bioc471/pages/Lecture2/Lecture2.html.

[224] M. Melvin, and D. Kealey, 'Electrophoresis', Wiley (1987)

[225] http://www.biolab.cn/plus/view-241801-1.html

[226] W. C. Dewey, B. A. Sedita and R. M. Humphrey, 'Radiosensitization of X chromosome of Chinese hamster cells related to incorporation of 5-bromodeoxyuridine', Science 152, 519(1966).

[227] K. Sano, T. Hoshino and M. Nagai, 'Radiosensitization of brain tumor cells with a thymidine analogue (Bromouridine)', J. Neurosurg. 28, 530(1968).

[228] T. J. Kinsella, P. P. Dobson, J. B. Mitchell and A. J. Fornace, 'Enhancement of X ray induced DNA damage by pre-treatment with halogenated pyrimidine analogs', Int. J. Radiat. Oncol. Biol. Phys. 13(5), 733 (1987).

[229] H. Sugiyama, Y. Tsutsumi and I. Saito, 'Highly sequence-selective photo reaction of 5-bromouracil-containing deoxyhexanucleotides', J. Am. Chem. Soc. 112, 6720 (1990).

[230] H. Sugiyama, K. Fujimoto and I. Saito, 'Stereospecific 1,2-Hydride Shift in Ribonolactone Formation in the Photoreaction of 2'-Iododeoxyuridine', J. Am. Chem. Soc. 117, 2945 (1995).

[231] K. Kawai, I. Saito and H. Sugiyama, 'Conformation-Dependent Photochemistry of 5-Halouracil-Containing DNA: Stereospecific 2'α-Hydroxylation of Deoxyribose in Z-form DNA', J. Am. Chem. Soc. 121, 1391 (1999).

[232] G. P. Cook and M. M. Greenberg, 'A novel mechanism for the formation of direct strand breaks upon anaerobic photolysis of duplex DNA containing 5-Bromodeoxyuridine', J. Am. Chem. Soc. 118, 10025 (1996).

[233] T. Chen, G. P. Cook, A. T. Koppisch and M. M. Greenberg, 'Investigation of the origin of the sequence selectivity for the 5-halo-2'-deoxyuridine sensitization of DNA to damage by UV-irradiation', J. Am. Chem. Soc. 122, 3861 (2000).

[234] T. Watanabe, T. Bando, Y. Xu, R. Tashiro and H. Sugiyama, "Efficient generation of 2'-deoxyuridin-5-yl at 5'-(G/C)AA^{x}U^{x}U-3' (x=Br, I) sequences in duplex DNA under UV irradiation", J. Am. Chem. Soc. 127, 44(2005).

[235] T. Watanabe, R. Tashiro and H. Sugiyama, 'Photoreaction at 5'-(G/C)AA^{Br}UT-3'sequence in duplex DNA: efficient generation of uracil-5-yl radical by charge transfer', J. Am. Chem. Soc. 129, 8163(2007).

[236] E. J. Hart and J. W. Boag, 'Absorption spectrum of the hydrated electron in water and in aqueous solutions', J. Am. Chem. Soc. 84, 4090 (1962).

[237] Revaz R. Dogonadze, Erika Kalman, Alexei A Kornysher and Jens Ulstrup, 'The chemical physics of solvation', Amsterdam: Elsevier (1985).

[238] J. V. Coe, G. H. Lee, J. G. Eaton, S. T. Arnold, H. W. Sarkas and K. H. Bowen, 'photoelectron spectroscopy of hydrated electron cluster anions, $(H_2O)^{-}_{n=2-69}$', J. Chem. Phys. 92(6), 3980 (1990).

[239] F. H. Long, H. Lu and K. B. Eisenthal, 'Femtosecond studies of the presolvated electron: an excited state of the solvated electron?', Phys. Rev. Lett., 64, 1469 (1990).

[240] X. L. Shi, F. H. Long, H. Lu and K. B. Eisenthal, 'Femtosecond electron solvation kinetics in water', J. Phys. Chem., 100, 11903 (1996).

[241] C. Silva, P. K. Walhout, K.Yokoyama and P. F. Barbara, 'Femtosecond solvation dynamics of the hydrated electron', Phy. Rev. Lett., 80, 1086 (1998).

[242] K. Yokoyama, C. Silva, D. H. Son, P. K. Walhout and P. F. Barbara, 'Detailed investigation of the femtosecond pump-probe spectroscopy of the hydrated electron', J. Phys. Chem. A102, 6957 (1998).

[243] P. Kambhampati, D. H. Son, T. K. Kee and P. F. Barbara, 'Solvation dynamics of the hydrated electron depends on its initial degree of electron delocalization', J. Phys. Chem. A106, 2374 (2002).

[244] M. S. Pshenichnikov, A. Baltuska and D. A. Wiersma, 'Hydrated electron population dynamcis', Chem. Phys. Lett., 389, 171 (2004).

[245] Q.-B. Lu, J. S. Baskin and A. H. Zewail, 'The presolvated electron in water: can it be scavenged at long range?', J. Phys. Chem. B108, 10509 (2004).

[246] B. C. Garrett et al. 'Role of Water in Electron-Initiated Processes and Radical Chemistry: Issues and Scientific Advances', Chem. Rev. 105, 355 (2005).

[247] P. J. Rossky and J. Schnitker, 'The hydrated electron: quantum simulation of structure, spectroscopy and dynamics', J. Phys. Chem., 92, 4277 (1988).

[248] B. J. Schwartz and P. J. Rossky, 'Aqueous solvation dynamics with a quantum mechanical solute: computer simulation studies of the photoexcited hydrated electron', J. Chem. Phys., 101, 6902 (1994).

[249] E. Neria, A. Nitzan, R. N. Barnett and U. Landman, 'Quantum dynamical simulations of nonadiabatic processes: solvation dynamics of the hydrated electron', Phys. Rev. Lett., 67, 1011 (1991).

[250] A. Staib and D. Borgis, 'Molecular dynamics simulation of an excess charge in water using mobile Gaussian orbitals', J. Chem. Phys., 103, 2642 (1995).

[251] T. Goulet, A. Bernas, C. Ferradini and J.-P. Jay-Gerin, 'On the electronic structure of liquid water: conduction-band tail revealed by photoioniaiton data', Chem. Phys. Lett., 170, 492 (1990).

[252] A. Bernas, C. Ferradini and J.-P. Jay-Gerin, 'on the electronic structure of liquid water: facts and reflections', Chem. Phys., 222, 151 (1997).

[253] R. E. Larsen, M. J. Bedard-Hearn and B. J. Schwartz, 'Exploring the Role of Decoherence in Condensed-Phase Nonadiabatic Dynamics: A Comparison of Different Mixed Quantum/Classical Simulation Algorithms for the Excited Hydrated Electron', J. Phys. Chem. B., 110, 20055 (2006).

[254] A. A. Zharikov and S. F. Fischer, 'Theory of electron solvation in polar liquids: A continuum model', J. Chem. Phys., 124, 054506 (2006).

[255] D. Borgis, P. J. Rossky and L. Turi, 'Quantized time correlation function approach to nonadiabatic decay rates in condensed phase: Application to solvated electrons in water and methanol', J. Chem. Phys., 125, 064501 (2006).

[256] J. E. Aldrich, K. Y. Lam, P. C. Shragge and J. W. Hunt, 'Fast Electron Reactions in Concentrated Solutions of Amino Acids and Nucleotides', Radiat. Res. 63, 42 (1975).

[257] Y. Gauduel, S. Berrod, A. Migus, N. Yamada and A. Antonetti, 'Femtosecond charge separation in organized assemblies: free-radical reactions with pyridine nucleotides in micelles', Biochemistry 27, 2509 (1988).

[258] Y. Gauduel, H. Gelabert and F. Guilloud, 'Real-Time Probing of a Three-Electron Bonded Radical: Ultrafast One-Electron Reduction of a Disulfide Biomolecule', J. Am. Chem. Soc. 122, 5082 (2000).

[259] P. Morales-Ramirez, T. Vallarino-Kelly and R. Rodriguez-Reyes, 'In vivo persistence of sister chromatid exchanges (SCE) induced by gamma rays in mouse bone marrow cells', Environ Mutagen. 6(4), 529 (1984).

[260] T. Tagichi and Y. Shiraishi, 'Increased sister-chromatid exchanges (SCEs) and chromosomal fragilities by BrdU in a human mutant B-lymphoblastoid cell line', Mutat. Res. 211 (1), 43 (1989).

[261] S. Zamenhof, R. De Giovanni and S. Greer, 'Induced gene unstabilization', Nature 181, 827 (1958).

[262] G. E. Adams, 'Current topics in radiation research', edited by M. Ebert and A. Howard, New York: John Wiley & Sons (1967).

[263] K. Bhatia and R. H. Schuler, 'Uracil radical production in the radiolysis of aqueous solutions of the 5-halouracils', J. Phys. Chem. 77(15), 1888 (1973).

[264] W. R. Hedrick, M. D. Webb and J. D. Zimbrick, 'Spin trapping of reactive uracil radicals produced by ionizing radiation in aqueous solutions', Int. J. Radiat. Biol 41 (4), 435(1982).

[265] J. D. Zimbrick, J. F. Ward and L. S. Myers Jr., 'Studies on the chemical basis of cellular radiolysis by 5-bromouracil substitution in DNA I. Pulse and steady-state radiolysis of 5-bromouracil and thymine', Int. J. Radiat. Biol., 16, 505 (1969).

[266] K. M. Bansal, L. K. Patterson and R. H. Schuler, 'The production of halide ion in the radiolysis of aqueous solutions of the 5-halouracils', J. Phys. Chem. 76 (17), 2386 (1972).

[267] E. Rivera and R. H. Schuler, 'Intermediates in the reduction of 5-Halouracil by e_{aq}^{-}', J. Phys. Chem. 87, 3966 (1983).

[268] C. D. Finch, R. Parthasarathy, H. C. Akpati, P. Nordlander and F. B. Hunting, 'Low-energy dissociative electron attachment to $CFCl_3$, CF_2Br_2 and 1,1,1- and 1,1,2-$C_2Cl_3F_3$: Intermediate lifetimes and decay energetics', J. Chem. Phys. 106, 9594 (1997).

[269] I. I. Fabrikant, 'Nondissociative electron attachment to molecules and clusters', Eur. Phys. J. D35, 193 (2005).

[270] H. Abdoul-Carime, M. A. Huels, E. Illenberger and L. Sanche, 'Sensitizing DNA to Secondary Electron Damage: Resonant Formation of Oxidative Radicals from 5-Halouracils', J. Am. Chem. Soc. 123, 5354 (2001).

[271] Q.-B. Lu, A. D. Bass and L. Sanche, 'Superinelastic Electron Transfer: Electron Trapping in H_2O Ice via the $N_2^-(^2\Pi_g)$ Resonance', Phys. Rev. Lett. 88, 147601 (2002).

[272] L. Turi and D. Borgis, 'Analytical investigations of an electron–water molecule pseudopotential. II. Development of a new pair potential and molecular dynamics simulations', J. Chem. Phys. 117, 6186 (2002).

[273] S. Cecchini, S. Girouard, M. A. Huels, L. Sanche and D. J. Hunting, 'Interstrand cross-links: a new type of γ- ray damage in bromodeoxyuridine-substituted DNA', Biochemistry, 44(6), 1932 (2005).

[274] D. Borgis, P. J. Rossky and L. Turi, 'Nuclear quantum effects on the nonadiabatic decay mechanism of an excited hydrated electron', J. Chem. Phys., 127, 174508 (2007).

[275] R. A. Crowell and D. M. Bartels, 'Multiphoton Ionization of Liquid Water with 3.0−5.0 eV Photons', J. Phys. Chem., 100, 17940 (1996).

[276] T. K. Kee, D. H. Son, P. Kambhampati and P. F. Barbara, 'A Unified Electron Transfer Model for the Different Precursors and Excited States of the Hydrated Electron', J. Phys. Chem. A105, 8434 (2001).

[277] T. F. Heinz, S. L. Palfrey and K. B. Eisenthal, 'Coherent coupling effects in pump-probe measurements with collinear, copropagating beams', Opt. Lett., 9, 359 (1984).

[278] M. W. Balk and G. R. Fleming, 'Dependence of the coherence spike on the material dephasing time in pump–probe experiments', J. Chem. Phys., 83, 4300 (1985).

[279] S. A. Kovalenko, N. P. Ernsting and J. Ruthmann, 'Femtosecond hole-burning spectroscopy of the dye DCM in solution: the transition from the locally excited to a charge-transfer state', Chem. Phys. Lett., 258, 445 (1996).

[280] Y.-X. Yan, E. B. Gamble, Jr. and K. A. Nelson, 'Impulsive stimulated scattering: General importance in femtosecond laser pulse interactions with matter and spectroscopic applications', J. Chem. Phys., 83, 5391(1985).

[281] P. Vöhringer and N. F. Scherer, 'Transient Grating Optical Heterodyne Detected Impulsive Stimulated Raman Scattering in Simple Liquids', J. Phys. Chem., 99, 2684 (1995).

[282] A. C. Chernovitz and C. D. Jonah, 'Isotopic dependence of recombination kinetics in water ', J. Phys. Chem., 92, 5946 (1988).

[283] S. M. Pimblott and J. A. Laverne, 'On the Radiation Chemical Kinetics of the Precursor to the Hydrated Electron ', J. Phys. Chem. A, 102, 2967 (1998).

[284] Q.-B. Lu and L. Sanche, 'Effects of cosmic rays on atmospheric chlorofluorocarbon dissociation and ozone depletion', Phys. Rev. Lett. 87, 078501 (2001).

[285] C.-R. Wang, K. Drew, T. Luo, M.-J. Lu and Q.-B. Lu, 'Resonant Dissociative Electron Transfer of the Presolvated Electron to CCl_4 in Liquid: Direct Observation and Lifetime of the $CCl_4{}^{*-}$ Transition State', J. Chem. Phys.128, 041102 (2008).

[286] J. Block and W. S. D. Verhey, 'The attack of free radicals on biologically active DNA in irradiated aqueous solutions', Radiat. Res. 34, 689 (1968).

[287] C.-R. Wang, T. Luo and Q.-B. Lu, 'On the Lifetimes and Physical Nature of Prehydrated Electrons in Liquid Water', Phys. Chem. Chem. Phys. 10, 4463 (2008).

[288] P. Foggi, L. Bussotti and F. V. R. Neuwahl, 'Photophysical and photochemical applications of femtosecond time-resolved transient absorption spectroscopy', Int. J. Photoenergy 3(2), 103(2001).

[289] P. A. Terpstra, C. Otta and J. Greve, 'Subpicosecond dynamics in nucleotides measured by spontaneous Raman spectroscopy', Biopolymers 41(7), 751(1997).

[290] A. Hernanz, I. Bratu and R. Navarro, 'IR study on the relaxation of the phosphate group of 5'-dCMP in ^2H_2O and H_2O solutions', J. Phys. Chem. B108, 2438 (2004).

[291] S. Gregoli, M. Olast and A. Bertinchamps, 'Charge-migration phenomena in γ-irradiated costacking complexes of DNA nucleotides: II An ESR study of various complexes in frozen solution', Radiat. Res. 77, 417 (1979).

[292] W. A. Bernhard, ‘Sites of electron trapping in DNA as determined by ESR of one-electron-reduced oligonucleotides’, J. Phys. Chem. 93, 2187 (1989).

[293] I. Zell, J. Huttermann and A. Graslund, A. Rupprecht and W. Kohnlein, ‘Free radicals in irradiated oriented DNA fibers: results from B-form DNA and from deuterated DNA samples’, Free Radical Res. 6, 105 (1989).

[294] W. Saenger, ‘Principles of nucleic acid structure’, New York: Springer-Verlag, pp. 368-384, (1984).

[295] J. Texter, ‘Nucleic acid-water interactions’, Prog. Biophys. Mol. Biol. 33, 83 (1978).

[296] S. M. Lindsay, S. A. Lee, J. W. Powell, T. Weidlich, C. Demarco, G. D. Lewen, N. J. Tao and A. Rupprecht, ‘The origin of the A to B transition in DNA fibers and films’, Biopolyers 27, 1015 (1988).

[297] N. J. Tao, S. M. Lindsay and A. Rupprecht, ‘Structure of DNA hydration shells studied by raman spectroscopy’, Biopolyers 28, 1019 (1989).

[298] M. Falk, A. G. Poole and C. G. Goymour, ‘Infrared study of the state of water in the hydration shell of DNA’, Can. J. Chem. 48, 1536 (1970).

[299] N. Mroczka and W. A. Bernhard, ‘Hydration effects on free radicals yields in DNA X-irradiated at 4K’, Radiat. Res. 135, 155 (1993).

[300] P. O’Neil, A. T. Al-Kazwini, E. J. Land and E. M. Fielden, ‘Diffuse reflectance pulse radiolysis of solid DNA; the effect of hydration’, Int. J. Radiat. Biol. 55, 531 (1989).

[301] P. O’Neil, ‘Pulse radiolysis of DNA-effects of environment’, Free Radical Res. Commun. 6, 153 (1989).

[302] R. O. Rahn and J. L. Hosszu, ‘Influence of relative humidity on the photochemistry of DNA films’, Biochim. Biophys. Acta 190, 126 (1969).

[303] J. Huttermann, M. Rohrig and W. Kohnlein, ‘Free radicals from irradiated lyophilized DNA: influence of water of hydration’, Int. J. Radiat. Biol. 61, 299 (1992).

[304] S. G. Swarts, M. D. Sevilla, D. Becker, C. J. Tokar and K. T. Wheeler, 'Radiation-induced DNA damage as a function of hydration I. Release of unaltered bases', Radiat. Res. 129, 333 (1992).

[305] N. Mroczka and W. Bernhard, 'Hydration effects on free radical yields in DNA X-irradiated at 4K', Radiat. Res. 135, 155 (1993).

[306] W. Wang, D. Becker and M. D. Sevilla, 'The influence of hydration on the absolute yields of primary ionic free radicals in γ-irradiated DNA at 77K: Total radical yields', Radiat. Res. 135, 146 (1993).

[307] K. J. Visscher, M. P. de Haas, H. Loman, B. Vojnovic and J. M. Warman, 'Fast Protonation of Adenosine and of Its Radical Anion Formed by Hydrated Electron Attack; A Nanosecond Optical and Dc-conductivity Pulse Radiolysis Study', Int. J. Radiat. Biol. 52, 745(1987).

[308] K. J. Visscher, M. Hom, H. Loman, H. J. W. Spoelder and J. B. Verberne, 'Spectral and kinetic properties of intermediates induced by reaction of hydrated electrons with adenine, adenosine, adenylic acid and polyadenylic acid: A multicomponent analysis', Radiat. Phys. Chem. 32, 465(1988).

[309] A. Hissung and C. von Sonntag, 'The reactions of the 2'-deoxyadenosine electron adduct in aqueous solution. The effects of the radiosensitizer p-nitroacetophenone. A pulse spectroscopic and pulse conductometric study', Int. J. Radiat. Biol. 39(1), 63(1981).

[310] L. P. Candeias and S. Steenken, 'Electron adducts of adenine nucleosides and nucleotides in aqueous solution: protonation at two carbon sites (C2 and C8) and intra- and intermolecular catalysis by phosphate', J. Phys. Chem. 96, 937 (1992).

[311] Y. Zheng, P. Cloutier, D. J. Hunting, L. Sanche and J. R. Wagner, 'Chemical Basis of DNA sugar-phosphate cleavage by low energy electrons', J. Am. Chem. Soc. 127, 16592 (2005).

[312] J. Bergys, I. Anusiewicz, P. Skurski and J. Simons, 'Damage to model DNA fragments from very low energy (<1ev) electrons', J. Am. Chem. Soc. 126, 6441 (2004).

[313] S. G. Ray, S. S. Daube and R. Naaman, ‘On the capturing of low-energy electrons by DNA’, Proc. Natl. Acad. Sci. USA 102, 15 (2005).

[314] M. Haranczyk, M. Gutowski, X. Li and K. H. Bowen, ‘Bound anionic states of adenine’, Proc. Natl. Acad. Sci. USA, 104, 4804 (2007).

[315] S. T. Stokes, X. Li, A. Grubisic, Y. J. Ko and K. H. Bowen, ‘Intrinsic electrophilic properties of nucleosides: Photoelectron spectroscopy of their parent anions’, J. Chem. Phys. 127, 084321 (2007).

[316] P. P. Bera and H. F. Schaefer III, ‘(G-H) ·-C and G-(C-H) · radicals derived from the guanine·cytosine base pair cause DNA subunit lesions’, Proc. Natl. Acad. Sci. USA 102, 6698 (2005).

[317] S. Ptasinska, S. Denifl, S. Gohlke, P. Scheier, E. Illengerger and T. D. Mark, ‘Decomposition of Thymidine by low-energy electrons: implications for the molecular mechanisms of single-strand breaks in DNA’, Angew. Chem. Int. Ed. 45, 1893 (2006).

[318] I. Bald, J. Kopyra and E. Illengerger, ‘Selective excision of C5 from D-ribose in the gas phase by low-energy electrons (0-1 eV): Implicatons for the mechanism of DNA damage’, Angew. Chem. Int. Ed. 45, 4851 (2006).

[319] E. E. Blatter, Y. W. Ebright and R. H. Ebright, ‘Identification of an amino acid–base contact in the GCN4–DNA complex by bromouracil-mediated photocrosslinking’, Nature (London) 359, 650 (1992).

[320] M. C. Willis, B. J. Hicke, O. C. Uhlenbeck, T. R. Cech and T. H. Koch, ‘Photocrosslinking of 5-iodouracil-substituted RNA and DNA to proteins’, Science 262, 1255 (1993).

[321] C. Nase, Z. Yuan, M. N. Schuchmann and C. von Sonntag, ‘Electron Transfer from Nucleobase Electron Adducts to 5-bromouracil. Is Guanine an Ultimate Sink for the Electron in Irradiated DNA?’, Int. J. Radiat. Biol. 62, 527 (1992).

[322] S. Cecchini, S. Girouard, M. A. Huels, L. Sanche and D. J. Hunting, 'Single-Strand-Specific Radiosensitization of DNA by Bromodeoxyuridine', Radiat. Res. 162, 604 (2004).

[323] A. O. Colson and M. D. Sevilla, 'Elucidation of primary radiation damage in DNA through application of ab initio molecular orbital theory', Int. J. Radiat. Biol. 67 (6), 627 (1995).

[324] M. Hutter and T. Clark, 'On the enhanced stability of the guanine-cytosine base-pair radical cation', J. Am. Chem. Soc. 118, 7574 (1996).

[325] I. Saito, T. Nakamura, Y. Y. Nakayati, K. Yamaguchi and H. Sugiyama, 'Mapping of the hot spots for DNA damage by one-electron oxidation: efficacy of GG doublets and GGG triplets as a trap in long-range hole migration', J. Am. Chem. Soc. 120, 12686 (1998).

[326] F. Prat, K. N. Houk and C. S. Foote, 'Effect of guanine stacking on the oxidation of 8-oxoguanine in B-DNA', J. Am. Chem. Soc. 120, 845 (1998).

[327] H. Sugiyama and I. Saito, 'Theoretical studies of GG-specific photocleavage of DNA via electron transfer: significant lowering of ionization potential and 5'-localization of HOMO of stacked GG bases in B-form DNA', J. Am. Chem. Soc. 118, 7063 (1996).

[328] Y. Yoshioka, Y. Kitagawa, Y. Takano, K. Yamaguchi, T. Nakamura and I. Saito, 'Experimental and theoretical studies on the selectivity of GGG triplets toward one-electron oxidation in B-form DNA', J. Am. Chem. Soc. 121, 8712 (1999).

[329] L. Sanche, 'Biological Chemistry: Beyond radical thinking', Nature 467, 358 (2009).

[330] H. Garn, H. Krause, V. Enzmann and K. Drossler, 'An improved MTT assay using the electron-coupling agent menadione', J. Immunol. Methods 168, 253 (1994).

[331] B. Djordjevic and W. Szybalski, 'Genetics of human cell lines: III. Incorporation of 5-bromo- and 5-Iododeoxyhridine into the deoxyribonucleic acid of human cells and its effect on radiation sensitivity', J. Exp. Med. 112,509 (1960) and references therein.

Appendices:

Appendix A: List of Symbols and Abbreviations

Symbols:

A	adenine (one of the DNA bases)
C	cytosine (one of the DNA bases)
C	carbon
C	molecular concentration
D	dose
e_{pre}^-	precursors to the fully solvated electron
e_{solv}^-	fully solvated electron
eV	electron volt (a unit of energy, 1 eV = 1.6×10^{-19} J)
fs	femtosecond (1 fs = 10^{-15} second)
G	guanine (one of the DNA bases)
Gy	Gray (a radiation dose unit, 1 Gy = 1 J/kg)
J	joule (an energy unit)
kg	kilogram
KI	potassium iodide
L	liter
M	molar (a molar concentration unit, 1M = 1 mol/L)
ms	millisecond (1 ms = 10^{-3} s)

ns nanosecond (1 ns = 10^{-9} s)

MTT 3-(4,5-Dimethylthiazol-2-yl)-2,5-diphenyltetrazolium bromide

O oxygen

ρ density

ps picoseconds (1 ps = 10^{-12} s)

γ gamma

t tert

T thymine (one of the DNA bases)

μs microsecond (1 μs = 10^{-6} s)

Abbreviations:

AP apurinic / apyrimidinic site

BrdU bromodeoxyuridine

DD dipolar dissociation

DEA dissociative electron attachment

DET dissociative electron transfer

DMSO dmethyl sulfoxide

DNA deoxyribonucleic acid

DSB double strand break

dsDNA double strand DNA

5’-dCMPH	2’ -deoxycytidine-5’ -monophosphate
5’-dTMPH	2’ -deoxythymidine-5’ –monophosphate
ESR	electron spin resonance
FDA	food and drug administration
HIF	hypoxia-inducible factor
H_2O_2	hydrogen peroxide
IdU	iododeoxyuridine
IFP	interstitial fluid pressure
IGRT	image-guided radiotherapy
IMRT	intensity-modulated radiotherapy
IR	infrared
LEFE	low energy free (kinetic) electron
LET	linear energy transfer
MDS	multiply damaged site
N_2O	nitrous oxide
PDT	photodynamic therapy
SC	supercoil
SCE	sister chromatid exchange
SDS	sodium dodecyl sulfate
SSB	single strand break

ssDNA	single strand DNA
TAE	Tris-acetate-EDTA
UHV	ultrahigh vacuum

Appendix B: List of Publications

[1] **Chun-Rong Wang,** Anmin Hu and Qing-Bin Lu, 'Direct Observation of the Transition State of Ultrafast Electron Transfer Reaction of a Radiosensitizing Drug Bromodeoxyuridine', J. Chem. Phys. 124, 241102 (2006). [selected for republications in the Virtual Journal of Biological Physics Research (July 1, 2006) http://www.vjbio.org and in the Virtual Journal of Ultrafast Science (July 2006), http://www.vjultrafast.org].

[2] **Chun-Rong Wang** and Qing-Bin Lu, 'Real-Time Observation of Molecular Reaction Mechanism of Aqueous 5-halo-2'-deoxyurimidines under UV/Ionizing Radiation', Angew. Chem. Int. Ed. 46, 6316 (2007).

[3] Qing-Bin Lu, Saeed Kalantari and **Chun-Rong Wang**, 'Electron Transfer Reaction Mechanism of Cisplatin with DNA at the Molecular Level', Mol. Pharmaceutics 4, 624 (2007).

[4] **Chun-Rong Wang**, Kristine Drew, Ting Luo, Mei-Jun Lu and Qing-Bin Lu, 'Resonant Dissociative Electron Transfer of the Presolvated Electron to CCl_4 in Liquid: Direct Observation and Lifetime of the $CCl_4{}^{*-}$ Transition State', J. Chem. Phys.128, 041102 (2008).

[5] **Chun-Rong Wang**, Ting Luo and Qing-Bin Lu, 'On the Lifetimes and Physical Nature of Prehydrated Electrons in Liquid Water', Phys. Chem. Chem. Phys. 10, 4463 (2008) [Selected as a **Hot Article** for PCCP].

[6] **Chun-Rong Wang**, Jenny Nguyen and Qing-Bin Lu, 'Bond breakage of nucleotides by dissociative electron transfer of nonequilibrium prehydrated electrons: a new molecular

mechanism for reductive DNA damage', J. Am. Chem. Soc. 131, 11320 (2009) [This paper was highlighted in a News & Views article in NATURE 461, 358 (2009)].

[7] **Chun-Rong Wang** and Qing-Bin Lu, 'Molecular Mechanism of the DNA Sequence Selectivity of 5-Halo-2'-Deoxyuridines as Potential Radiosensitizers', J. Am. Chem. Soc. 132, 14710 (2010).

[8] Ting Luo, Jianqing Yu, Jenny Nguyen, **Chun-Rong Wang,** Robert. G. Bristow, David. A. Jaffray, Xiao Zhen Zhou, Kun Ping Lu and Qing-Bin Lu, 'Electron-Transfer Based Combination Therapy of Cisplatin with Tetramethyl-p-Phenylenediamine for Ovarian, Cervical and Lung Cancers', Proc. Natl. Acad. Sci. USA (PNAS), Published online before print June 8, 2012, doi: 10.1073/pnas.1203451109, (2012).

[9] **Chun-Rong Wang**, Xiao-Juan Chen, Chang-Cang Huang, Han-Hui Zhang, Zhao-Xun Lian, and Guang-Can Xiao, "Potassium trihydrogen 1,2,4,5-benzenetetracarboxylate trihydrate", Acta Crystallographica Section E. 60: m641-m643 (2004).